IVW - Schriftenreihe Band 100
Institut für Verbundwerkstoffe GmbH - Kaiserslautern

Thomas Bayerl

Application of Particulate Susceptors for the Inductive Heating of Temperature Sensitive Polymer-Polymer Composites

Bibliografische Information Der Deutschen Bibliothek

Die Deutsche Bibliothek verzeichnet diese Publikation in der Deutschen Nationalbibliografie; detaillierte bibliografische Daten sind im Internet über <http://dnb.ddb.de> abrufbar.

Bibliographic information published by Die Deutsche Bibliothek

Die Deutsche Bibliothek lists this publication in the Deutsche Nationalbibliografie; detailed bibliographic data is available in the Internet at <http://dnb.ddb.de>.

Herausgeber: Institut für Verbundwerkstoffe GmbH
Prof. Dr.-Ing. Ulf Breuer
Erwin-Schrödinger-Straße
TU Kaiserslautern, Gebäude 58
67663 Kaiserslautern
http://www.ivw.uni-kl.de

Verlag: Institut für Verbundwerkstoffe GmbH

Druck: Technische Universität Kaiserslautern
ZBT – Abteilung Foto-Repro-Druck

D 386

Als Manuskript gedruckt. Printed in Germany.
ISSN 1615-021X
ISBN 978-3-934930-96-4

Application of Particulate Susceptors for the Inductive Heating of Temperature Sensitive Polymer-Polymer Composites

Vom Fachbereich Maschinenbau und Verfahrenstechnik
der Technischen Universität Kaiserslautern
zur Verleihung des akademischen Grades

Doktor-Ingenieur (Dr.-Ing.)

genehmigte Dissertation

von

Dipl.-Ing. Thomas Bayerl
aus Mainz

Tag der mündlichen Prüfung:	30. April 2012
Vorsitzender:	Prof. Dr.-Ing. Paul Geiß
Referent:	Prof. Dr.-Ing. Peter Mitschang
Koreferent:	Prof. Dr.-Ing. Ralf Schledjewski

D386

Für meine Großeltern

„Ihrer wahren Wesensbestimmung nach ist die Wissenschaft

das Studium der Schönheit der Welt.“

Simone Weil (1909 - 1943), französische Philosophin

Vorwort

Die vorliegende Arbeit entstand während meiner Tätigkeit als wissenschaftlicher Mitarbeiter in der Abteilung Verarbeitungstechnik an der Institut für Verbundwerkstoffe GmbH.

Mein herzlichster Dank gilt meinem Doktorvater Professor Dr.-Ing. Peter Mitschang, der die Erstbegutachtung dieser Arbeit übernahm und mir in den letzten Jahren die Gelegenheit gab, meine Fähigkeiten in einem exzellenten wissenschaftlichen Umfeld zu entwickeln. Er ermöglichte mir stets ein eigenständiges und selbstbestimmtes wissenschaftliches Arbeiten. Des Weiteren danke ich Professor Dr.-Ing. Paul Geiß für die Übernahme des Vorsitzes der Prüfungskommission und meinem ehemaligen Gruppenleiter Professor Dr.-Ing. Ralf Schledjewski für die Zweitbegutachtung der Arbeit.

Allen Kolleginnen und Kollegen des IVWs danke ich für die gute Zusammenarbeit und Unterstützung. Viele von ihnen betrachte ich mittlerweile als Freunde.
Ich bedanke mich bei Lars Moser für die Diskussionen und Anregungen zum Induktionsschweißen und zur Simulation induktiver Prozesse. Besondere Erwähnung sollen hier auch Dr.-Ing. Sebastian Schmeer und Stefan Gabriel für tiefer gehende Einblicke in die Welt des Zerstörens finden. Überaus dankbar bin ich auch Markus Brzeski, der zu manch anregender Diskussion über Degradationsmechanismen von Polymeren in mein Büro stürmte. Erhard Natter und Michael Päßler seien an dieser Stelle nochmals herzlich gedankt, da sie mir immer einen Blick für die praktische Anwendung meiner Ergebnisse bewahrt haben. Des Weiteren danke ich Dr.-Ing. Lada Gyurova, Zdravka Rasheva, Dr. Miro Duhovic, Michael Bierer, Irene Hassinger, Martin Priebe, Klaus Hildebrandt, René Holschuh und Marcel Christmann für ihre Freundschaft und ihre vielfältige Unterstützung.

Ich danke meinen fleißigen Studenten Andreas Elmer, Jörg Rief, Loubna Kandri, Timo Grieser, Felix Schulte-Hubbert, José Sanchez-Sansano, Manuel Martínez-Tafalla, Juan Ignacio Andrés, Jovana Džalto, Florian Kühn, Jie Zou, Hristo Valchev und Nick König für ihren Beitrag zum Gelingen dieser Arbeit. Meine beiden „Ober-Hiwis“

Pascal Bernd und Christian Engel sollten bereits wissen, wie dankbar ich ihnen für ihre exzellente Arbeit bin.

Ein besonderer Dank gilt weiterhin meinen Projektpartnern aus dem europäischen Projekt „Esprit“, im Speziellen Uta Schönwald-Otten und Dr. Adolfo Benedito Borrás, die stets ein offenes Ohr für meine Anliegen hatten.

Schließlich danke ich meiner Familie, allen voran meinen Eltern, die mir durch ihre Unterstützung während meines Studiums all dies erst möglich gemacht haben. Meiner Schwester Anke bin ich dankbar für die sprachliche Verfeinerung dieser Arbeit. Zuletzt, aber von Herzen, danke ich meiner Frau Anna, die jederzeit für mich da war und mich immer gestärkt hat.

Kaiserslautern im Mai 2012 Thomas Bayerl

Table of Contents

Abstract

Thermoplastic polymer-polymer composites consist of a polymeric matrix and a polymeric reinforcement. The combination of these materials offers outstanding mechanical properties at lower weight than standard fiber reinforced materials. Furthermore, when both polymeric components originate from the same family or, ideally, from the same polymer, their sustainability degree is higher than standard fiber reinforced composites.

A challenge of polymer-polymer composites is the subsequent processing of their semi-finished materials by heating techniques. Since the fibers are made of meltable thermoplastic, the reinforcing fiber structure might be lost during the heating process. Hence, the mechanical properties of an overheated polymer-polymer composite would decline, and finally, they would be even lower than the neat matrix. A decrease of process temperature to manage the heating challenge is not reasonable since the cycle time would be increased at the same time. Therefore, this work pursues the adaption of a fast and selective heating method on the use with polymer-polymer composites. Inductively activatable particles, so-called susceptors, were distributed in the matrix to evoke a local heating in the matrix when being exposed to an alternating magnetic field. In this way, the energy input to the fibers is limited.

The experimental series revealed the induction particle heating effect to be mainly related to susceptor material, susceptor fraction, susceptor distribution as well as magnetic field strength, coupling distance, and heating time. A proper heating was achieved with ferromagnetic particles at a filler content of only 5 wt-% in HDPE as well as with its respective polymer fiber reinforced composites. The study included the analysis of susceptor impact on mechanical and thermal matrix properties as well as a degradation evaluation. The susceptors were identified to have only a marginal impact on matrix properties. Furthermore, a semi-empiric simulation of the particle induction heating was applied, which served for the investigation of intrinsic melting processes.

The achieved results, the experimental as well as the analytic study, were successfully adapted to a thermoforming process with a polymer-polymer material, which had been preheated by means of particle induction.

Kurzfassung

Die Klasse der eigenverstärkten Verbundwerkstoffe umfasst Thermoplaste, die mit einer polymeren Verstärkung ausgestattet sind. Diese meist faserförmige Verstärkung ist dabei der gleichen Polymerfamilie zugeordnet, der auch die Matrix angehört. Im Hinblick auf die Faser/Matrix-Haftung und aus Recyclinggründen sind beide Komponenten im idealen Fall aus demselben Material hergestellt. Solche Systeme sind seit einigen Jahren bereits im Bereich der Polyolefine, meist in Form von tafelförmigen Halbzeugen, auf dem Markt etabliert. Diese eigenverstärkten Kunststoffe weisen Vorteile im Bereich der Zugeigenschaften, der Schlagzähigkeit, der Dichte sowie der Rezyklierfähigkeit im Vergleich zu Faserkunststoffverbunden mit anorganischer Verstärkung auf. Hierdurch ist ein extremer Leichtbau mit hoher Energieabsorption des Bauteils möglich. Die Anwendungsmöglichkeiten reichen von Unterbodenblechen für Automobile über Schalenelemente in Transportboxen und Koffern bis hin zu verstärkter persönlicher Schutzausrüstung im Sportbereich.

Bei der Verarbeitung eigenverstärkter Verbundwerkstoffhalbzeuge besteht die Gefahr, die thermoplastische Verstärkungsphase thermisch zu schädigen und damit die mechanischen Eigenschaften des Verbunds zu reduzieren. Eine extrinsische Erwärmung, d.h. eine Erwärmung von außen, erweist sich als problematisch, da die bei Thermoplasten übliche Verwendung einer Verarbeitungstemperatur oberhalb der Schmelztemperatur des Polymers zu einem Schmelzen der verstärkenden Polymerfaserstruktur führen würde. Selbst bei unterschiedlichen Schmelztemperaturen von Matrix und Faser, die innerhalb einer Polymerfamilie realisiert werden könnten, würden Fasern im Randbereich stärker erwärmt und damit auch eher geschädigt als im Zentrum des Verbunds. Eine moderatere Arbeitstemperatur würde zwar die Faserkomponente nicht schädigen, aber auch zu längeren Prozesszeiten führen.

Aufgrund dieser Problematik wurde eine neuartige Methode zur induktiven Erwärmung eigenverstärkter Verbunde über in die Matrix eingebrachte Partikel, sog. Suszeptoren, untersucht und validiert. Die Partikel werden benötigt, um die Energie eines von außen wirkenden elektromagnetischen Induktionsfelds in Wärmeenergie im Verbund umzusetzen. Thermoplastische Polymere sind ohne diese Additive transparent gegenüber magnetischen Feldern. Da die Partikel nur in der Matrix

eingebracht sind, kann eine lokale Heizwirkung erzielt werden. Durch die Distanz zu den partikelförmigen Wärmequellen werden die ohne Partikel ausgerüsteten Fasern vor einem zu großen Wärmeeintrag geschützt.

Als Suszeptoren wurden marktübliche, in großer Stückzahl vorhandene Partikel verwendet, wie z.B. Graugusseisen, Magnetit, Nickel und Rußpartikel sowie nanoskalige Kohlenstoffröhrchen. Diese elektrisch als auch magnetisch unterschiedlichen Partikel wurden gewählt, um die bekannten Wirkmechanismen induktiver Erwärmung, die auf elektrischen Eigenschaften basierten Wirbelstromverluste und die magnetischen Hystereseverluste, hinsichtlich ihrer Wirkungsweise zu unterscheiden. Zur Verringerung des Aufwands der experimentellen Reihe wurden die grundsätzlichen Zusammenhänge der Heizwirkung an zwei unverstärkten Polymeren untersucht. Ein niedrigschmelzendes Polyethylen (HDPE) und ein hochschmelzendes Polyamid (PA6) wurden gewählt, um die Umsetzbarkeit in zwei unterschiedlichen Temperaturbereichen zu testen.

Gute Heizwirkungen wurden bei ferromagnetischen Suszeptoren erzielt, was auf magnetischen Hystereseverlust als primären Heizmechanismus der induktiven Erwärmung schließen lässt. Durch die fortwährende Umpolung des magnetischen Materials, insbesondere der Weißschen Bezirke, entsteht ein Wärmeverlust, der als Temperaturanstieg im Polymermaterial beobachtet wird. Im Gegensatz dazu wurde bei rein elektrischen Additiven keine Erwärmung festgestellt. Diese Beobachtung zeigt, dass Wirbelstromverluste, d.h. Wärmeverluste, die durch die Umpolung eines elektrischen Stromes und damit zu Jouleschen Verlusten führen, nicht auftreten.

Die Untersuchungen ergaben eine Abhängigkeit der Heizwirkung ferromagnetischer Suszeptoren von ihrem Füllgehalt im Verbund. Ein Schmelzen der Matrix konnte unabhängig vom Polymer bereits bei einem Suszeptorgehalt von nur 5 Gewichtsprozent beobachtet werden. Neben dem Füllgehalt wurden der Einfluss der Partikelgröße sowie prozessseitige Parameter wie Frequenz, Induktionsstrom und Kopplungsabstand untersucht. Die besten Ergebnisse wurden bei einer Frequenz von 453 kHz mit einem 10 kW Generator bei einem möglichst minimalen Abstand erzielt.

Die Auswirkung der Partikelerwärmung auf die Eigenschaften der Matrix wurde sowohl in thermischen als auch mechanischen Experimenten untersucht. Da es bislang keine standardisierte Vorgehensweise zum Nachweis thermischer Degradation bei Partikelerwärmung existiert, wurde eine neue Methodik entwickelt, die aus der Höhe der nominellen Schmelztemperatur auf den Degradationsgrad des Polymers schließen lässt. Eine Polymerdegradation konnte zwar nachgewiesen werden, deren Schädigungswirkung aber im Vergleich zu Referenzheizverfahren, Infrarot- oder Lasererwärmung, deutlich geringer ausfiel. Weiterhin zeigte sich in mechanischen Studien, dass die Partikel mit Ausnahme der Schlagzähigkeit keinen signifikanten negativen Einfluss auf die Eigenschaften der Matrix haben.

Für den Einsatz mit polymerverstärkten Materialien wurden die ferritischen Partikel, Graugusspulver und Magnetit, ausgewählt. Eigenverstärkte Komposite konnten mit Hilfe des induktiven Verfahrens innerhalb von drei Minuten in den schmelzflüssigen Bereich überführt werden. Eine Beeinträchtigung der Fasern wurde optisch und mechanisch widerlegt. Da die Vorgänge um die Partikel bei der Erwärmung nicht direkt beobachtbar sind, wurde ein simulativer Ansatz für Untersuchungen zum intrinsischen Aufheizverhalten gewählt. Die Simulation zeigte, dass die Verteilung der Wärmeenergie vom Dispersionsgrad der Partikel abhängig ist und gleichermaßen Matrix und Faserbereiche erreicht. Dadurch ist es theoretisch möglich, dass Fasern schneller zum Schmelzen gebracht werden könnten als die Matrix. Eine Selektivität des Aufheizverhaltens durch das Einbringen von Partikeln in die primär zu erwärmende Matrix wurde damit widerlegt. In der experimentellen Versuchsreihe wurde aber eine eingeschränkte ortsgebundene Aufheizung nachgewiesen, welche sich dadurch charakterisiert, dass die Erwärmung über das Magnetfeld lokal sehr gut steuerbar ist. Hierdurch wird die Erwärmung von Teilbereichen eines Bauteils ermöglicht. In einem Umformprozess könnten dadurch Bereiche von der Erwärmung ausgespart werden, die keiner späteren Deformation unterliegen. Damit wird insbesondere ein Faserschrumpf der polymeren Verstärkung, der auch in konkurrierenden Prozessen beobachtet wurde, über die Bauteilgesamtheit minimiert.

Die gewonnen Erkenntnisse wurden auf einen Thermoformprozess eines eigenverstärkten Materials im Kleinstmaßstab angewendet und erfolgreich umgesetzt.

Abbreviations

Abbreviation	Meaning
AC	Alternating current
BMC	Bulk molding compound
CB	Carbon black
CNT	Carbon nano tubes
D-LFT	Direct LFT
DSC	Differential scanning calorimetry
E-LFT	Endless LFT
ETFE	Ethylene tetrafluoroethylene
GF	Glass fiber
GFRP	Glass fiber reinforced polymer
GMT	Glass mat reinforced thermoplastic
HDPE	High density polyethylene
IH	Induction heating
IR	Infrared
LDPE	Low density polyethylene
LFT	Long fiber reinforced thermoplastic
MFC	Microfibrillar composite
NF	Natural fibers
PA	Polyamide
PA 12	Polyamide 12
PA 46	Polyamide 46
PA 6	Polyamide 6

PA 66	Polyamide 66
PBT	Polybutylene terephthalate
PEEK	Polyetheretherketone
PET	Polyethylene terephthalate
PET-A	Amorphous polyethylene terephthalate
PET-C	Crystalline polyethylene terephthalate
POM-Copo	Polyoxymethylene (copolymer)
POM-H	Polyoxymethylene (homopolymer)
PP	Polypropylene
PP-H	Polypropylene (homopolymer)
PPS	Polyphenylene sulfide
PSU	Polysulfone
PTFE	Polytetrafluoroethylene
PVDF	Polyvinylidene fluoride
PZT	Lead zirconate titanate
ref	Reference
SEM	Scanning electron microscopy
SMC	Sheet molding compound
SRP	Self-reinforced polymer
srPA	Self-reinforced polyamide
srPET	Self-reinforced polyester
srPO	Self-reinforced polyolefin
UHMWPE	Ultra high molecular weight polyethylene
wk	Week

Symbols

Symbol	Unit	Denotation
ΔH_m	[J/g]	Specific melting heat
ΔH_m^0	[J/g]	Theoretical specific latent heat (100 % crystallinity)
ΔT_m	[K]	Melting temperature gap
σ_p	[m]	Penetration depth
μ	[-]	Magnetic permeability
μ_0	[-]	Magnetic permeability of vacuum
μ_r	[-]	Relative magnetic permeability
ρ	[kg/m³]	Mass density
ρ_e	[Ω/m]	Electric resistivity
χ	[m³/kg]	Magnetic susceptibility
X_c	[%]	Degree of crystallinity
a	[mm]	Sample width
a_{cN}	[kJ/m²]	Notch impact strength
b	[mm]	Sample height
B	[T]	Magnetic flux density
B_0	[T]	Magnetic flux density in vacuum
c	[mm]	Width
c_p	[J/kgK]	Specific heat capacity
d	[mm]	Material thickness
d_c	[µm]	Critical particle size

F	[N]	Force
f	[1/s]	Frequency
f_s	[-]	Shape factor
H	[A/m]	Magnetic field strength
h_r	[K/s]	Linear heating rate
I_C	[A]	Effective current in the coil
k	[W/mK]	Thermal conductivity
L	[H]	Inductance
n	[-]	Number of coil windings
P_H	[J]	Hysteresis loss energy
P_m	[J]	Energy of a magnetic field
R^2	[-]	Coefficient of determination
r	[mm]	Coupling distance
r_c	[mm]	Coil radius
t	[s]	Time
T	[°C]	Temperature
t_0	[s]	Reference time
T_c	[°C]	Crystallization peak temperature
T_{Cu}	[°C]	Curie temperature
T_g	[°C]	Glass transition temperature
T_m	[°C]	Crystallite peak melting temperature
Q	[J]	Heat energy
V	[mm³]	Volume

W_{25}	[J]	Impact energy after 25 mm displacement
W_I	[J]	Charpy impact energy
W_L	[J]	Loss energy
W_m	[J]	Magnetic work
W_{max}	[J]	Impact energy at maximum force
$W_{max,s}$	[Jm^3/kg]	Specific impact energy at maximum force
w_s	[wt-%]	Susceptor weight fraction

1 Introduction and Motivation

1.1 Introduction

Fiber reinforced composites have become an important material class within the industrial world. The development from the beginning of polymer appearance starting in 1907 with the invention of Bakelite, the first synthetic polymer material, and the first industrialized production of composites in 1945, reached its breakthrough with complex designed composite parts for high performance space and aircraft applications in the 1960s [1,2]. Today's composites are not exclusive for specialized, high-end applications. Even children talk about the lightness of their new "carbon bike frame" or the smooth running of their "nano inline wheels". Composites and their advantages of being lightweight, extremely strong, and stiff, besides other additional attributes have become well-known and accepted within the society in the past years, thus, representing goods of high value. Nevertheless, especially carbon fiber reinforced composite components are still expensive and not affordable to everybody as well as suitable for every application. By regarding the economic and ecological situation at the beginning of the 21st century, two factors have gained in importance: environmental and economic sustainability. Accordingly, on the one hand, materials still have to provide the specific mechanical, chemical, and thermal needs within an application. On the other hand, they have to be recyclable and have to arouse only low initial costs. These factors are extremely important for commodity goods, where a slightly higher priced component may cause an extremely high profit loss due to the high lot size. At worst case, the economic factor defines the material choice, which leads to lower costs for the producer but only to the second best choice for potential customers. As a consequence, the development of new materials, which face this challenge of being highly versatile and customizable as well as ecologic and economic bearable should be pushed forward. New approaches, which try to compete with these needs, include the use of natural fibers, new energy-saving hybrid metal-fiber-polymer composites, and the development of self-reinforced materials.

Natural fibers (NF) perform the needs of ecological sustainability, but their flammability and their water absorption mark factors for their rejection for most challenging applications [3,4,5,6,7]. Furthermore, when natural fibers are in contact with a thermoplastic or thermoset matrix, the recyclability has to be revised, since the end-of-life separation is an additional challenge. Therefore, the approach of using 100 % bio-compatible materials for the manufacturing of composites has been recently pursued. These bio-composites are bio-degradable or consist of renewable, organic material. To some extent, they are already used in small-scale applications. For developing a market for a broad field of applications, many challenges still have to be solved including the hydrophilic behavior of natural fibers, their low service temperature, and their rather poor mechanical properties in comparison to inorganic fibers [3,6,8].

Other approaches deal with hybrid composites containing metallic and polymeric structures. Metal fiber reinforced polymer hybrids usually reveal high impact performance at lower weight than neat metal structures, since they combine the advantages of metallic ductility with polymer weight and corrosion resistance. By the use of metallic grids in polymers, especially improved crash absorption has been achieved [9,10]. The metallic reinforcement meets the economic demands in comparison to carbon or glass fibers. Furthermore, the recyclability of these compounds may be solved with certain efforts, but its high specific weight limits its broader usability.

A very promising approach to withstand all economic, ecological, and structural demands is characterized by the group of polymer-polymer composites. They consist of a polymer matrix and reinforcing polymer fibers. In order to fulfill the recyclability demands, both, polymer fiber and polymer matrix, originate from the same polymer family (polyolefins, polyamides etc.). These special types of polymer-polymer composites are also referred to as self-reinforced polymers (SRP) [11]. To achieve the highest sustainability degree, polymer and matrix are produced from the same type of polymer (e.g. polypropylene reinforcement in polypropylene matrix). First approaches to manufacture these single-polymer composites date back to the 1970s [12,13]. As being of high lightweight potential, self-reinforced polymers especially offer high impact strength in comparison to neat materials of the same density as well

as the ability for low-cost recycling [14]. The currently market available SRP materials are on a polyolefin basis and are either manufactured from a plain sheet of unidirectional polyolefin fibers by heat compaction or from tapes by co-extrusion [15,16]. Recently, this material is used for suitcase covers, soccer shin pads, automotive underbody panels, and other applications, where a high impact resistance is demanded.

Nowadays, no direct processes for the manufacturing of components made of SRP are market-ready yet. Consequently, a reheating of the semi-finished materials is necessary to achieve the final component shape in a subsequent forming process. During this process, the danger of reinforcement melting occurs, which will reduce the mechanical properties of the final component.

The major problem for the development of any new SRP material is to prevent the melting of the reinforcement phase during the (re-)heating process. In order to handle this dilemma, two main approaches, one on the material and one on the process side, are pursued. Firstly, the difference between the melting temperatures of matrix and fiber has to be large enough to permit conventional heating. Although originating from the same polymer family, SRP components can be chosen among a range of polymers with different properties, including different melting temperatures. For example, the melting temperature of polyamide 6 (PA 6) is about 40 °C lower than polyamide 6.6 (PA 66). PA 66 fibers in a PA 6 matrix could be an option for easy processible self-reinforced semi-finished materials. Nevertheless, the application of conventional heating techniques, such as the use of a convection oven, at low temperatures is rather slow since the heat energy is transferred into the component to be heated from its surface. To achieve a complete heating throughout the composite, the heat energy has to be conducted from the surface to the center. This process is very time-intensive in case of thermoplastics which are usually of low thermal conductivity. For increasing the heating speed, a common procedure for neat thermoplastics is choosing a processing temperature above the polymer's melting temperature. Since the surface would be affected more from the increased heat, this would result, in case of SRP, in a surface near fiber damage followed by a loss of mechanical properties.

To overcome this dilemma of either damaging polymer-polymer composites by external heat sources or accepting higher cycle times, a selective heating of the matrix phase without affecting the fibrous reinforcement would be the silver bullet. Consequently, the emphasis of this work lies on the adaption of a selective heating technique on the basis of electromagnetic induction for polymer-reinforced composites.

1.2 Motivation and Scope of the Work

By their extreme lightweight and high impact resistance at increased recyclability, polymer-polymer materials offer various application possibilities in the automotive, sports and leisure, and construction sectors (Figure 1.1).

Figure 1.1: Selected applications for self-reinforced materials [17,18,19]

The motivation of this work is related to the exploitation of new application markets for SRP. For this purpose, the development of a suitable heating technique especially designed for SRP materials would be beneficiary. The heating should primarily affect the matrix and prevent an overheating of the polymer reinforcement. The so-called selective heating method has to fulfill the requirements of energy-saving and high automation potential. Furthermore, the method should be applicable to various kinds of SRP semi-finished materials while guaranteeing an accurate temperature control. Energy-saving techniques have a high degree of efficiency, which implies that a main part of the invested energy is transferred into the component to be heated and not to the surrounding environment. In this context, Table 1.1 lists important polymer heating methods and their efficiency degrees presented as their respective power densities.

Table 1.1: Power densities of various polymer heating techniques [20]

Process	Power density [kW/m²]
Convection	5 – 10
Radiation (e.g. infrared)	10 – 100
Resistance heating	20 – 30
Induction heating	300 – 600
Dielectric heating (e.g. microwave)	1000 – 2000

For its selective working, the method has to be locally applicable or can be shielded to limit its influence on a specific area. By the use of additives, so-called heating promoters or susceptors, which introduce the heat into the material, a selectiveness is predetermined. This method has the advantage of offering an intrinsic nature which helps to achieve a homogeneous heating and limits the damage to surface near fibers as it would be the case for extrinsic surface heating methods.

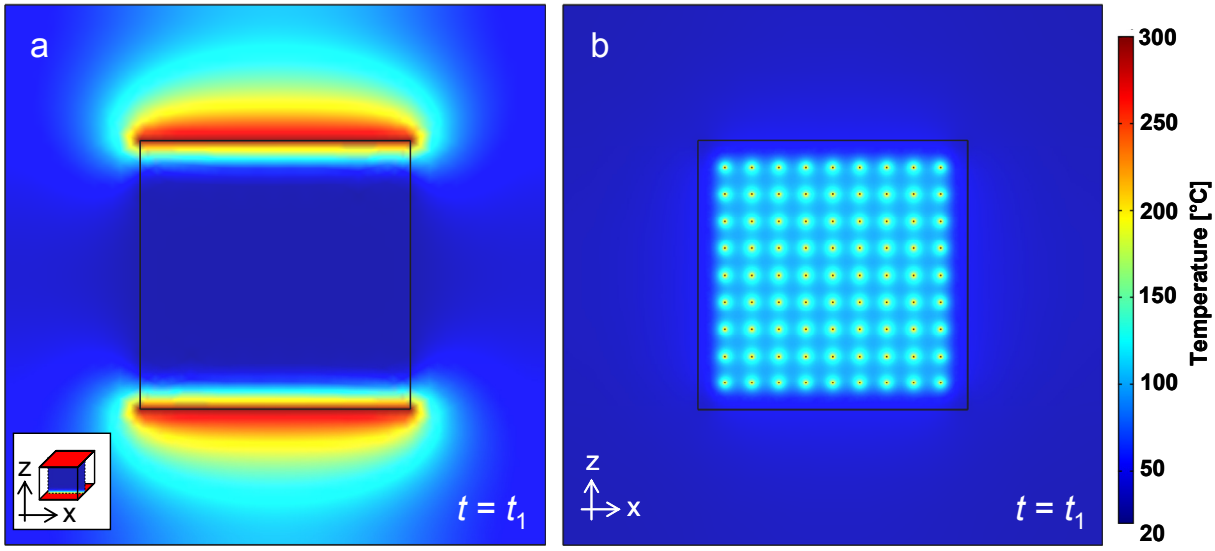

Figure 1.2: Simulation of extrinsic (a) versus intrinsic (b) heating – the low thermal conductivity of polymers prevent a homogenous extrinsic heating for bulk materials

The expected homogeneity increase within a bulk material is demonstrated by a simulative approach. An exemplary cubic polymer surface with an edge length of 10 cm is heated by a constant temperature input on two opposite surfaces. Figure 1.2 demonstrates that this extrinsic heating does not achieve the desired homogeneous heating of the bulk. A large part of the induced energy is lost to the environment. An intrinsic heating, consisting of particulate heat sources, which sum up to the same used energy as for the extrinsic heating simulation, result in a more homogenous heating of the bulk within the same time in this ideal case even without

losses to the environment. Consequently, the intrinsic method is expected to be of higher efficiency resulting in shorter process cycles.

Contactless heating techniques using electromagnetic fields like microwave and induction heating are predestined to meet the demands of selectiveness. Both techniques need additional particles for a sufficient energy transfer into the compound since most polymers are transparent to electromagnetic radiation. The particles act then as heat sources within the material. This work focuses on heating by inductive means, since this method is able to comply with the stated requirements and furthermore provides good automation perspectives.

Induction heating has previously proven its selective heating abilities in various other fields of research, such as in induction welding applications and even as medical treatments [21,22,23,24,25]. Nevertheless, an approach for the heating by induction of self-reinforced material does not exist. The scope of this thesis includes an analysis of the heating abilities of commonly available ferromagnetic and non-ferromagnetic particulate induction heating susceptors and their influence on compound properties in combination with neat thermoplastic materials. The study was focused on susceptors which fit to the price level of the used matrix materials and could serve as suitable additives in subsequent mass production applications. In this context, from related patents is known that ferromagnetic alloys can be tailored according to their hysteresis ability [26], but particles of these alloys were rejected in this study for their bad market availability and their high price. Furthermore, ferromagnetic nano particles were not considered due to their low master batch availability on the market.

The feasibility of particle based induction heating was investigated with neat matrix systems first, before adapting the knowledge for the manufacturing of inductively heatable polymer-polymer compounds.

Two different matrix systems were primarily used, a polyolefin and a polyamide, for demonstrating the application of particle induction in their respective melting temperature range. In the experimental series, the influence on heating effects of particle material and fraction were investigated, which, in turn, covered the influence of the susceptors. Succeedingly, the machine parameters of the induction generator,

which were used for the control of the electromagnetic field, were adapted to suitable particulate susceptors. This optimization included common process parameters, like power, frequency, and coupling distance. The influence of the coil, which is defined by its shape and thus very complex, was not investigated.

The feasibility of the induction heating process with polymer-polymer composites was proven by the use of the optimized susceptor and machine properties. Since intrinsic phenomena, like temperature distribution and possible reinforcement melting processes, could not be observed during the experimental series, a multi-physics simulation tool was used to simulate the inductive particle heating.

Conventional and competing compression molding processes were compared to the results of compressed sheets which have been previously heated by particle based induction. Within this scope, also fast heating methods, like the innovative RocTool® technology, were examined to prove the feasibility of the developed heating method.

For dissemination means of this work, design concepts for an industrial application of particle induction as well as for economic considerations were discussed. Figure 1.3 illustrates the general layout of the work.

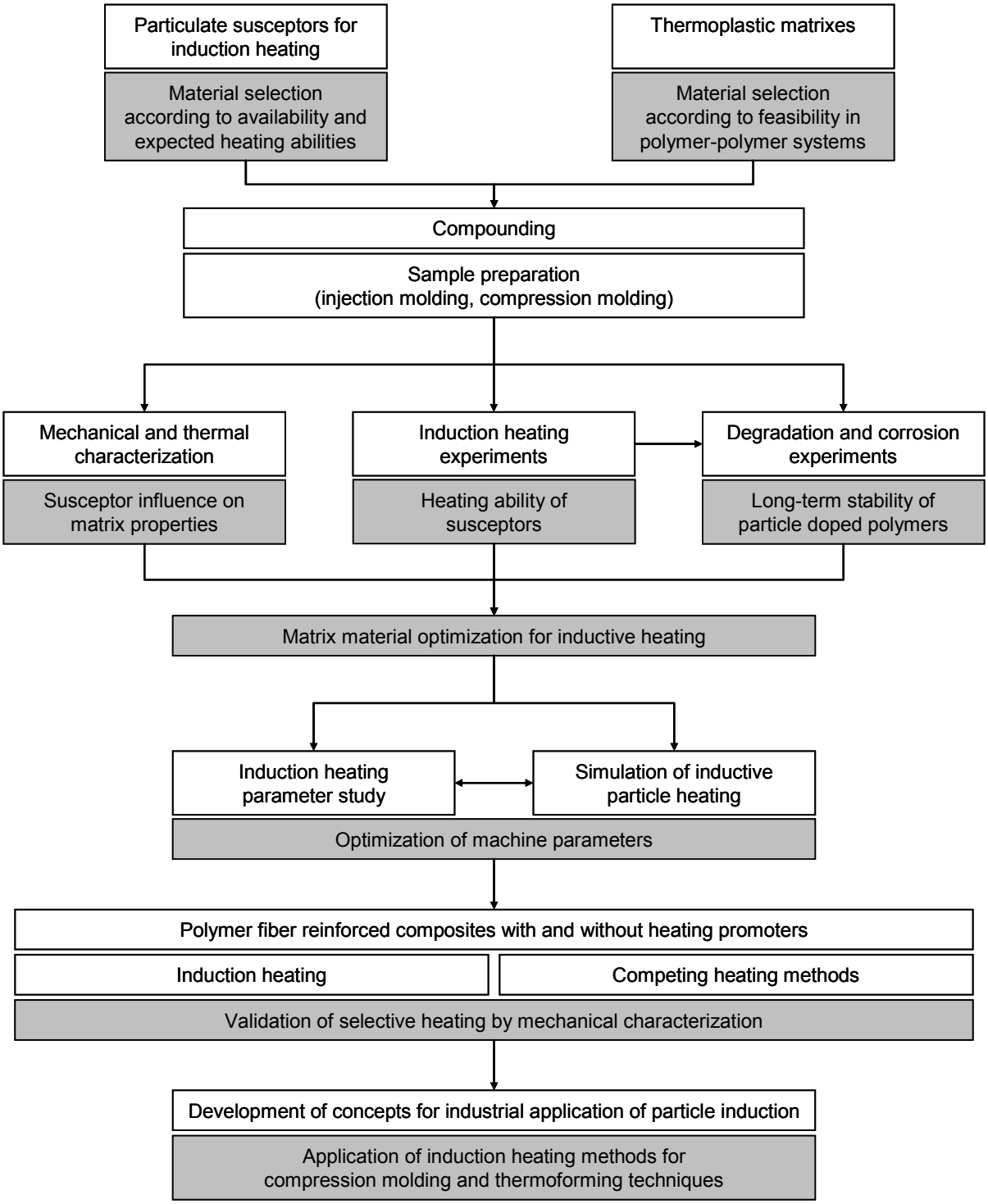

Figure 1.3: Scope and layout of the work

2 State of the Art

2.1 All-Polymeric and Self-Reinforced Materials

In contrast to standard fiber reinforced composites which use a polymer matrix and fibers made of glass or carbon, all-polymeric materials consist of a thermoplastic polymer matrix phase and a thermoplastic polymeric reinforcement. To conform to the term self-reinforced polymer (SRP), matrix and reinforcement of such materials have to be from the same polymer type (e.g. polypropylene matrix and polypropylene fiber).

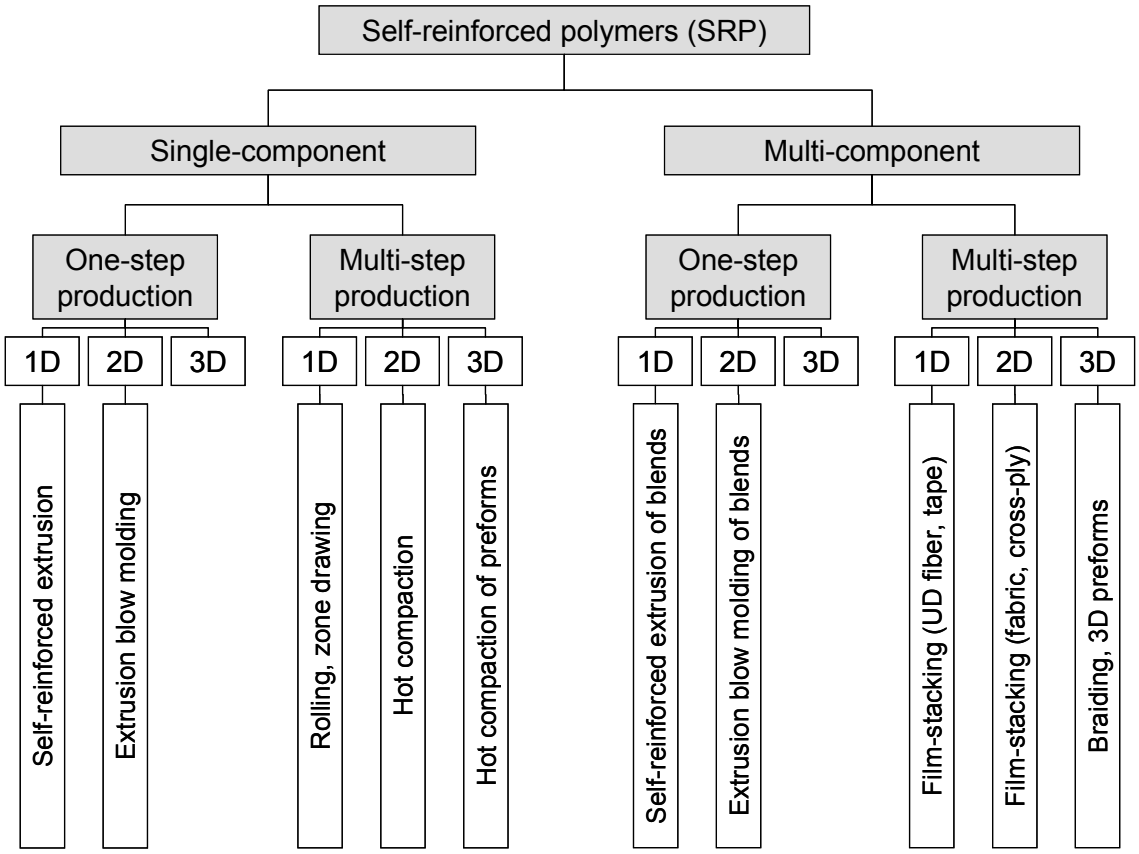

Figure 2.1: Classification of self-reinforced polymers (extract from [11])

In literature and recent research, the definition of self-reinforced polymers refers also to reinforced materials which consist of a polymer matrix and reinforcement from the same polymer family (e.g. polyolefins like high density polyethylene and polypropylene) [11]. To distinguish between these types, the concurrent definition of single-component (same polymer) and multi-component (same polymer family) SRP

is applied. Further classifications respect the production process steps (single or multi) and the spatial distribution of the reinforcement (1D, 2D, 3D) [11].

Table 2.1: Properties of commercially available sheet-like SRP material in comparison to a PP reference material [16,27,28,29,30,31]

Property	Test method	Unit	Moplen HP500V	Curv® C100A	Armordon® Panel	Tegris Sheet	PURE® Sheet
Manufacturer	-	-	Basell	Propex Inc.	Don & Low Ltd.	Milliken & Co.	Lankhorst Pure Composites bv
Material combination	-	-	PP	PP/PP	PP/PP	PP/PP	PP/PP
Density	ISO 1183	g/cm³	0.91	0.92	0.83	0.78	0.78
Tensile strength	ISO 527	MPa	35	120	200	200	200
Tensile modulus	ISO 527	GPa	1.55	4.2	4.4	5-6	5.5
Flexural modulus	ISO 178	GPa	Not provided	3.5	3.8	5-6	4.5 - 5.5
Charpy impact (notched, 20 °C)	ISO 179-2	kJ/m²	2	120	137	Not provided	140 (part. break)
Izod impact (notched, 20 °C)	ISO 180-2	kJ/m²	Not provided	400	115	Not provided	126 (part. break)
Puncture impact, (20 °C, 2.1 mm, impactor diam. 20 mm)	ISO 6603-2	J	Not provided	40	Not provided	Not provided	51.46

Commercial SRP materials are already available from a small amount of manufacturers, but are exclusively made of polyolefins. The polypropylene (PP) materials offer outstanding mechanical properties at extreme lightweight (Table 2.1). Besides them, a high density polyethylene (HDPE) self-reinforced composite has recently appeared on the market, which is offered as tapes as well as organic sheets originating from stacked tapes.

Curv®, a self-reinforced polypropylene, is available as sheet material, which has been pre-consolidated by a hot compaction process (Figure 2.2). The manufacturing process of Curv® consists of an orientation of the polypropylene chains by stretching. The stretched fibers are either aligned for UD reinforcement or woven into a fabric.

The know-how within the Curv® manufacturing process lies in the consequent heating of the fibers above melting temperature without melting the whole fiber and preventing the fiber to lose its stretched state. In this context, polypropylene reveals a beginning material softening at 90 - 100 °C, which is lower than the respective melting peak temperature. The molten material forms the matrix phase after recrystallization resulting in a two-dimensional SRP [15]. In literature, this is referred to as hot compaction process which is also used by Nextrusion for the manufacturing of HDPE based kaypla® [11].

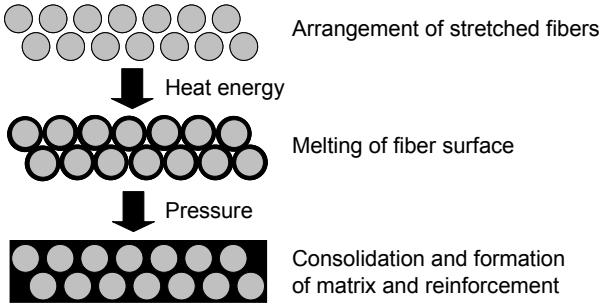

Figure 2.2: Principle of hot compaction process used for the manufacturing of materials like Curv® and kaypla®

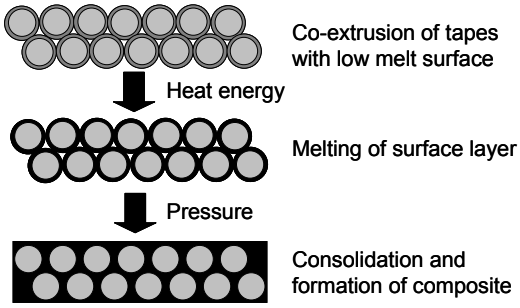

Figure 2.3: Principle of co-extrusion process used for the manufacturing of PURE® and Tegris™

The co-extrusion of polymers is the second manufacturing process, which can cover the market needs at the moment. PURE® and Tegris™ (former MFT) materials are produced in this manner based on the extrusion of a skin on a highly oriented core (Figure 2.3). A subsequent compaction leads to organic sheets [32].

Table 2.2: Properties of commercially available SRP tapes [33,34,35]

Property	Test method	Unit	Nextrusion kaypla®	Armordon® Tape	Lankhorst PURE® tape
Manufacturer	-	-	Nextrusion GmbH	Don & Low Ltd.	Lankhorst Pure Composites bv
Material combination	-	-	HDPE/HDPE	PP/PP	PP/PP
Tensile Strength	ISO 527	MPa	not provided	not provided	500
Tensile Modulus	ISO 527	GPa	20 – 62	not provided	14

Additionally, various scientific approaches exist for the manufacturing of either self-reinforced or polymer-polymer materials [11,36,37,38,39]. Neither of them has successfully found its way onto the market, yet.

Besides the self-reinforced materials, a special group of thermoplastic polymer-polymer composites have been developed, which do not fulfill the demands for being self-reinforced. Within this group, matrix and fiber do not originate from the same polymer family. Usually, they consist of two polymers from different families and form a blend. By using an adequate heating/stretching process, so-called microfibrillar composites (MFC) are manufactured, which have similar properties as glass fiber reinforced materials [11,40]. Various material combinations have been examined in the last years, including polypropylene-polyethylene terephthalate (PP/PET), polypropylene-polyamide (PP/PA), and polyethylene terephthalate-polyamide (PET/PA) combinations [40]. These materials offer the same advantages like self-reinforced materials but have to face the same challenges as well.

The challenges of polymer-polymer composites include the limitation of polymer fiber shrinkage and the optimization of fiber-matrix adhesion.

Polymer shrinkage describes the relaxation of an oriented polymer structure due to internal forces. For polymer-reinforced materials, mainly the triggering of shrinkage by thermal processes is of relevance. Shrinkage within a material is mainly predetermined by the respective manufacturing process. For the manufacturing of polymer fibers, as used in SRP composites, thermoplastic polymers are melted, spun, and drawn to gain certain properties. An additional drawing process of a fiber in cold state causes a higher orientation of the molecular chain and a higher perfection of crystallites. The cold-drawing process consequently results in increased tensile properties, but also the shrinkage of the fiber is higher because of higher frozen-in relaxation forces. Besides the processing, the fiber material, including the crystallite orientation and the molecular structure of amorphous regions, and the material's thermal history influence the shrinkage behavior [41,42].

Thermally triggered shrinkage usually occurs below the melting temperature of semi-crystalline thermoplastics. For fibrous PP materials, a high shrinkage was reported between 140 °C and 155 °C, which is close to the respective melting temperature. The shrinkage related softening effect for PP was even observed at an earlier state beginning from 80 – 90 °C [43]. PET fibers revealed a softening around their glass

transition temperature at 65 °C, whereas the shrinkage was monitored to be linearly increasing from this point with increasing temperature [41,43].

As every fiber-reinforced composite, the performance of all-polymer composites is dependent on the adhesion between matrix and reinforcement. Within SRP material systems, which originate from a single-polymer approach like the formerly mentioned hot compaction process, the use of only one polymer guarantees a high compatibility between matrix and reinforcement. Nevertheless, the good compatibility does not necessarily guarantee a high adhesion but is dependent on processing parameters. Hence, recent research activities focus on the optimization of adhesion quality also of market-ready material combinations [11,44].

2.2 Polymer Melting

Polymers can be classified by numerous parameters, e.g. molecular setup, mechanical and chemical properties, their processing or according to their specific field of application. In the scope of this work dealing with thermoplastic melting phenomena, a classification according to their molecular structure and their respective molecular mobility is appropriate. The molecular mobility describes the ability of the molecular chains to oscillate and even to move within a material and is closely linked to the melting behavior of a polymer [45].

The Brownian mobility is connected to the molecular setup of each polymer. Thermoset polymers possess a low Macro- and Micro-Brownian mobility in comparison to thermoplastic materials (Figure 2.4). The thermoset consists of cross-linked macromolecules, which is one molecule in an ideal cured state. This molecular setup implies a strong covalent bonding between atoms. The Brownian mobility is limited and can be best observed while heating the material – where the material does not reveal a plastic melting state – and is destroyed after exceeding a temperature, which is distinct for each polymer. This temperature is named decomposition temperature.

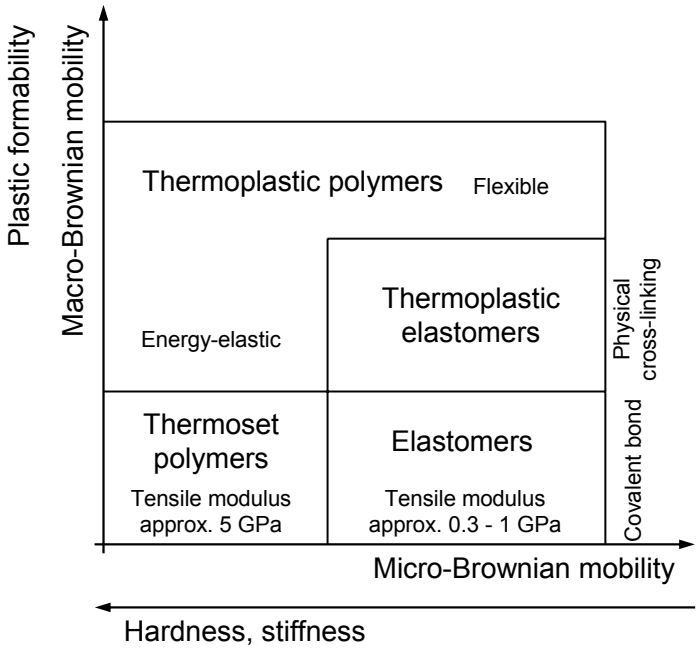

Figure 2.4: Classification of polymers according to their molecular mobility at room temperature [45]

In comparison, thermoplastic materials consist of polymer chains, which are not cross-linked. The stability of these polymers are connected to electrostatic forces, like Van-der-Waals-Forces and hydrogen bonds, as well as to physical cross-linking due to interlocking and to the formation of ravels of the polymer chains. By an exposure to a higher temperature, the polymer chains are able to move because of their Brownian mobility, which results in a melting of the macroscopic material.

During thermoplastic polymer melting, several distinct states are distinguished from each other (Figure 2.5). Beginning from absolute zero (0 K), the polymer is in a glass-like brittle state. Amorphous thermoplastic materials lose a large amount of their mechanical properties by exceeding the glass transition temperature, T_g, which characterizes the shift from the glass-like to the elastic state. Crystalline thermoplastics, which contain an additional crystallite phase, also display a declining of mechanical properties at this point, but only with a marginal effect due to the softening in amorphous regions. The semi-crystalline thermoplastic materials forfeit their mechanical performance when reaching the crystallite melting temperature or peak melting temperature, T_m, at which the polymer changes its state from elastic to plastic behavior. Therefore, for a processing, meaning the molding of amorphous thermoplastics, T_g is the relevant factor, whereas for crystalline thermoplastics, T_m is

of higher importance. Since both temperatures, T_g as well as T_m must not be seen as distinct values but as a transition region, the processing temperatures are often chosen in a higher range [46].

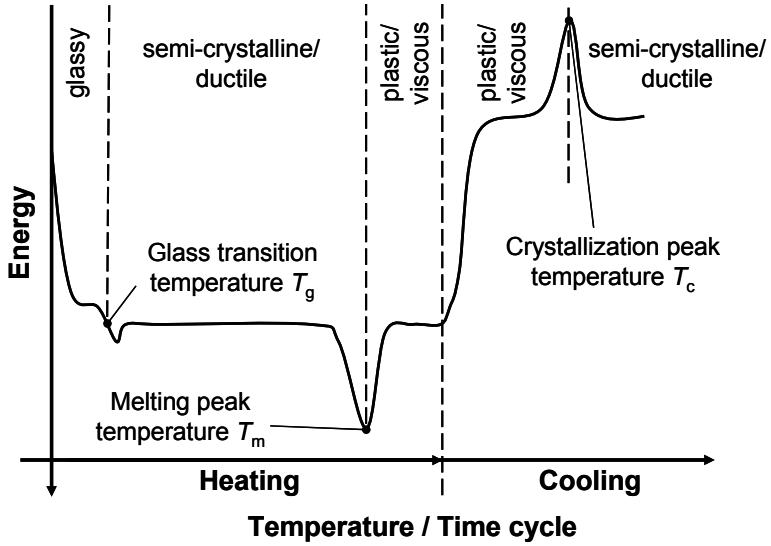

Figure 2.5: Exemplary differential scanning calorimetry (DSC) record providing details of important states of a semi-crystalline thermoplastic polymer [46]

2.3 Thermal Degradation of Polymers

Degradation mechanisms and appropriate analysis methods of thermoplastics within standard heating processes were discussed in various papers and handbooks before [1,46,47,48,49].

Heating of thermoplastic polymers above their respective decomposition temperature, which usually lies several decades higher than the melting peak temperature, leads to changes in the configuration of the molecular chain. The most common observed phenomenon is the molecular deterioration which is characterized by a separation of parts from the polymer chain backbone, often referred to as molecular scission. This effect can also be noticed at temperatures higher than the nominal melting temperature and below the decomposition temperature [47]. Besides by directly observable properties like color and surface morphology, the molecular weight and the degree of crystallinity are affected by molecular scission. Additionally, thermal and mechanical properties of the polymer are often negatively influenced [50,51,52,53].

Thermal degradation is accelerated through higher temperatures. Longer exposition times at lower temperatures do not necessarily promote increased polymer degradation. Holmström et al. reported in this context a molecular chain enlargement for polyethylenes at temperatures close to the melting point [54,55]. From other materials is also known that cross-linking may appear, which consequently increases the molecular weight [56].

2.4 Heating Techniques

Heat transfer mechanisms and their respective technical applications have been described to a large extent before [57,58,59,60,61]. According to Nußelt's classification, the main mechanisms are conduction and radiation [62].

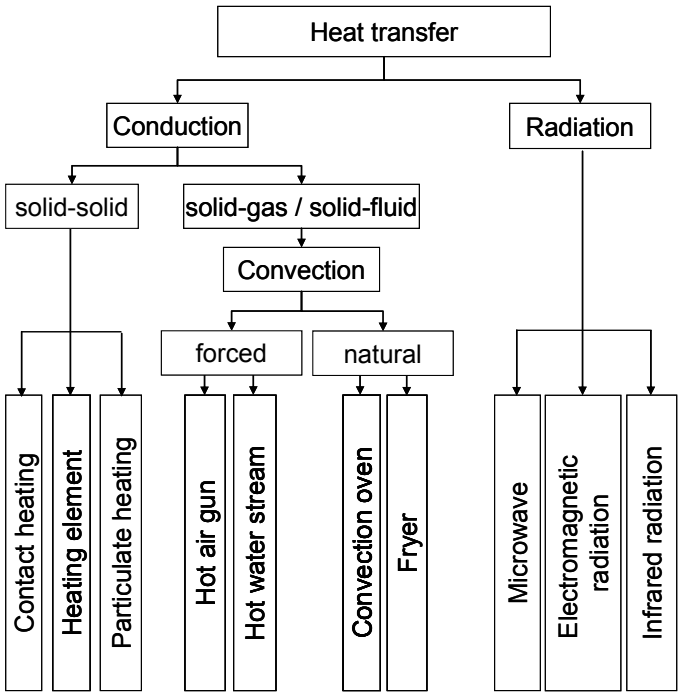

Figure 2.6: Heat transfer mechanisms with exemplary applications (based on [62])

Conduction heating is characterized by the contact of a hot (tool) surface with a material of lower temperature. Without a continuous energy supply, a steady state is formed, in which both materials possess the same mean temperature. This is avoided by continuous tool heating. Hot plate welding is an example hereof. According to Nußelt, conduction heating also refers to systems, where a medium is used as a conveyer of the energy, as the air in a convection oven, for instance [62].

The radiative heat mechanism depends on the energy transfer by electromagnetic radiation and is therefore of contactless character without the need of a medium. Infrared heating, an example for radiative heat transfer, is a standard method in thermoforming processes.

The particle based induction heating investigated within this study can be classified as a combination of radiation and conduction heating. The particulate susceptors are affected contactless from the electromagnetic field, which offers all advantages of radiative heating applications. The heat transfer to the matrix is based on conduction since matrix and susceptor strive for forming a temperature balance.

2.4.1 Induction Heating

2.4.1.1 Inductive Heating Theory

The electromagnetic induction is based on Lenz's law and the principles found by Michael Faraday [63]. The heating phenomena of ferromagnetic and conductive materials, which appear when these materials are exposed to an alternating electromagnetic field, are based on eddy currents and magnetic polarization effects. The latter is referred to as hysteresis heating or the magnetic hysteresis loss in literature. The mathematical description of both phenomena is included in the basic equations, which originate from the work of Maxwell [64].

Eddy currents are formed within a closed electric circuit in a conductive material through either an alternating electromagnetic field or the alternating movement of an electric conductor in a static magnetic field. According to Lenz's law, each induced current forms an electromagnetic field which counteracts the causative, exterior field. The continuous pole reversal of induced currents and fields results in the emergence of thermal energy due to the Joule effect [65]. The heating behavior during the exposition of a closed electric circuit to an alternating magnetic field is common for all electrically conductive materials [63,65].

The magnetic hysteresis loss is based on the polarization and depolarization of ferromagnetic and ferrimagnetic materials, when they are exposed to an electromagnetic field. In contrast to the eddy current heating, the alternating magnetic dipoles within the material lead to frictional heat [66]. The form of the

corresponding curve of the magnet flux density *B* as a function of the magnetic field strength *H* follows a hysteresis curve (Figure 2.7).

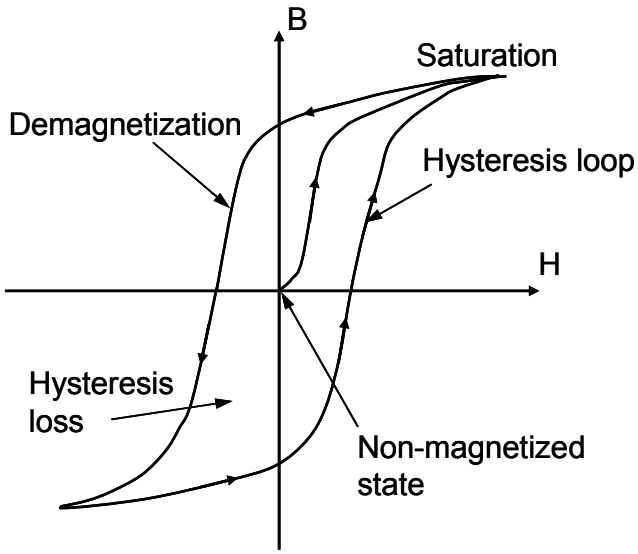

Figure 2.7: Hysteresis curve of a ferromagnetic material (based on [63])

The hysteresis loss energy P_H within a magnetic volumetric element d*V* can be generally described as function of *B* and *H* (2.1). The enclosed area of the respective hysteresis curve quantifies the energy derived from the hysteresis loss within a time step [67].

$$dP_H = dV \oint B dH \tag{2.1}$$

Consequently, the larger the enclosed area of the hysteresis curve, the larger is the induced thermal energy [65].

A simplified expression of the hysteresis loss (2.3) can be derived from the relation between *B* and *H* through the magnetic permeability μ. This approach also respects the influence of the frequency *f* (2.3) [68].

$$B = \mu H \tag{2.2}$$

$$P_H = V \cdot f \cdot \int_0^H B_{(H)} dH = V \cdot f \cdot \frac{\mu \cdot H^2}{2} \tag{2.3}$$

The magnetic hysteresis heat loss is much lower than through eddy currents [69]. Nevertheless, the hysteresis loss is regarded as the dominant mechanism for

inductive particle heating in general since macroscopic electrically conductive circuits are not formed in particle doped materials [70].

One main effect accompanying inductive heating, is the skin effect. The skin effect describes the limitation of the penetration depth of the causative electromagnetic field into the heated conductive or magnetic material. The observable limitation is caused by the formation of induced counteracting magnetic fields. This behavior implies that the main energy input in a homogeneous magnetic or conductive sample lies in or close to the surface. Since the skin effect is dependent on the induced currents and the accompanied electromagnetic fields, the penetration depth δ_P is related to the frequency *f* of the causative field, the electrical resistivity ρ_e, and the magnetic permeability μ_r of the absorbing material [69].

$$\delta_P = 503\sqrt{\frac{\rho_e}{\mu_r f}} \tag{2.4}$$

As indicated by this equation, the higher the frequency, the lower is the penetration depth. Concluding from this, a homogeneous heating of material bulks is better realized at lower frequencies. Typical induction applications use frequencies between several kilohertz up to the megahertz range.

2.4.1.2 Induction Heating Applications in the Composite Industry

Induction heating applications in the composite industry include melting and welding processes of thermoplastics as well as the curing of thermoset matrix systems.

Induction welding techniques cover the welding of composite-composite joints as well as hybrid metal-composite joints. Since polymer matrix materials are generally not affected by an electromagnetic field, the heat is brought into the composite either by the use of electrically conductive reinforcements like carbon fiber fabrics, or by additional welding susceptors, like metal fabrics and grids [25,57,66,71,72,73]. These additives provide closed electric circuit structures and, therefore, eddy current heating is the dominant heating mechanism, whereas the hysteresis heating is negligible. This domination of eddy currents results in relatively high process speeds. Since ferromagnetic particles only rely on the slower hysteresis heating, they are only used for exceptional welding cases. For heating the surrounding matrix, the

susceptor material is at best case placed directly in the joint zone. When reaching the melted state, the joint partners are pressed against each other to achieve the welded joint. The used frequency of the applied magnetic field lies often in the range of 200 to 1000 kHz [25,57]. For the quality of the joint, important welding parameters include joint pressure, weld speed, coupling distance, as well as the geometry of the weld zone. Since the weld zone needs to be heated homogeneously and consequently requires a homogenous magnetic field originating from an electrically driven coil, the coil design is an important variable, too [57].

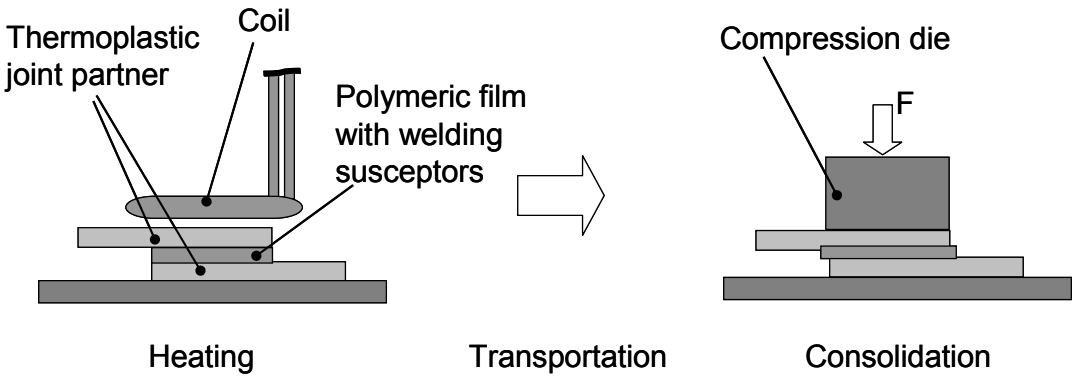

Figure 2.8: Exemplary process chain of semi-continuous induction welding

In case of welding hybrid metal-polymer structures, the metallic joint partner can also serve as a main susceptor material [74,75].

2.4.2 Infrared Heating

Infrared (IR) radiation is a state-of-the-art heating technology for plastics processing. Each material absorbs infrared radiation in a distinct wave length region which corresponds to the respective molecular vibration. The method is based on electromagnetic radiation and therefore works contactless without the need of a medium. In general, infrared heating is dependent on the temperature of the radiating body, the relative position between emitter and receiver, the surface roughness of the heated material, chemical properties, and color [76,77]. For polymeric materials, the carbon-hydrogen bond is mainly responsible for the good absorption at wave lengths between 3.2 and 3.5 µm. Depending on the material, other spectra fractions are reflected; others interpenetrate the component. Only the absorbed spectrum is transferred into heat [77].

As IR sources, a large variety of radiators with different spectra and power levels is available on the market. The variety range covers the wave lengths up to 10 µm from short-wave halogen infrared bulbs (0.76 - 2 µm) to carbonous and ceramic dark radiators (4 - 10 µm) [78].

Thin materials are transparent to short-wave radiation and are consequently heated less than with long-wave IR radiation. In contrast, massive materials are more homogeneously heated by the use of short-wave IR radiators since the absorption at this wave-length is less and leads to a good material penetration. When using medium-wave and long-wave radiators, the main energy is absorbed surface-near, which therefore leads to a higher temperature at the surface.

2.4.3 Application of Heating Susceptors for Contactless Heating

Particulate susceptors as heating sources work with a broad range of electromagnetic frequencies, covering the whole range from infrared to induction and microwave applications. In combination with polymeric materials, only a few applications are known for the particle based induction heating.

The domination of magnetic properties within particle induction heating provides the option to use the loss of these properties for a self-controlling process. The for magnetic materials common Curie temperature T_{Cu} marks the range at which a distinct material loses its magnetic properties. This effect immediately stops an induction heating process and can be used as a limitation of the maximum reachable temperature. In the melting range of thermoplastic materials only a few commonly available materials possess a Curie temperature, one of them nickel (T_{Cu} = 358 °C) which could work with high performance thermoplastics like polyetheretherketone (PEEK, T_m = 345 °C) and polyphenylene sulfide (PPS, T_m = 285 °C). This lack of more commonly available particles has driven research groups to tailor ferromagnetic particles with improved heating abilities [79,80,93].

Table 2.3: Curie temperature of magnetic materials (selection) [81,82]

Material	Industrial availability as particle	Curie temperature [°C]
Goethite	None/rare	120
Lepidocrocite	None/rare	196
Ilmenite	Frequently	233
Nickel	Common	358
Magnetite	Common	575
Hematite	Common	680
Iron	Common	768
Cobalt	Frequently	1121

For the realization of a welding process based on inductive means, Suwanwatana et al. have developed a polysulfone (PSU) material system containing nickel particles [83,84]. The Curie temperature of nickel (358 °C) lies in the range of the process temperature of polysulfone around 320 °C which realizes a self-controlled process. The particle loading was chosen between 10 and 20 vol-% (respective 44 and 64 wt-%) with varying particle sizes in the nano and micro range. The best heating results using an alternating current (AC) magnetic field with 2.25 MHz were obtained from the smallest particles applied in the study (79 nm). The time to reach the process temperature took in this case 80 seconds. The resulting bond strengths for PSU/nickel welded joints were lying in the range of 18 MPa which was 20 % less than neat PSU reference samples manufactured in the autoclave [84].

Mohr et al. used inductively heated magnetite particles for triggering a shape-memory effect in thermoplastic polymers [85]. The nano-sized magnetite particles which were activated at a frequency of 258 kHz substitute an extrinsic heating and were applied in a weight fraction of 5 to 10 wt-%. For the shaping, a temperature of maximum 88 °C was sufficient and resulted in an almost instant deformation effect of the sample after two seconds.

Besides the melting and the reshaping of thermoplastics, several applications and patents also cover the curing of thermosets by reaction activation via particle heating [86,87].

Furthermore, particle based induction heating has recently gained in importance by the development of a novel technique to destroy human cancer cells. A so-called artificial hyperthermia is triggered either by a cloth containing inductive heatable

particles placed on a cancerous cell or by magnetic nano particles being directly injected into the cell body (magnetic fluid hyperthermia) [22,23]. An alternating electromagnetic field heats the magnetic particles whereby the cancer cell is destroyed thermally. Mainly ferrous particles like magnetite and maghemite in various sizes are used as susceptors for induction based hyperthermia. The frequency of the magnetic field in these applications usually lies in the range of 50 to 500 kHz. [22,23,24,88,89,90,91,92,93,94].

For optimizing the hyperthermia effect, Hergt et al. investigated the influence of particle size and magnetic field strength on heating effects regarding magnetite nanoparticles. A general correlation between particle size and heating effect could not be found. Each material and particle size exhibited a different heating behavior which is also influenced by the magnetic field [24]. This conclusion fits to the results which have been published in relation to polymer heating applications before [83,84,85].

2.4.4 Conduction Heating Techniques

Thermal conduction is an important mechanism for heating materials in many different processes [58,59,95]. This includes also semi-finished polymer materials, as for example, the preheating of textile piles in an oven or the through heating of bulky components in a heated mold.

Furthermore, thermal conduction is important in common thermoplastic welding processes, like heated tool welding, heated wedge welding, and impulse sealing [60,96]. The techniques are characterized by heating the joint zone from the component’s surface to the center by means of a hot tool. Since a medium temperature between hot tool and component is formed which is dependent on the thermal conductivity and the heat transfer coefficient between the engaged materials, the process is time-intensive. A higher tool temperature is consequently applied to increase process speeds. In this case, the danger of thermal material degradation has to be regarded and discussed.

In compression molding processes, the use of a heated tool, either for thermoplastic or for thermoset applications, is common. A hot tool is used for thermosets to initiate

curing, whereas for thermoplastics the material is heated first and has to be cooled down below the respective melting temperature in order to consolidate the component. With commonly used technologies, these heating processes are very time-intensive since a high energy has to be transferred until the large molds are completely heated or cooled, respectively. Recently, novel fast heating and cooling systems for large molds have been developed which are based on a conduction heating approach. The fast performance is either realized by a complete exchange of the heating and cooling fluid which is in contact with a relatively thin mold surface or by the use of an aligned inductive field. In either way, the benefit is that only a small mold volume is effectively heated so that the hot mold does not prevent a quick cooling, due to its heat capacity.

The main target of the Quickstep system is to substitute conventional autoclave processes. The Quickstep process uses a so-called heat transfer fluid which flows around a mold. The mold is floating in the fluid but segregated from it. By exchanging the complete fluid, high heating and cooling rates are achieved [97].

The systems developed by RocTool® operate on two different approaches. The Cage System® uses a coil cage which is arranged around a mold. The mold itself consists of two layers: a carrier frame made of stainless steel and permeable for electromagnetic radiation, and the mold which forms the contour of the part and can be activated by the electromagnetic field, since the mold is made of construction steel. A generator drives the inductor cage, and the resulting electromagnetic field induces a current mainly in the mold surface where the magnetic field is dimensioned to reach its highest degree of efficiency there. Since mainly the surface is heated, heating rates up to 200 K/min are possible. Furthermore, the surface cooling with an air-water mixture reaches levels around 150 K/min for the latter reason, too. The Cage System® is very effective with resin transfer molding and injection molding processes [98,99].

Another RocTool® technology, namely 3iTech®, has been especially developed for compression molding shear edge tools. Here, the induction coils are embedded in the mold structure, although being electrically isolated. The heat is also generated by inductive means. The measurable temperature rise is not affected by a direct heating

of the surface, but by indirect heating of the inner tool. This technique allows the same heating and cooling rates as the Cage System®, but with a short delayed response caused by the heat conduction through the inner tool to the surface. This technique is safer for compression molding since an electric short-cut by the tool shear edges is impossible [98].

2.5 Composite Compression Molding

Low material costs combined with high dimension accuracy at a high degree of automation and reproducibility offer excellent possibilities for mass production by compression molding. In contrast to these advantages, the restricted design complexity and the high initial costs for equipment have to be mentioned. Compression molding techniques are a standard way of automated manufacturing plastic components including applications in the electric, automotive and transportation, construction, as well as sports and leisure sectors.

Thermoplastic molding applications include the processing of long fiber reinforced thermoplastics (LFT) and glass mat reinforced thermoplastic materials (GMT) as well as the thermoforming of organic sheets and films. Thermoset materials are mainly processed as sheet molding compounds (SMC) or bulk molding compounds (BMC).

Processing methods have been developed for thermoset as well as thermoplastic semi-finished materials. The components' sizes vary from small-scale like door handle bars up to large parts like front ends for automotives and trucks [100,101,102].

LFT processes are based on the use of polymer pellets which are preliminarily melted by an extruder. The heat is transferred to the LFT by shear forces between pellets and screw. The reinforcing fibers are either distributed within the pellets or added directly within the extruding step. The latter is referred to as direct processing of LFT (D-LFT) which has recently been also developed to endless LFT (E-LFT) applications [103,104,105,106]. Since the manufacturing of low-cost components demand also low-cost materials, the most common reinforcement is made of glass fibers with a standard fiber length between 7 and 25 mm. Fiber volume fractions usually vary between 20 and 40 vol-%. The most common matrix material is

polypropylene - for high temperature applications, polyamides as well as polyesters are used [100]. Since the LFT dough is hot when brought into press, the mold needs to be cooled to 60 – 80 °C in order to solidify the molten material during the flow process in the mold. To prevent a melt flow-out, the use of shear edge molds is widely spread [100].

A convection oven or an infrared radiator unit is needed for the processing of GMT sheets which usually consist of pre-impregnated needled non-crimp glass fiber mats. Advanced GMT can also contain unidirectional fabrics [104]. The processing by flowing to fill the cavity is similar to LFT. In comparison to LFT, GMT provides a lower freedom of design since its viscosity and flowability is limited by its dense reinforcement [101].

In thermoforming processes semi-finished pre-consolidated fabric sheets (organic sheets) are reheated and molded. In contrast to LFT and GMT, the compressed material does not flow but forms the component shape due to a draping of the reinforcing structure. Hence, the sheets are usually clamped for transportation ease and to preserve the reinforcements' integrity. The use of an open mold without shear edges is standard in this case [100,101].

Thermoset SMC and BMC materials are usually based on unsaturated polyester resins. Besides the matrix, SMC and BMC contain various fillers – they either thicken the compound or deliver specific properties as, for example, pigments for color or fibers for mechanical improvement. Recently, also recycled materials are incorporated in order to improve the sustainability degree of these compounds [107,108]. The press molds for SMC are usually temperated at approx. 150 °C. The contact with the hot surface initializes the curing process and leads temporarily to a lower viscosity of the material [109]. The reduction of viscosity enables the material for flow processes within the cavity. SMC is widely used for automotive and electric applications. BMC usually possesses shorter fibers than SMC, which make the compound adaptable for injection molding purposes and allow a higher design freedom. Shorter fibers, however, give BMC also a lower mechanical profile [100].

3 Materials and Methods

3.1 Materials

3.1.1 Polymers and Polymer-Polymer Systems

For investigating the selective induction heating by particles, polymer-polymer composites were chosen within this work according to several different aspects. To preserve the status of being easily recyclable, the thermoplastic polymer-polymer composites had to originate from the same polymer family which implied that the chemical nature was similar among matrix and reinforcement. For a greater process safety in terms of not melting the polymer reinforcement during a reheating of the semi-finished material, polymer-polymer systems were also selected according to their melting temperature difference between reinforcement and matrix. A reasonable combination consisted of a low-melting polymer matrix and a high-melting reinforcement. In this way, the matrix melted before the reinforcement did. Additionally, the mechanical performance of the reinforcement, in this case the tensile strength, should be higher than the matrix performance. Otherwise, the composite would lose its main strength during melting of the matrix. Figure 3.1 exemplarily points out possible combinations within different polymer families. Suitable matrixes are found in a bottom-left direction from the chosen reinforcement polymer, which should be of high mechanical performance. Following this rule, sensible combinations can be found within the polyolefins, the polyesters, and the polyamides.

The applicability of particle induction at low as well as high matrix melting temperature was investigated with two SRP systems of different melting temperature regions, namely a low-melting self-reinforced polyolefin (srPO) and a high-melting self-reinforced polyamide (srPA) system. These two compounds not only covered different melting temperatures but also different tensile strength levels and therefore allowed insight on the impact of inductively heated particles on mechanical properties in two completely different systems.

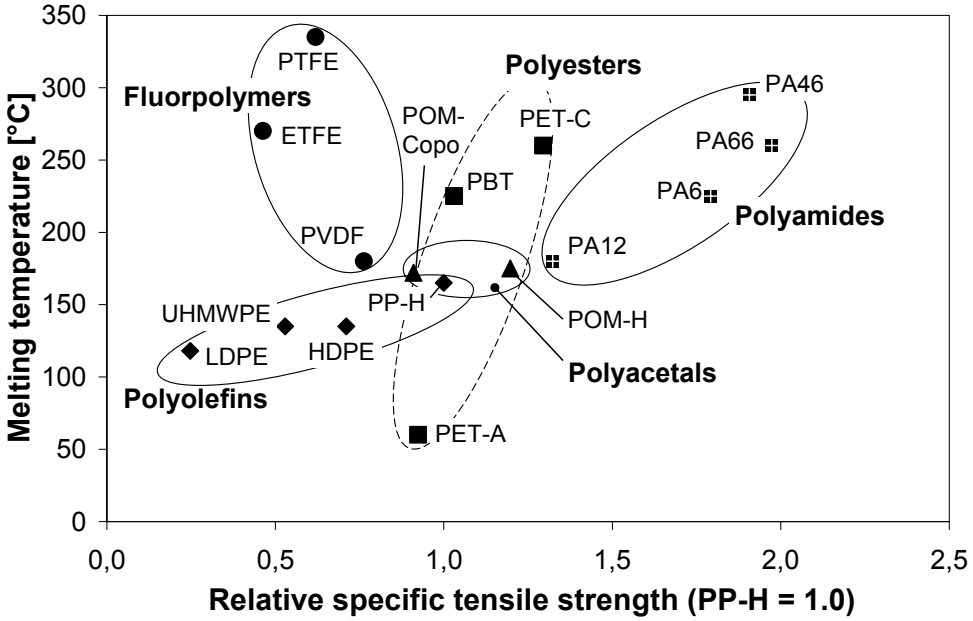

Figure 3.1: Polymers and their respective melting temperature within a polymer family (selection)

For the realization of a self-reinforced polyolefin composite, a high density polyethylene (HDPE) matrix was the desired option to be used with a polypropylene (PP) reinforcement. Although LDPE would offer a larger melting temperature difference in respect to PP, HDPE was chosen for its higher mechanical properties.

For a polyamide SRP, a polyamide 6 (PA6) matrix was suitable in combination with polyamide 46 (PA46) or polyamide 66 (PA66) reinforcement. Again, the higher mechanical performance of PA6 outnumbered PA12 as the desired matrix.

To reduce the time and effort for the basic induction heating experiments with particles, the matrix thermoplastics were used without reinforcement. The most important properties of the matrix materials are listed in Table 3.1. In the basic heating experiments, the results obtained from HDPE served for a parameter adaption to a polymer-polymer composite. The results of the doped polyamide matrix demonstrated the applicability of particle induction with high temperature melting matrixes.

Table 3.1: Properties of investigated matrixes for particle induction [110,111]

Property	Standard	HDPE	PA6
Polymer family	-	Polyolefins	Polyamides
Type	-	Rigidex HD6070EA	Akulon K222 D
Matrix manufacturer	-	Ineos Polyolefins	DSM
Melting temperature [°C]	-	135	220
Density [g/cm³]	ISO 1183	0.96	1.13
Tensile modulus [GPa]	ISO 527-2	1.5	3.8
Tensile stress (Yield) [MPa]	ISO 527-2	31	95
Strain (Yield) [%]	ISO 527-2	Not given	3.5
Charpy impact strength, 23 °C [kJ/m²]	ISO 179/1eA	4	8.0

The work with polymer-polymer composites was focused on a self-reinforced polyolefin system consisting of HDPE which was equipped with 50 wt-% polypropylene fibers.

In addition to the self-reinforced polyolefin, a polypropylene matrix was obtained for a model system in combination with polyethylene terephthalate (PET) fibers. The PP/PET model system provided a significant temperature gap between matrix and reinforcement of more than 85 °C. Thus, the induction heating process did not require an exact control to avoid fiber melting. This facilitated the material handling and the experimental effort in feasibility studies. The provided fiber weight fraction lay between 30 and 33 wt-%.

Self-reinforced semi-finished materials were obtained as pilot plant material from Celstran GmbH, Germany, and Fibroline France SARL, France.

The Celstran material was provided in form of reinforced tapes manufactured by hot melt impregnation which is similar to a pultrusion process. The fiber content was set to 30 wt-%. Celstran manufactured the used PP/PET model system with different susceptor materials and filler degrees. In contrast, Fibroline provided self-reinforced sheets from polyolefins (HDPE/PP) as well as the model system with a standard fiber

fraction of 50 wt-%. Fibroline used a powder impregnation process for the manufacturing of these fabrics (Figure 3.2).

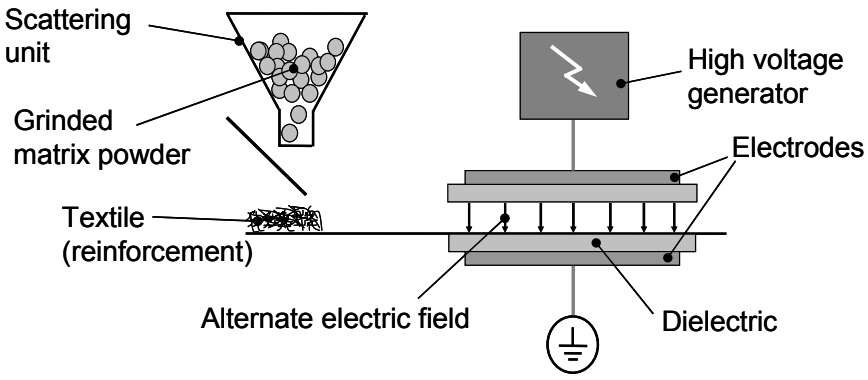

Figure 3.2: Electrically assisted powder impregnation process for textiles by Fibroline France SARL (based on [112])

The Fibroline process began with a dispersion of matrix powder on the surface of a textile. In this study, the textile consisted of non-impregnated randomly distributed polypropylene fibers. The powder coated textile was then transported into a high voltage electric field, which polarized the matrix particles. A continuous pole reversal led to a polarization of matrix particles which penetrated into the textile. For this process, no additional fillers in the matrix powder were needed [112]. Succeedingly, the textile surface layer was heated above the matrix melting temperature for sealing and therefore avoiding a separation of matrix and textile.

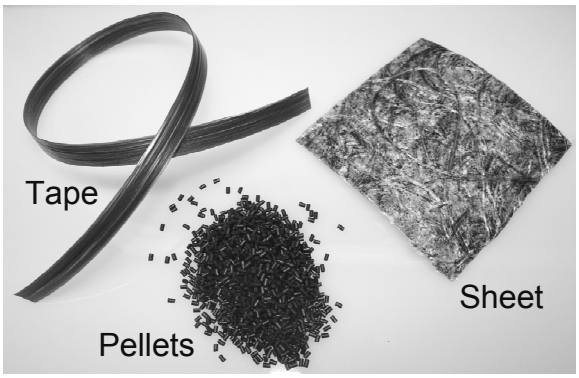

Figure 3.3: Inductively heatable semi-finished materials

Each used polymer-polymer system has been equipped with a particle doped polymer matrix to realize induction heating.

Table 3.2: Investigated polymer-polymer systems [27,110,111,113]

Property	HDPE/PP	PP/PET
Matrix polymer	Rigidex HD6070EA	Moplen HP500V
Matrix manufacturer	Ineos Polyolefins	Basell
Matrix melting temperature [°C]	135	163
Fiber type	Standard PP fiber	Standard PET fiber
Reinforcement manufacturer	Polisilk S.A.	Performance Fibers, Inc.
Reinforcement melting temperature [°C]	167	250
Reinforcement fraction [wt-%]	50	30-33
Nominal melting temperature gap ΔT_m [K]	30	87

3.1.2 Susceptors

Sufficient heating results were expected from ferromagnetic susceptors, like the used commercially available cast iron particles (iron fraction up to 94 wt-%, density 7.2 g/cm³), magnetite (iron oxide fraction more than 95 wt-%, density 4.9 - 5.5 g/cm³), and nickel (purity 99 %, density 8.9 g/cm³). These particles provided both, electrical and magnetic properties. Materials which offered only electrical properties have been carbon black (CB) and multi-wall carbon nano tubes (CNT). The latter did not meet the demand of being a low-cost additive, but were selected for their high impact on electric conductivity in composite materials [114]. Special particles with extraordinary properties, like piezoelectric lead zirconate titanate (PZT) and ilmenite, have been tested as well. Ilmenite was chosen due to its contents of ferromagnetic hematite (Fe_2O_3) and its low Curie temperature (see Table 2.3).

General properties of the used particles have been described by their respective manufacturers [115,116,117,118,119,120,121]. Important properties are listed in Table 3.3.

Table 3.3: Properties of susceptors applied in this study

Name	Brand Name	Manufacturer	Shape	Average Size / Composition
Carbon black	Raven® L Ultra	Columbian Chemicals Company	Spherical	30 nm
Carbon nano tubes (CNT)	NC 7000	Nanocyl S.A.	Multi-wall tube	9.5 nm (diameter), 1.5 µm (length)
Cast iron	FG 0000/0300	Gotthart Maier Metallpulver GmbH	Spherical, irregular	Max. 300 µm, see Table 3.4
Ilmenite	Type 90 W Type AU, SG	Mineralmühle Leun, Rau GmbH & Co. KG	Irregular	90 W: 75 – 250 µm AU, SG: 63 – 315 µm
Magnetite	FO 0000/0090/HA	Gotthart Maier Metallpulver GmbH	Irregular	Max. 100 µm, see Table 3.4
Nickel	0333/1/1	TLS Technik GmbH & Co Spezialpulver KG	Spherical	Max. 250 µm, see Table 3.4
Lead zirconate titanate (PZT)	PCM 55	Noliac Ceramics s.r.o.	Irregular	3 µm

The ferromagnetic particles have been used in various sizes to investigate the influence of particle size on heating behavior. Therefore, a vibratory sieve shaker (Fritsch Analysette 3 Pro) was applied for the analysis of approx. 250 g per sieve process. The sieving was repeated three times with different samples. The determined grain size distributions of the ferromagnetic particles at initial state are given in Table 3.4.

Table 3.4: Medium grain size distribution of ferromagnetic susceptors

Grain size [µm]	Cast iron	Magnetite	Nickel
< 24	3.0 ± 0.2 %	7.3 ± 1.6 %	13.1 ± 1.9 %
25 – 62	7.5 ± 0.2 %	25.0 ± 4.5 %	43.2 ± 1.0 %
63 – 124	14.0 ± 0.2 %	67.6 ± 3.1 %	23.1 ± 1.0 %
125 – 249	54.1 ± 0.3 %	0.1 ± 0.1 %	16.0 ± 2.0 %
250 – 300	21.4 ± 0.7 %	0.0 %	4.6 ± 1.2 %

The resulting particle size fractions were separated for the investigation of particle influence on heating abilities in polymer matrixes.

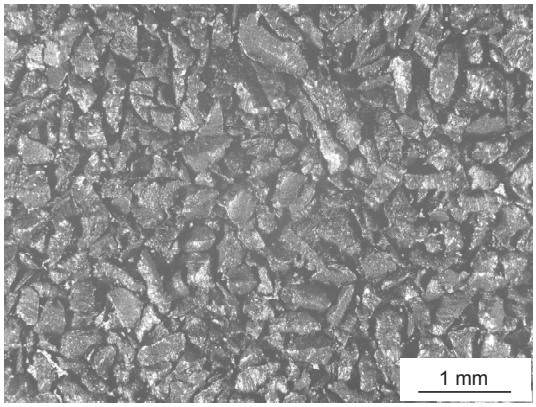

Figure 3.4: Cast iron powder in delivery state (grain size 0 - 300 µm)

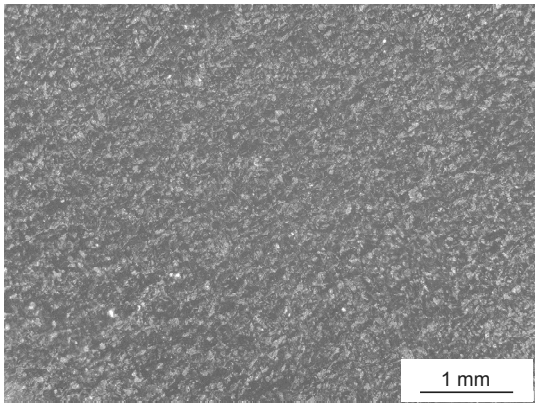

Figure 3.5: Sieved cast iron powder (fraction 24 - 62 µm)

The susceptor quantity is given in the experimental results as weight percentage (wt-%) of the entire composite (matrix and fibers).

3.2 Induction Heating Experiments

For the basic induction heating experiments, particle doped matrix thermoplastics without reinforcement were used.

Plates with the dimensions of 120 x 120 x 2 mm³ were manufactured from pellets of each compound by the application of a laboratory hot press. The press cycle was chosen accordingly to the demands of the polymers: a previously weighted amount of pellets was arranged in an aluminum frame mold and placed into the pre-heated press (200 °C for HDPE and PP matrixes, 260 °C for PA6). During the two minutes lasting melting, a constant force of 10 kN was applied, equal to approx. 0.7 MPa for the given area. The press was cooled with a cooling rate of 10 K/min to 100 °C for removing the mold. The manufactured plates were mechanically cut into four parts with the dimensions of 60 x 60 x 2 mm³.

To guarantee the comparability between pellet and fabric-like specimens, the fabrics were previous to the experiments consolidated by a manual hot press. For reasons of reinforcement protection, the maximum temperature was varied in comparison to the specimen preparation with pellets. The processing temperature did not exceed 155 °C for HDPE and 180 °C for PP matrixes, respectively. A constant force of 30 kN (~2 MPa) was applied during the whole compression molding procedure.

The compression molded plates were exposed to a magnetic field with a medium frequency of 450 kHz provided by a Hüttinger TruHeat 5010 MF generator (Trumpf Hüttinger, Germany). A high frequency generator (Trumpf Hüttinger IG 10/2000) was used to examine the material at a frequency of 2500 kHz. At both generators, a five-turn flat spiral coil (pancake shape) with a diameter of 100 mm and an internal water cooling to reduce a self-heating of the coil was applied (Figure 3.6).

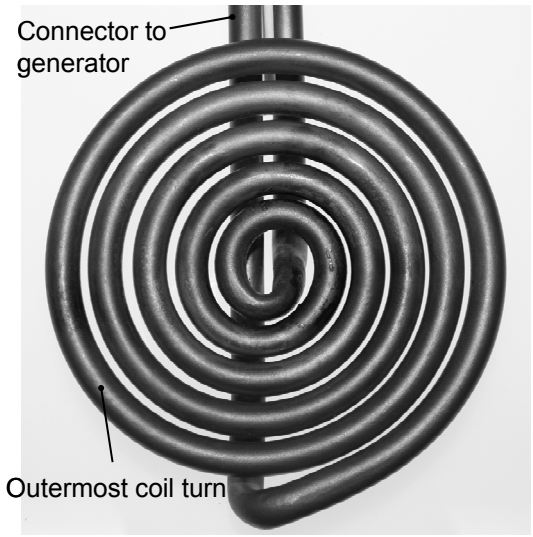

Figure 3.6: Applied five-turn spiral coil with a diameter of 100 mm

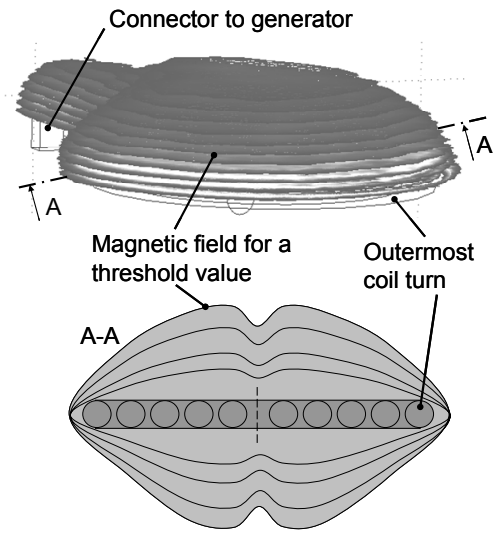

Figure 3.7: Simulation of the upper magnetic field distribution of the used spiral coil for an exemplary threshold value – the field follows a dome shape

The magnetic field distribution for a spiral coil has been previously described by independent researchers by a model based on the Biot-Savart Law [83,84,122,123]. The shape of the magnetic field distribution follows a dome with the highest magnetic field strength located close to the center of the coil. Figure 3.7 illustrates a finite element simulation (Comsol Multiphysics 3.5a) of the magnetic field density for the used five-turn coil at an exemplary magnetic field strength threshold. The density close to the coil is higher and increases from the edge towards the center. The achieved results correspond to the magnetic field distribution described in literature.

In accordance with the magnetic field distribution, the center of the sample was aligned with the center of the coil in standard experiments. The generator power was set to a maximum, which resulted in a nominal current of 280 A in the coil [124]. The distance between specimen and inductor was kept constantly at 2 mm. As spacers,

non-conductive wooden bars were applied. During the three-to-five-minutes-lasting experiment, the temperature of the sample was obtained by a fiber-optical temperature sensor at two points on the opposite side of the coil: close to the center position and in a distance of 10 mm from the edge of the sample. In order to guarantee an intimate contact between temperature sensors and the sample surface, the sensors were fixed with high temperature resistant adhesive tape (Kapton® polyimide film) and additionally clamped by another wooden bar.

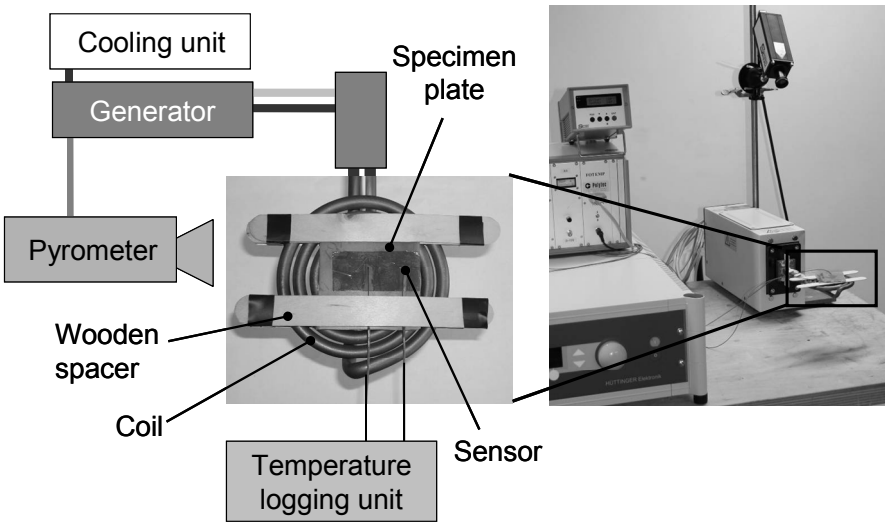

Figure 3.8: Experimental setup for the induction heating tests

3.3 Material Characterization

3.3.1 Mechanical Characterization

3.3.1.1 Tensile Tests

For standard mechanical tensile tests performed with a Zwick Roell 1474 universal testing machine (Zwick Roell, Germany), doped pellets were injection molded into tensile bars according to DIN EN ISO 527-2, sample type 1BA [125]. For each material, a minimum of 8 specimens were examined at a test speed of 5 mm/min. The elastic modulus was obtained within a range up to 1 % strain by a macro extensometer. A 10 kN load cell was applied for the measurement of the maximum force.

The high maximum strain of HDPE up to more than 400 % exceeded the maximum test range of the machine and did not allow a reasonable testing (Figure 3.9). Consequently, the experiment was terminated when a maximum displacement of 25 mm was reached in which all samples revealed their maximum tensile strength and ductile samples could be well distinguished from brittle samples.

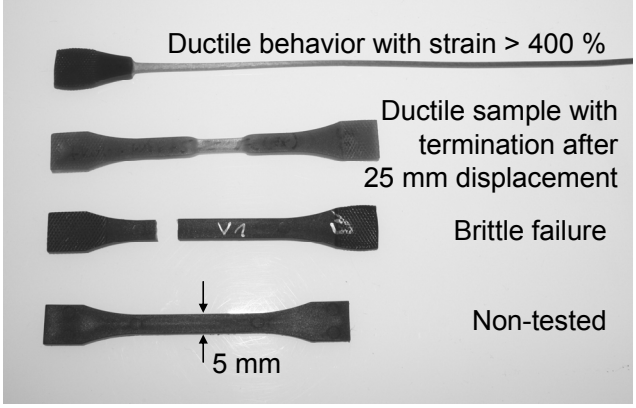

Figure 3.9: Observed failure patterns during tensile testing

The dimensions of each sample were measured separately, and a correcting shape factor was employed to calculate the true cross section of each sample. The factor was previously determined to 0.926 for HDPE and 0.968 for PA6.

3.3.1.2 Charpy Notched Impact Tests

Since polymer-polymer composites are known for their high impact properties, Charpy impact tests were performed. They served to reveal whether the used susceptors negatively influenced the impact behavior of the matrix, and should prove the impact performance of inductively heated reinforced composites.

For the investigation of susceptor influence, notched bars of sample type 1eA were manufactured according to DIN EN ISO 179 by a Babyplast injection molding machine (Christmann Kunststofftechnik GmbH) from particle doped matrix polymers [126]. The Charpy pendulum was equipped with a 4 J hammer for non-reinforced and with a 15 J hammer for self-reinforced samples. Each experimental series consisted of the testing of ten samples. The notch impact strength a_{cN} was calculated from the measured impact energy (W_I), the loss energy (W_L), the sample cross section ($a \cdot b$), and a correcting shape factor f_s for injection molded samples (HDPE: 0.926, PA6: 0.968).

$$a_{cN} = (W_I - W_L)\cdot(a\cdot b\cdot f_s)^{-1}\cdot 10^3\ \text{kJ/m}^2 \quad (3.1)$$

Charpy tests were conducted with particle doped matrix systems to investigate the impact of the fillers on matrix ductility. Additionally, the polymer-polymer materials were tested to investigate the effect of the polymeric reinforcement.

3.3.1.3 Dart Impact Tests

Besides the Charpy impact experiments, the impact performance of SRP was tested with a dart impact test rig. The results demonstrated the performance of particle doped compression molded polymer-polymer sheets. For this purpose, the within this study investigated material was compared to industrially available composites like self-reinforced PP, Curv®, and glass fiber reinforced polymers (GFRP) on PP basis, TwinTex®.

The tests were conducted on a drop tower with a maximal drop height of 15 m.

Table 3.5: Compared sheet materials in dart impact tests

Material	Manufacturer	Matrix	Reinforcement	Density [g/cm³]
Curv®	Propex Inc.	PP	PP	0.93
HDPE/PP	Fibroline	HDPE	50 % PP	1.07
TwinTex®	Owens Corning	PP	60 % GF	1.50

The composites were tested in sheet-like shape with the dimensions of 80 x 80 mm² at various thicknesses from 3.0 mm to 4.6 mm. A cylindrical impactor with a diameter of 20 mm was applied on the sledge with a total weight of 65.05 kg. At a height of 1.07 m, this weight results in an impact velocity of 4.4 m/s and equals to a maximum impact energy of 100 J which conforms with the parameters given by the standard DIN EN ISO 6603-2 [127]. The maximum force, the energy at maximum force W_{max} and the energy after 25 mm from impactor contact, W_{25}, were evaluated by a 60 kN load cell. Additionally, a specific value $W_{max,s}$, which considered the density ρ, was calculated to demonstrate the advantage of polymer-polymer composites in respect to glass fiber reinforced materials.

$$W_{max,s} = \frac{W_{max}}{\rho} \quad (3.2)$$

3.3.2 Differential Scanning Calorimetry (DSC)

DSC experiments were used for the investigation of susceptor influence on crystallinity and melting temperature within doped matrix systems as well as for the analysis of thermal degradation due to the occurrence of hot spots around susceptors in neat and polymer reinforced matrixes. Changes of thermal properties were especially expected due to thermal degradation, whereas the susceptor presence was not regarded to significantly influence matrix properties.

A standard differential scanning calorimetry device Mettler Toledo DSC 821 served for the investigation of the degree of crystallinity and melting temperature of polymer compounds before and after heating. The samples had a weight of approx. 10 mg. The DSC experiments were conducted in nitrogen atmosphere to prevent material oxidation. The time-temperature program consisted of two cycles; each cycle was characterized by a temperature increase and a cooling step. Only the second cycle of each program was finally analyzed since the first cycle served to quasi-eliminate the thermal history of the samples, especially dissimilar cooling rates [46]. In accordance with the proceeding described in standard DIN 53765, the experiment was repeated with two different samples for each material [128,129]. The most important parameters of the DSC experiments are summarized in Table 3.6.

Table 3.6: Parameters for DSC measurements

Polymer	Max. temperature [°C]	Heating rate [K/min]	Cooling rate [K/min]	Comments
HDPE	200	10	10	Nitrogen 30 ml/min
PA6	260	10	10	Nitrogen 30 ml/min

The degree of crystallinity was calculated for particle doped matrixes according to equation (3.3).

$$X_c = \frac{\Delta H_m}{\Delta H_m^0 (1 - w_s)} \tag{3.3}$$

The specific melting heat of the sample ΔH_m was recorded by the DSC, whereas ΔH_m^0 is the theoretical specific latent heat of a 100 % crystalline polymer. For ΔH_m^0,

293 J/g was used for HDPE and 190 J/g for PA6. The susceptor weight fraction is given by w_s.

3.3.3 Water Immersion Experiments (Corrosion Tests)

Suwanwatana et. al. reported a decreased induction heating ability of corroded nickel particles due to the emergence of an oxide layer [130]. Since ferromagnetic particles, especially cast iron, were used in this study, an investigation of the corrosion influence was considered as mandatory.

Tensile bars as well as sheet specimens were aged by a complete immersion in artificial sea water according to standard DIN 50905-4 [131]. To remove contaminants, the samples were cleaned with isopropanol prior to aging. The immersion duration was chosen to one week and four weeks, respectively. After aging, the samples were cleaned with demineralized water to remove the sea water, and they were dried in a convection oven for 2.5 h at 70 °C for reaching a conditioned state before the mechanical tests. The aged samples were tested on their tensile properties and their heating abilities according to the procedures described before. Besides non-immersed specimens, also samples which have been tested in demineralized water were applied as references in these tests.

3.3.4 Electric Conductivity

The investigation of the electric conductivity served to decide whether a particle heating effect can be traced to an overall closed electric circuit. For the tests, bulks (20 x 10 x 4 mm³) were prepared from injection molded bars. Smaller samples (20 x 10 x 2 mm³) were obtained from compression molded plates. The front and rear faces were grinded and coated with silver conductive paint (G 3692, Plano GmbH). The conductivity was recorded from a four-point resistivity test, according to DIN EN ISO 3915 with a series of five samples per material [132].

3.3.5 Microscopy

Light microscopy as well as scanning electron microscopy (SEM) images served for the investigation of susceptor distribution and fiber analysis. The samples were either

embedded in an epoxy resin and polished, or directly observed after a cryo-fracture in liquid nitrogen. The light microscopy images were obtained from a reflected light microscope (Leitz Group, Germany) providing magnifications up to 500 x. The samples for the SEM (Zeiss Supra 40, Germany, and Jeol JSM 6300, Japan) had to be coated with a conductive platinum-gold layer with a sputtering device (Oerlikon Balzers, Liechtenstein).

Moreover, a computed micro tomography system (nanotom by Phoenix x-ray systems + services GmbH, Germany) provided three-dimensional insights of particle distributions and composite structures.

3.4 Compression Molding and Thermoforming Applying Different Heating Techniques

As competing heating techniques, standard processes for compression molding and thermoforming were considered which included infrared, conduction, and convection heating. All competing processes were not subject to optimization, but were regarded as feasibility studies for the self-reinforced materials.

3.4.1 Infrared Heating Experiments

Infrared (IR) experiments were conducted to test the selective melting ability of infrared radiation for the use with SRP materials. Two infrared radiators with different wave lengths were available for this investigation (Table 3.7).

Table 3.7: Wavelength fractions for the used infrared radiators [133,134,135]

Model	Wavelength		
	< 2 µm	2 - 4 µm	> 4 µm
Dark radiator (ceramics)	2.2 %	37.2 %	60.6 %
Halogen infrared lamp	73.3 %	21.0 %	5.7 %

The long-wave ceramic dark radiator (elstein FSR, Elstein Werk M. Steinmetz GmbH & Co. KG, Germany) was adjusted to 300 °C and preheated until the temperature reached the desired value. The distance between radiator and specimen was 100 mm to minimize a convective heat transfer.

The short-wave halogen radiator (Spot IR Model 4085, Research Inc., USA) provided a spot of approx. 20 mm² (diameter 0.25 inch) at a distance of 200 mm of the bulb. The energy supply of this type of IR radiator was not controlled. Due to its high heating rate, a preheating of the 750 W spot was unnecessary. HDPE and PA6 plates (120 x 120 x 2 mm³) with and without susceptors were placed at the focal point of the spot. For avoiding conduction to the metallic base plate, all sheet-like samples were placed on ceramic blocks. Furthermore, the specimen preparation and sensor placement were kept the same for infrared and induction heating.

3.4.2 Conduction and Convection Heating

Various standard conduction and convection heating techniques were applied with SRP to investigate critical states in these processes.

A convection oven (model VL / D, Ernst Reinhardt GmbH) was used for preheating polymer reinforced fabrics. The heated fabrics were, like in the related glass mat reinforced thermoplastics (GMT) process, afterwards consolidated in a Dieffenbacher hydraulic press (J. Dieffenbacher, Germany) with a maximum force of 8000 kN. The press possesses a parallel controlled press ram and realizes closing speeds of up to 80 mm/s. The mold for the manufacturing of sheets was heated to a temperature of 90 °C. Additionally, convectively preheated sheets were also used in combination with a safety shoe cap mold. The shoe cap mold provided a complex shape and was previously used in thermoforming processes. The mold was mounted on a medium-scale hydraulic press with a maximum press force of 1200 kN and heated to 90 °C.

The conduction heating was realized by using a heated mold mounted in the medium-scale press. The mold was heated by thermal oil, which resulted in long cycle times of more than one hour. A conduction heating could also be realized by the application of the induction assisted RocTool® technology (see chapter 2.4.4) which significantly reduced the cycle time of conduction processes.

Furthermore, an extruder (Kannegießer KMH60S, Germany) was applied, which is a standard in compression molding LFT process chains. Although the energy input into the material only marginally relies on thermal conduction and is mainly attributed to

shear effects, the LFT process was used as a reference for the preheating of polymer-polymer pellets before compression molding.

Figure 3.10: Dieffenbacher hydraulic press with mounted RocTool® mold

4 Discussion of Particle Induction Heating Results

All experimental results presented in this section have been tested upon their integrity. Every experiment was repeated several times, for thermal measurements at least three times, for mechanical measurements at least eight times. In the case of temperature runs, the data presented below show an exemplary recorded evolution, which fits best to the most often observed behavior. Due to inhomogeneous material distribution and ambient effects, it was likely to detect deviations to the exemplary run within heating experiments as well. For this reason, a reliable value for distinct measured data, as for instance, for the below-mentioned linear heating rate, was found by the calculation of a mean value. Preliminary to this, outliers were uncovered by the help of a Nalimov outlier test at a confidence level of 95 %. The outliers were not taken into account for the calculation of the mean value. The confidence interval for the mean value was then calculated by the help of the standard deviation and the student factor at a confidence level of 95 %. The used procedure was described in detail by Kaiser and Gottschalk [136].

4.1 Particle Induction Heating within Neat Matrix Systems

For investigating the heating abilities of particles for polymer-polymer systems, neat thermoplastic materials were particle doped, which were designed for the later use as matrix in SRP.

An exemplary temperature evolution of a doped thermoplastic from a sensor located in the coil's center is given in Figure 4.1. At the beginning, the temperature follows a linear trend which will be later referred to as linear heating rate h_r. With increasing heating time and temperature level, the curve first displays a degressive trend and then flattens. The flattening lies in the region of the peak melting temperature of the polymer. The exact peak melting temperature T_m as corresponding base line to the flat region was detected in neither case since the temperature measurement was limited to the sample surface, whereas the heating was intrinsic. The measurement of heating time of the whole sample, by sensor placement on the sample's opposite in respect to the coil, further influenced an offset of T_m. The side which faced the coil

usually melts prior to the side facing away. The energy provided by the particles is needed in this temperature range for the crystallite melting and is expressed as latent heat in literature. After the crystallites are mainly molten, the temperature increases again with a faster heating rate.

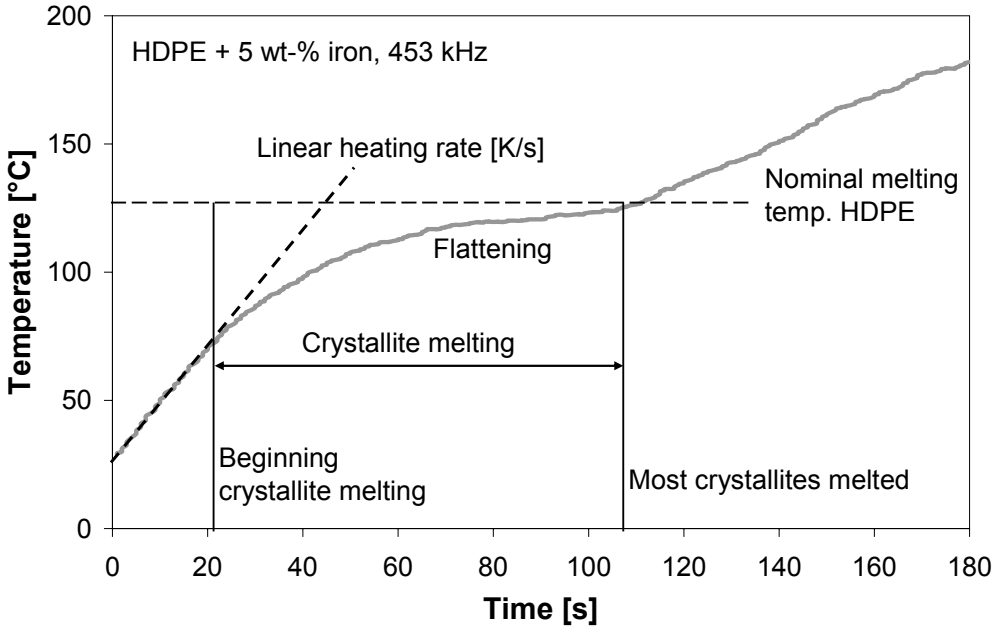

Figure 4.1: Exemplary temperature evolution of particle induction heated sample

Unless otherwise stated, the presented temperature evolutions were obtained in the center of the sample on the side facing away from the coil. The temperature homogeneity and records of the edge sensors will be discussed in detail in chapter 4.1.3.

Experiments with other matrixes exhibited that neither of the heating phenomena could be attributed to the polymeric matrix. Neat HDPE as well as neat PA 6 and PP do not heat from a magnetic field. Furthermore, the polymers do not limit the heating ability of the particles since they are transparent for electric and magnetic fields.

4.1.1 Susceptor Material Influence

The experiments with different susceptor materials revealed that the electric conductivity of an inductive susceptor material is not a required property (see Figure 4.2). Neither the carbon black materials nor the CNT doped compounds were significantly more affected by the electromagnetic field than a non-doped reference

sample. The small temperature increases observed in these cases were attributed to a conductive heating of the sample caused by the moderate warming of the coil surface due to self-induction effects. A heating attributed to inductive means was excluded. This led to the assumption that the eddy current losses, which are based on an electric current and therefore need electrically conductive paths within a material, were negligible in this case. Although a particle in itself presents a microscopic closed electric loop, an influence in terms of temperature increase on the surrounding polymer material was not found. Particle doped materials which are electrically conductive from a macroscopic point of view did not show a heating effect either (compare chapter 4.1.1.2).

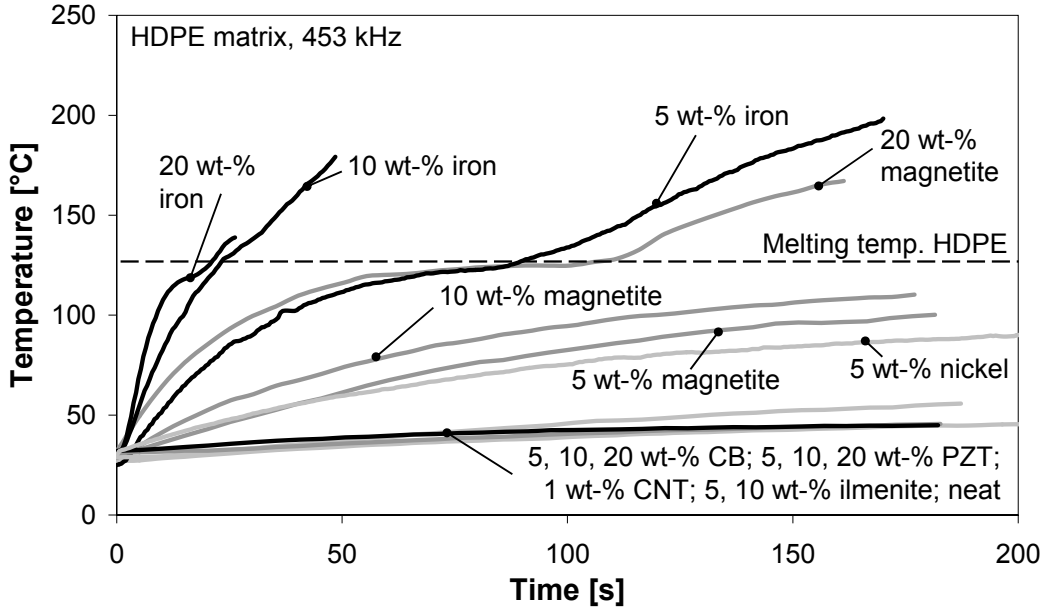

Figure 4.2: Influence of the susceptor material on the heating performance within a HDPE matrix

In comparison, the ferromagnetic material was highly activated from an electromagnetic field. Even with a filler fraction as low as 5 wt-%, the material could be melted within a range of less than 100 s. This behavior proved that the dominant heating mechanism is related to the magnetic properties of the particles. Particle induction heating below the percolation threshold is based on magnetic hysteresis loss. The eddy current losses can be neglected. This discovery corresponded to results given in literature [70].

Nickel and magnetite resulted in a moderate heating effect than the investigated iron particles on the one hand. On the other hand, the reactivity of iron made it unsuitable for most industrial applications. Therefore, the work was focused on iron, which gave the best heating effect, and magnetite, which delivered the best possibility for a later implementation in an industrial application at lower heating effectiveness. The gradation among the ferromagnetic particles was attributed to their respective magnetic properties, especially the shape of their hysteresis loop.

Despite their magnetic character, PZT and ilmenite were not affected by the field at all. Reasons for this can be found in their piezo-magnetic behavior (PZT) and their varying ferromagnetic content (ilmenite), which is a condition of manufacturing. The ferromagnetic content was assumed to be too low for the use as susceptor in this study.

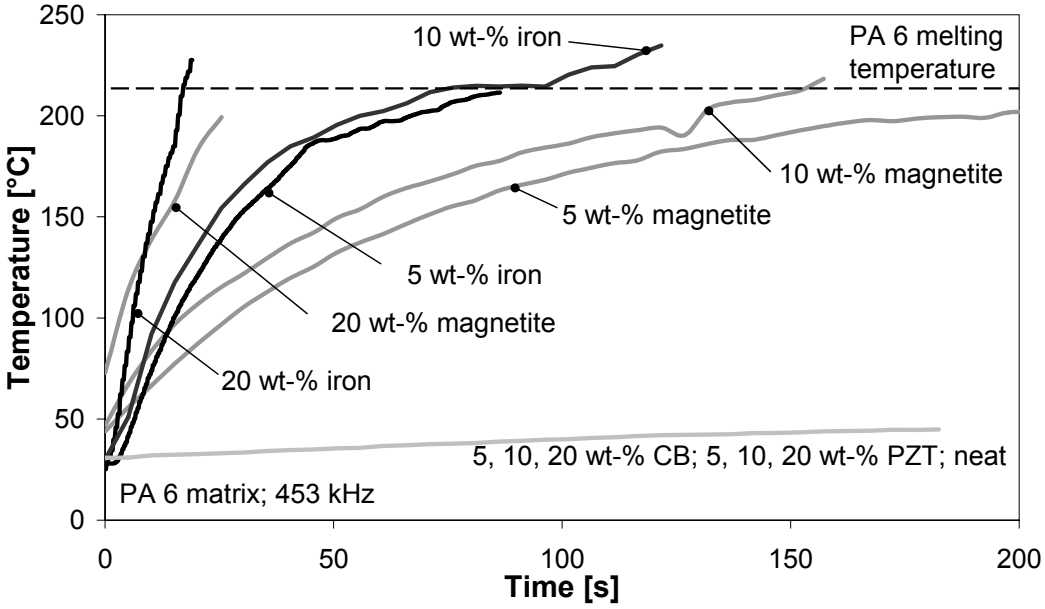

Figure 4.3: Susceptor material influence on heating performance of PA6

4.1.1.1 Susceptor Fraction

The analysis of susceptor fraction influence on heating effectiveness led to an expected result. The more susceptors were incorporated in the polymer, the higher was the heating effect (Figure 4.4). For cast iron powder, the border between reasonable material melting and heating without reaching the melted state was found

between 2.5 and 5 wt-%. The melting of HDPE could be reached with 5 wt-% of iron particles within approx. 90 seconds. Following from the temperature evolution, the increase of susceptor fraction increased the heating speed on the one hand. On the other hand, a further increase of susceptors was not desired since the particles also increased the composite density. Additionally, a higher number of particles led to increased matrix contamination which thus caused a reduction of the mechanical performance and a higher economic effort. For this study, a fraction of 5 to 10 wt-% was regarded as sufficient concerning the heating abilities.

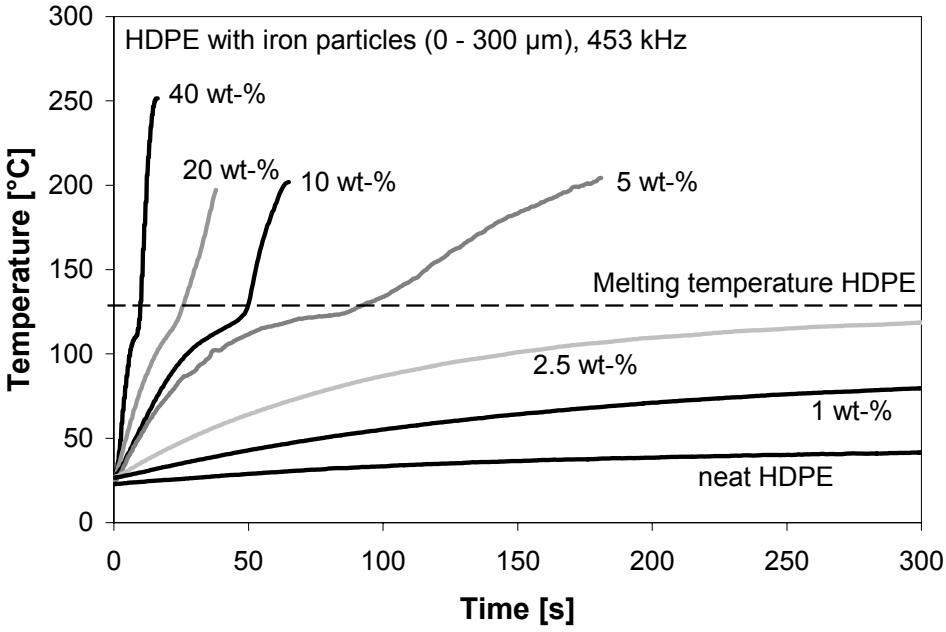

Figure 4.4: Influence of filler fraction on heating effect of iron particles in HDPE

The analysis of heating rates revealed an asymptotic behavior in the investigated borders. From a theoretic point of view, the heating rate increases with filler fraction as long as the hysteresis heating is the dominant mechanism. When reaching the percolation threshold at a distinct filler fraction, the mechanism was supposed to change due to the more effective eddy current heating. The maximum heating was expected close to a filler degree of 100 wt-%, which would be the pure susceptor material.

The recorded heating rates h_r for the investigated materials could be well fit with a function including an exponential part which contains the susceptors fraction w_s.

$$h_r \sim e^{\frac{w_s - const.}{const.}} \qquad (4.1)$$

The exponential relationship between filler fraction and heating effect was analyzed by the help of the coefficient of determination R^2 which is a criterion for the quality of a linear approximation. R^2 values close to 1 indicate a high accordance between predicted data (model) and experimental results; values close to 0 are evidence of low agreement. In case of the filler-fraction-to-heating-rate correlation, three of four materials revealed a R^2 value of more than 0.92. Since the nickel material was only available with two different filler fractions, the predicted correlation could only be approximated with a R^2 value of 0.7.

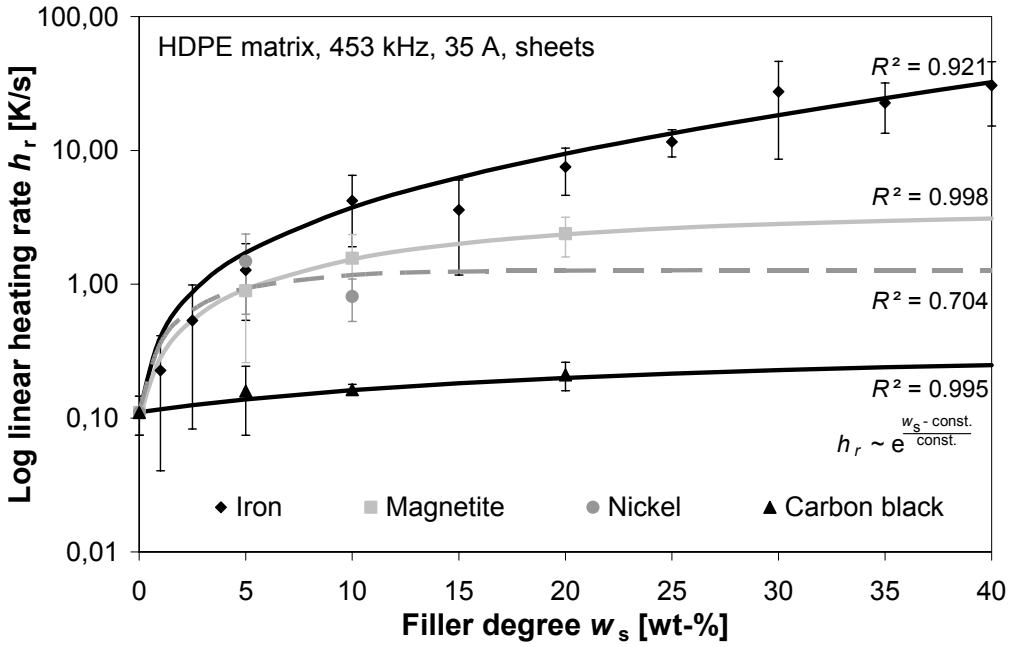

Figure 4.5: Logarithmic plot of heating rate of HDPE in dependence on different filler fractions

The experiments pointed out that the susceptor fraction has a high influence on the successful and economic heating of a component. For visualizing the influence of the susceptor fraction on the heating performance, a theoretic analysis of the through heating time of a thermally insulated flat sheet heated from only one side was performed. The analysis revealed that the inductive heating performance, depending on the susceptor fraction, may result in a lower or higher heating time than competing heating techniques (Figure 4.6). For example, the inductive heating with a very low susceptor fraction will not be able to be faster than a convective heating in an oven.

Nevertheless, a very low and a very high susceptor fraction are not ideal: the low one has a too low heating efficiency, whereas the higher will increase the compound's weight dramatically. Furthermore, the analysis demonstrates that a certain material thickness exists, at which inductive heating, although the material possesses a sufficient amount of particles, loses its performance. The performance loss is attributed to the lower magnetic field strength with increasing distance from the coil. This effect is discussed in detail in chapter 4.1.2.2.

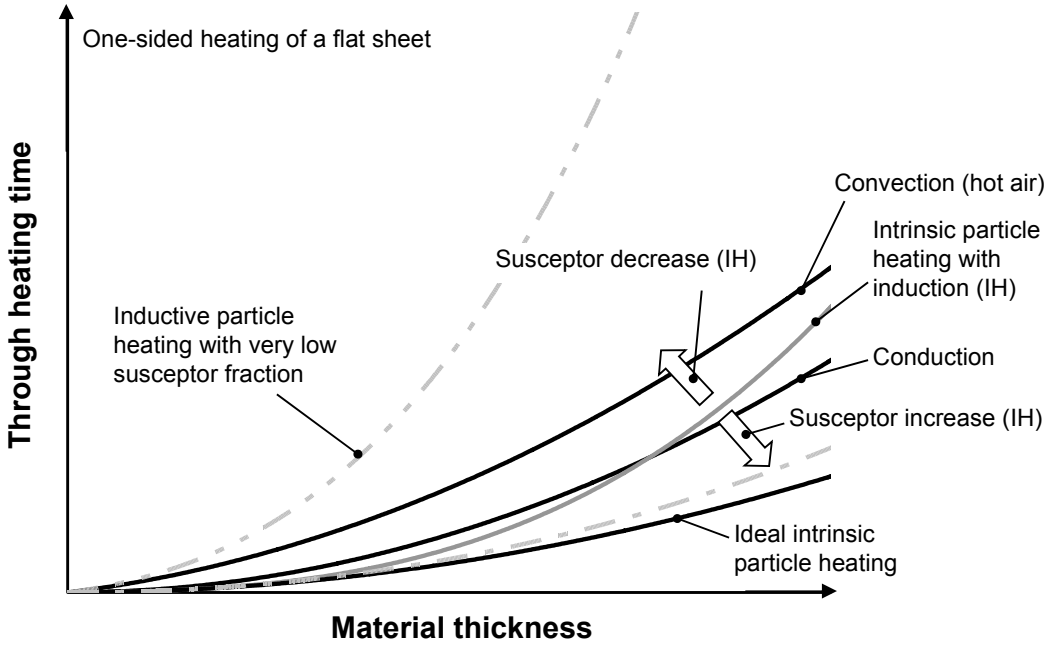

Figure 4.6: Influence of susceptor fraction on performance of inductive particle heating of an exemplary component

4.1.1.2 Influence of Electric Conductivity

None of the particle doped matrixes with an outstanding heating performance had an electric conductivity higher than 10^{-15} S/m. Since this value lies in the region of isolators, the formation of eddy currents within the samples could definitely be neglected. The observed heating mechanism is limited to the magnetic hysteresis, which was best observed at the weak heating of carbonous particle doped polymers. For composites containing these particles, a higher electric conductivity in the range of 10^{-7} to 10^{-9} S/m was determined, which generally classifies them as semi-

conductors. From tests with carbon fibers is known that the conductivity has to be at least in the range of 10^{-3} S/m and above to reach an eddy current dominated heating.

As already mentioned, a significant change of the heating behavior for all particles was expected when the material reaches a conductive state. Within a conductive material, closed electrical loops as well as eddy currents are possible which have a considerable higher heating effect. For spherical electrically conductive particles, the filler fraction has to be as high as 33 vol-% to exceed the percolation threshold at which the overall compound becomes conductive [79]. Even with a filler fraction of 40 wt-%, the volume fraction for iron is only as high as approx. 7.5 vol-%. Since the use of susceptors is connected to an increased recycling effort in terms of separating the components, the amount of particles should be reduced to a necessary minimum. Although it is expected that ferromagnetic particles can easily be separated from polymers in melted state by the use of magnetic forces, the amount of particles was not further increased in this study.

In the approach of heating an electrically conductive compound, carbon nano tubes offered the possibility to reach a conductive composite with only small amounts of incorporated fillers. For a specimen with 3 wt-% CNT, an electric conductivity was measured in the region of 10^{-3} S/m. Unexpectedly, the bar could not be heated when exposed to an alternating magnetic field. The reason was the bar representing itself a single non-closed conductor loop. But, for eddy current heating, a closed electric circuit is necessary. By attaching a conductive carbon fiber at both ends of the bar, the circuit was closed and a heating could be observed (Figure 4.7).

Similar observations were even made with conductive pellets filled with carbonous particles in a small scale. The arrangement of pellets within the test tube led to coincidentally emerging closed loops, which were affected by the electromagnetic field. Nevertheless, in all cases the emerging heating was only little faster than the standard hysteresis based ferromagnetic particle heating and much slower than the eddy current based heating of carbon fiber fabrics. This result was attributed to the high electric resistivity in the specimens.

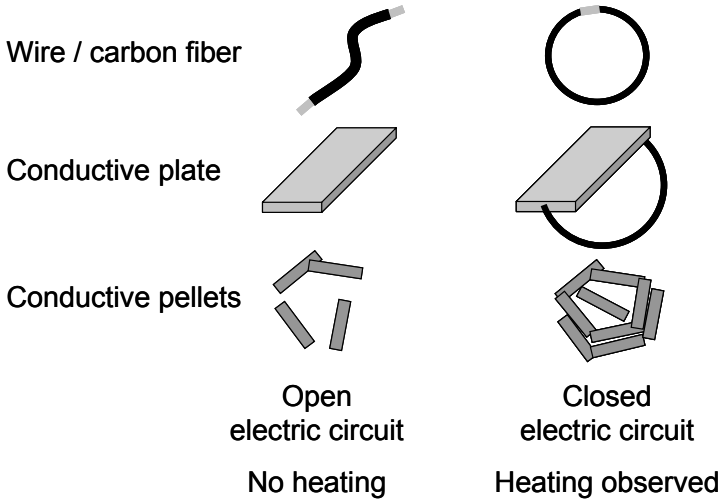

Figure 4.7: Induction heating trials with non-metallic, conductive materials

The same results were detected with a knotted and an unknotted carbon fiber. Only the short-cut, knotted fiber was heated within an induction experiment.

The poor heating in combination with a relatively high economic effort when using CNT filled materials disqualified them for further use with the demanded low-cost materials in this study. Nevertheless, the application of CNT in circular, closed loop structures could generate local heatability and make welding processes with defined shapes possible.

4.1.1.3 Susceptor Size

The influence of susceptor size was investigated for the ferromagnetic particles, nickel, and cast iron. A general rule for the relationship between particle size and heating ability was not found. Each material indicated a distinct behavior. This size-dependent heating behavior for ferromagnetic particles has been previously reported by other researchers for medical as well as plastic applications [24,94,83,84,137].

In the investigated borders, nickel follows a linear relation so that fractions which contain larger particles generate more heat. Only materials filled with the largest particles were able to melt the material sufficiently.

For cast iron powder, the heating experiment revealed a non-linear correlation to the particle size. A maximum heating performance was observed at a size between 24 and 62 µm. In contrast to nickel, the lowest heating was found with the largest particle sizes, which was also the only particle size not exceeding the melting

temperature of HDPE. This non-linear behavior was previously described by Ma et. al. for magnetite particles at a frequency of 80 kHz [138].

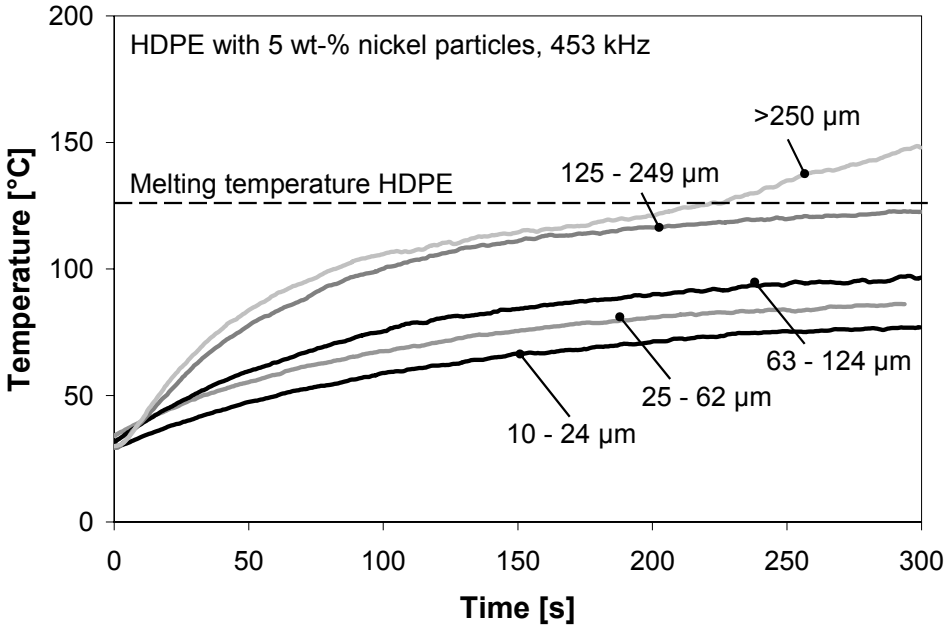

Figure 4.8: Influence of particle size on material heating of nickel filled HDPE

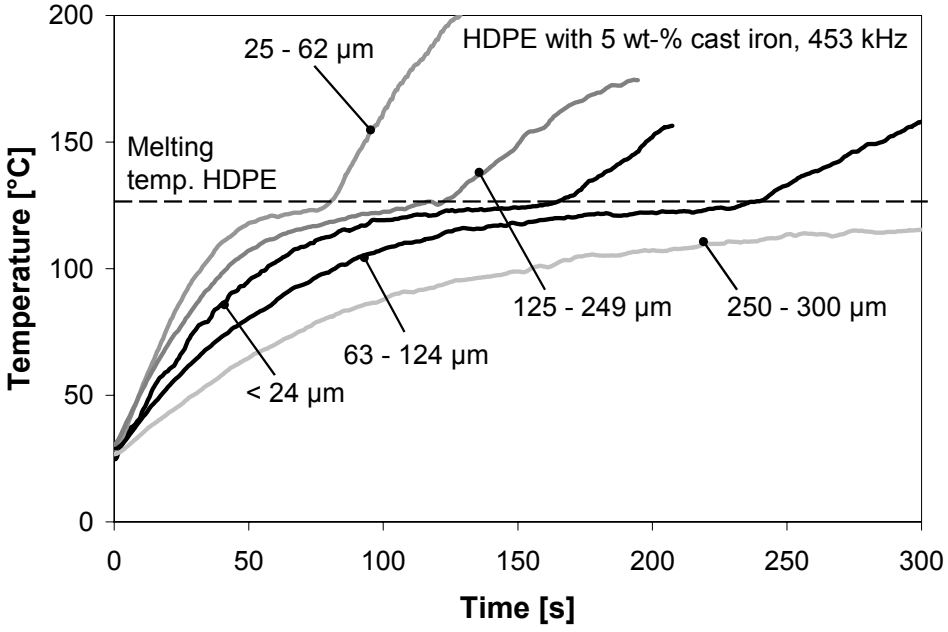

Figure 4.9: Temperature progression of cast iron doped HDPE with different susceptor sizes

Magnetite revealed a quasi-linear correlation between particle size and heating effect although the obtained heating rates were not as distinct from each other as this was

observed with nickel doped samples. The highest linear heating rates were recorded for the largest used particles, whereas the lowest rates were obtained from the smallest ones (Figure 4.10).

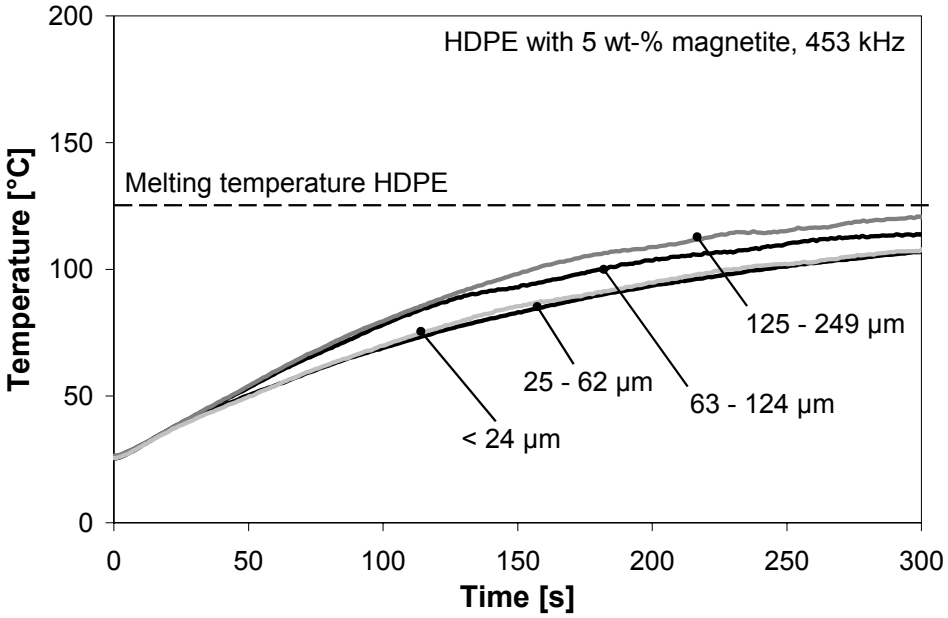

Figure 4.10: Influence of particle size on material heating of magnetite doped HDPE

According to Ma et. al. and Frauenhofer, the heat effect of spherical magnetic ferrites, which is actually a dissipation loss, can be described as a proportional function of susceptibility [138,139]. Furthermore, the existence of a correlation between particle size and susceptibility is known fact. For related magnetite, Svoboda has described the influence of particle size on susceptibility (Figure 4.11) [81].

The reason for the susceptibility function is the change of magnetic single domain structures to multi-domain structures in larger grains. A single-domain particle possesses only one magnetic dipole, whereas corresponding multi-domain particles are so large that they contain more than one magnetic dipole. The amount of dipoles influences the magnetic properties of the entire particle. Each material has a distinct critical particle size d_c for this change [81,140]. The value of the critical particle size lies at approximately 0.05 µm for magnetite [82] which signifies that the applied particles within this study are of a multi-domain structure character. Consequently, the susceptibility increases with larger magnetite particles. The higher is the

susceptibility, the better is the heating performance which was proven by the experiments.

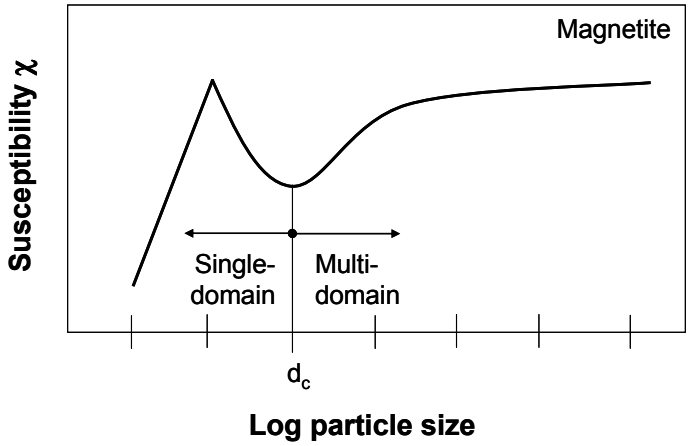

Figure 4.11: Relation between susceptibility and particle size [81]

The obtained heating results indicate that the influence of the susceptibility might be the driving factor for the observed behavior of cast iron powder. Because of the findings of Svoboda and Nagata, who pointed out that the critical particle size d_C for Hematite can also lie around 200 – 300 µm [141], the investigated cast iron particles were assumed to scatter around their respective d_C, which is expected to lie in the same size range as hematite. Consequently, a general correlation between heat efficiency and particle size cannot be given, but depends on the chosen particle material and its magnetic history [140].

Furthermore, the particle distribution was affirmed an evident criterion. Smaller particles, which were not well dispersed and formed agglomerate-like structures, revealed a strong inhomogeneous heating pattern comparable to the heating of large particles (Figure 4.12). The appearing hot spots could not guarantee a sufficient polymer melting, whereas smaller, well-dispersed susceptors led to better temperature homogeneity within the sample. They primarily heated the sample effectively in areas with a high magnetic field strength such as visible in Figure 4.13 at the edges of the innermost coil turn.

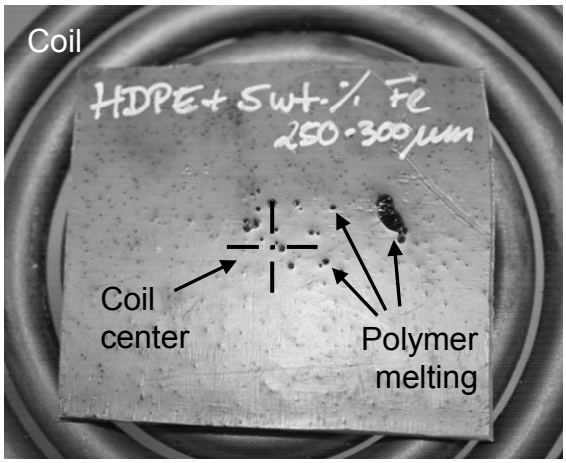

Figure 4.12: Heating pattern of 250 – 300 µm sized iron particles (5 wt-%) in HDPE

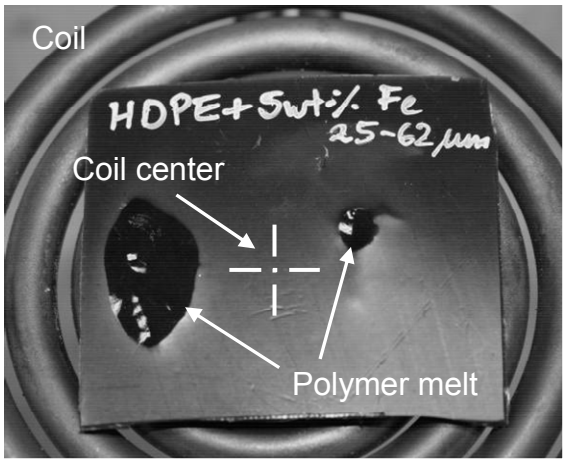

Figure 4.13: Heating with well-dispersed iron particles of 25 – 62 µm size (5 wt-%) in HDPE

4.1.2 Influence of the Electromagnetic Field

The control parameters for the generation of the electromagnetic field were varied in the feasible limits. The frequency, a product of the oscillating circuit, which consisted of generator, matchbox with capacitors, and coil, was changed by a hardware modification. The strength of the electromagnetic field was altered by changing the generator current level, whereas the dependent power output (max. 10 kW) and the circuit voltage (max. 1400 V) remained at the peak levels.

4.1.2.1 Frequency Variation

The frequency is a product of the complete setup of the oscillating circuit. Generally, the generator, the matchbox with changeable capacitors, the coil, and even the sample to be heated can have influence on the frequency. In case of samples with low overall magnetic properties, like the particle-filled polymer plates, the experiments indicated that the sample influence on the frequency could be neglected. The frequency did not change when the samples were placed on the coil.

Table 4.1: Realized frequencies with the used pancake coil

Matchbox capacitors [µF]	100	170	270	330	430	500	600	670	830
Frequency [kHz]	744	565	453	408	360	334	305	289	262

Since the generator and the coil remained the same for all experiments, the frequency could be altered in distinct steps according to the available capacitor pairs within the matchbox (Table 4.1). Nevertheless, for frequencies higher than the nominal working frequency of 500 kHz, the generator current had to be reduced. The current was changed to the maximum possible level. In that way, the highest possible frequency with full generator power was found at 453 kHz.

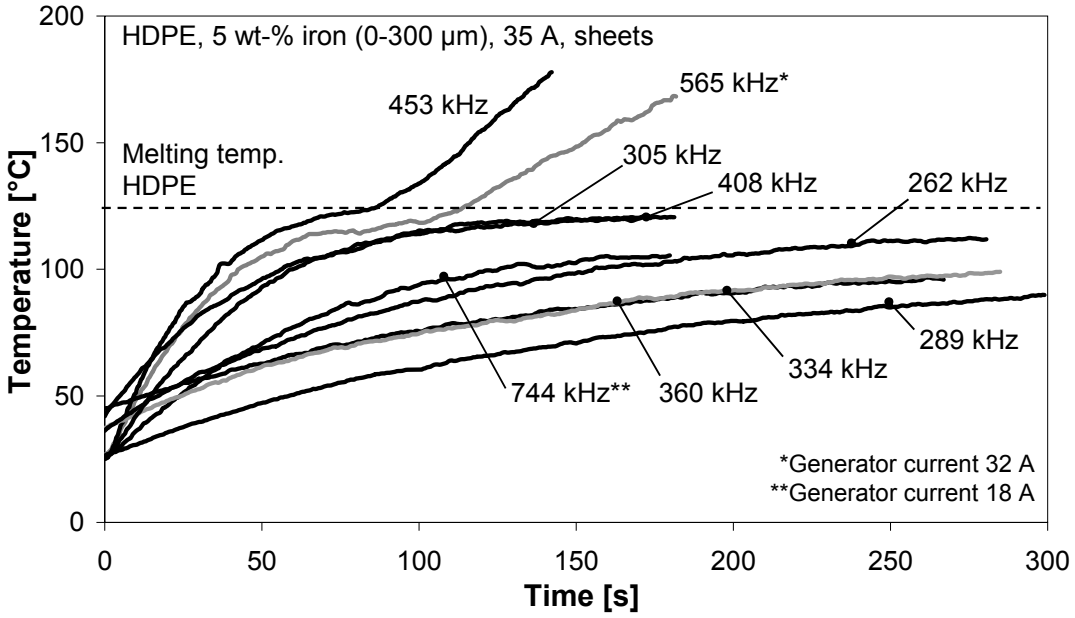

Figure 4.14: Temperature evolution of iron doped HDPE at various frequencies

From the theory of induction heating of bulk materials, higher frequencies were expected to deliver higher power input to the material (compare eq. (2.3)).

The power level displayed at the generator varied non-linearly, depending on frequency changes. In this context, Orfeuil stated that the increase of frequency theoretically led to an improved heating of conductive materials. But the frequency increase was related to a changed inductor impedance, losses in mountings, and various other negative phenomena. These negative effects reduced the efficiency achieved by the higher frequency [142].

A well-working frequency with good heating results was found close to the nominal working frequency of the generator at 453 kHz for iron (Figure 4.14) as well as for magnetite (Figure 4.15). Lower frequencies, which could be reached with full

generator power, resulted in lower heating efficiency. Higher frequencies than 453 kHz were possible and even led to good heating, as for example 565 kHz. However, as mentioned before, the power level had to be reduced for this frequency due to machine restrictions which prevented a better result with this standard equipment.

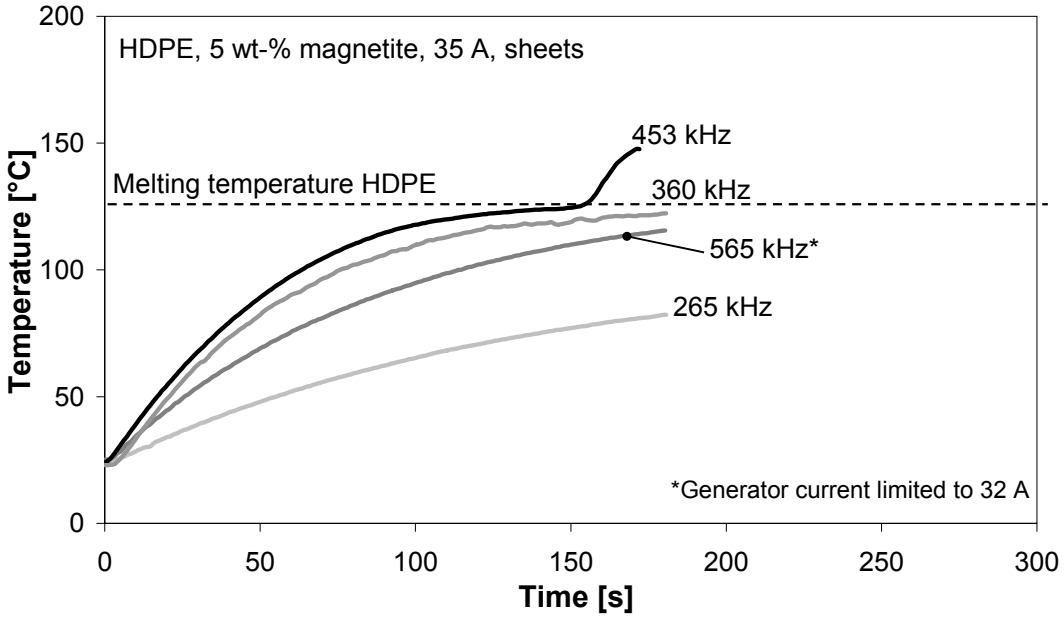

Figure 4.15: Temperature evolution of magnetite doped HDPE at various frequencies

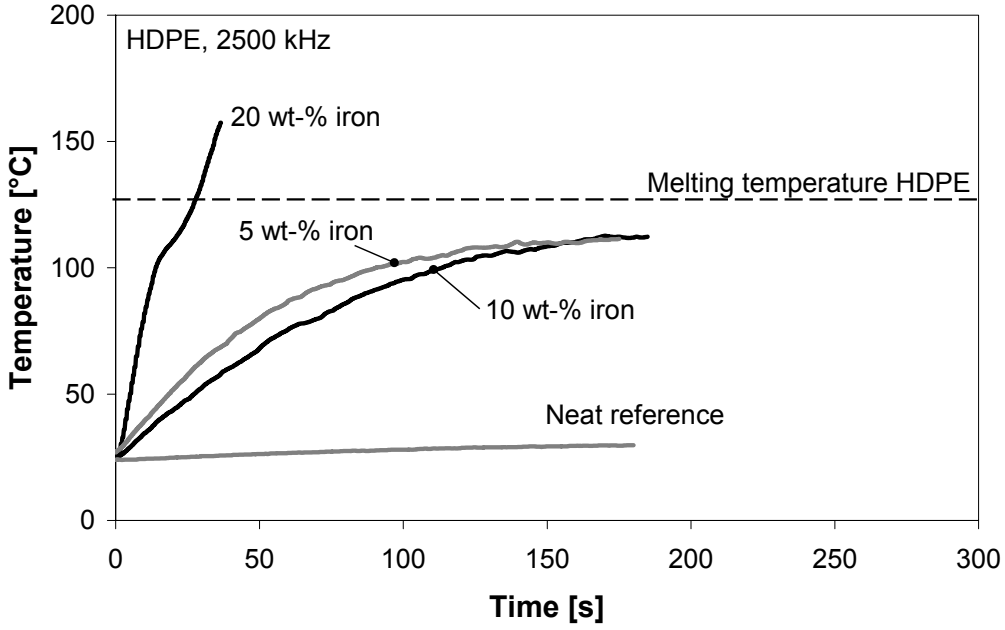

Figure 4.16: Heating of iron-doped HDPE at a frequency of 2500 kHz

To verify the theoretically better heating efficiency at higher frequencies, the Trumpf Hüttinger IG 10/2000 high frequency generator was used to examine the material at a frequency of 2500 kHz. The pancake coil remained the same.

Unexpectedly, a better heating at higher frequencies was not observed (Figure 4.16). The heating was even noticed to be worse than at around 500 kHz. Also other tested particles, such as magnetite and carbon black, were not evidence for an improved sample heating. An explanation is given by the results of Orfeuil, which have been already mentioned [142].

Since related studies also point out that sufficient heating is possible at lower and higher frequencies [93,143], a general rule of higher frequencies generating better heating is concluded to be only applicable in theory, and strongly depends on generator setup.

By drawing a conclusion from the experimental results of this study, the frequency has to be selected according to the generator in relation to the coil and the susceptor material. A general rule cannot be given. The frequency of 453 kHz was found to be the best suitable option for all examined ferromagnetic particles in this study. Independent researchers described a suitable frequency for particle heating in the same range between 400 and 500 kHz for ferromagnetic particle induction heating [22,94,144,145].

4.1.2.2 Coupling Distance

The coupling distance is defined as the gap between coil and specimen. A decreased heating effect with higher distance was expected due to the lower magnetic field strength. A continuous decline was observed for both tested susceptor materials in various filler degrees, magnetite and cast iron.

The magnetite revealed a very regular behavior. For 10 wt-% magnetite filled HDPE, the heating effect was sufficient for a material melting within 5 minutes even at a distance of 6 mm (Figure 4.17). Above this distance, the heating was dramatically decreased until the largest tested distance of 12 mm was no longer able to reach 75 °C after 5 minutes. The low magnetite filled HDPE could only be melted at a maximum distance of 2 mm, which indicated that a strong magnetic field was needed

to transfer sufficient amounts of energy into a heat effect. The results with cast iron particles were similar to the ones with magnetite (see Figure 5.4).

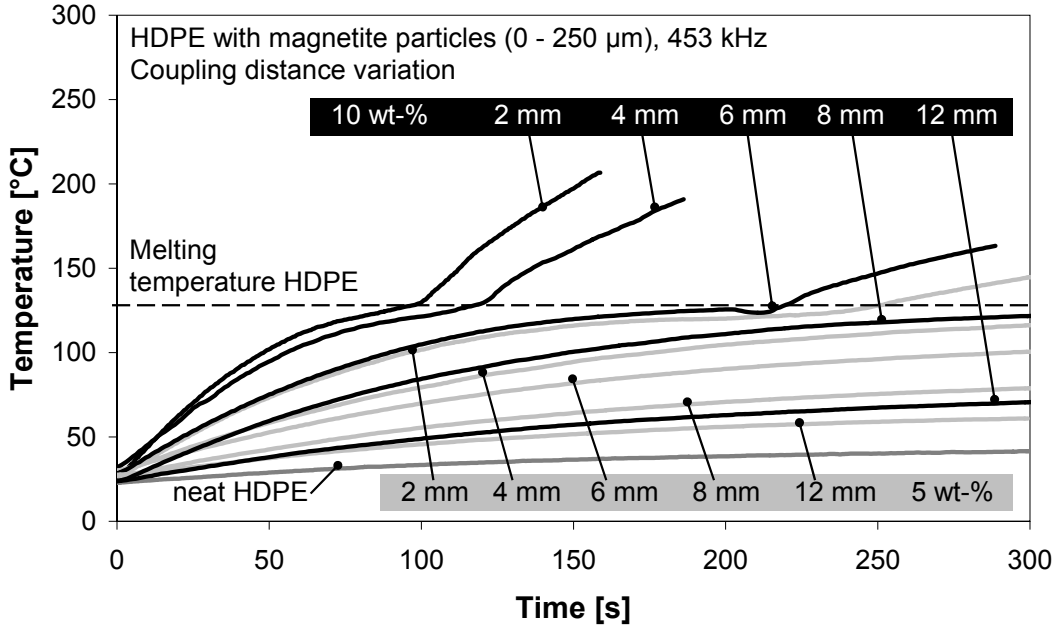

Figure 4.17: Temperature run in relation to coupling distance of 5 wt-& (grey) and 10 wt-% (black) magnetite filled HDPE

For describing the reduction of heat effect caused by an increasing coupling distance, the magnetic potential function was considered. The potential function depicts the energy distribution in relation to an individual point in space. Generally expressed, the energy decreases from its origin in a reciprocal way [146]. This fact is also explicated in the Biot-Savart law. By concluding from the mathematical approach, a reciprocal relationship between the coupling distance r and the linear heating rate h_r was anticipated (4.2).

$$h_r \sim \frac{1}{r} \tag{4.2}$$

The assumed reciprocal correlation could be validated with high accordance due to an analysis of the linear heating rate (Figure 4.18).

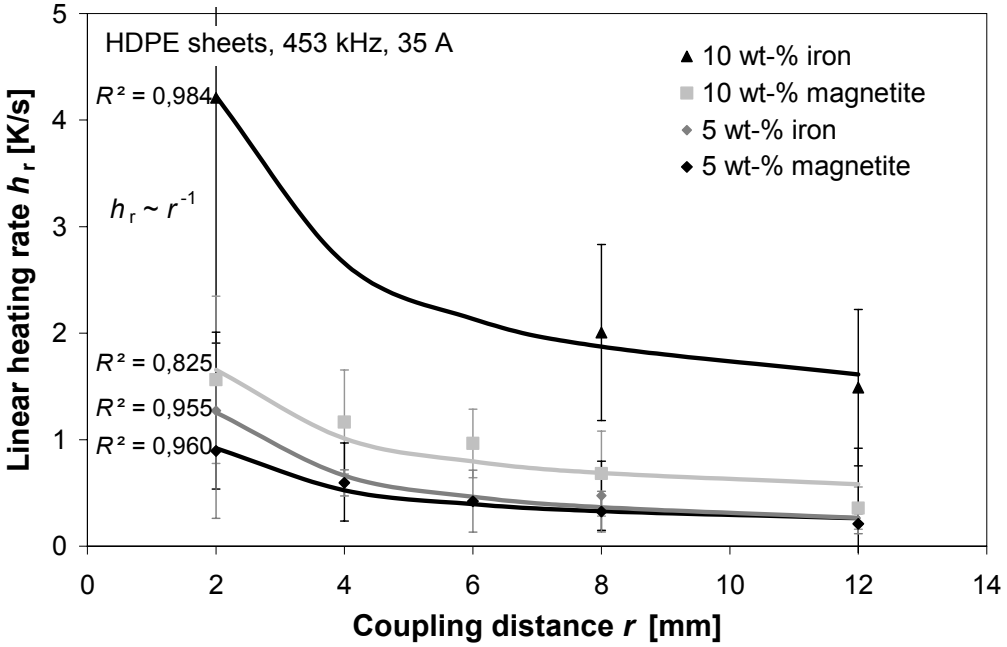

Figure 4.18: Plot of linear heating rate in comparison to coupling distance of magnetite and iron doped HDPE

4.1.2.3 Generator Power

The generator power level was changed by varying the generator current. At its maximum level, the generator delivered 35 A, which was transformed by the attached coil circuit to a nominal value of 280 A. In the related diagrams, the generator current is the referred current.

The experiments are evidence that the generator current had a high influence especially on low filled polymer systems (Figure 4.20). Whilst 5 wt-% iron doped HDPE exceeded the melting temperature after 90 seconds at 35 A, the heating time to reach this level extended more than 300 % by the use of a reduced current of 20 A. The induced energy in the particles was at a power level of 10 A so low that a heating could not be significantly measured.

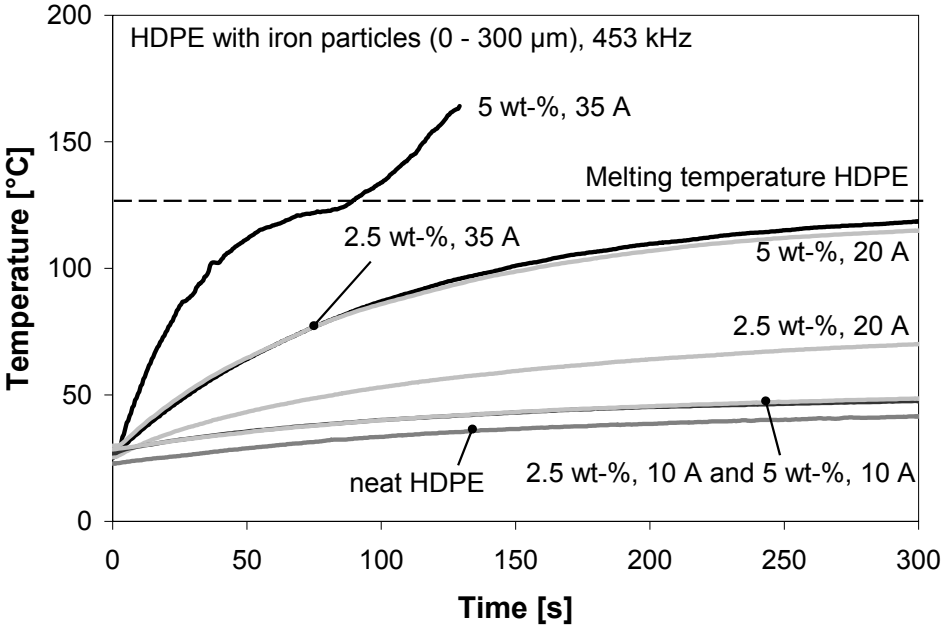

Figure 4.19: Influence of generator power on heating of low iron doped HDPE

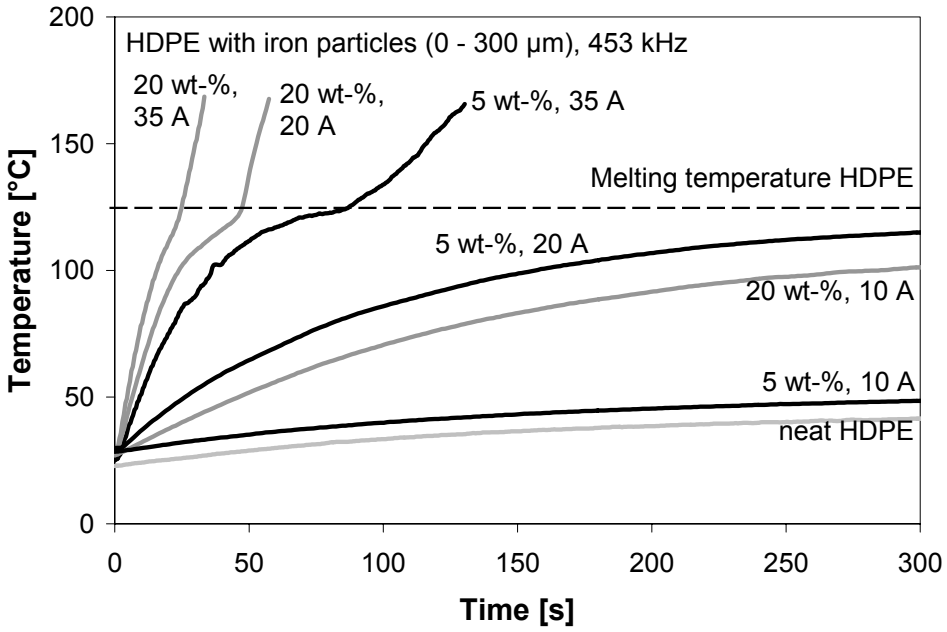

Figure 4.20: Influence of generator power on heating of high iron doped HDPE

The dramatic decrease of heating effect was less distinctive for high filled 20 wt-% iron containing HDPE (Figure 4.20). The melting temperature was also exceeded in this case at 20 A by a doubling of heating time. Furthermore, the higher amount of particles led to a significant increase of sample temperature at 10 A. This result

demonstrates that the generator power is a decisive factor for a successful particle induction heating.

In order to quantify the influence of the generator power, the energy of the magnetic field P_m was considered. The energy of a coil with the inductance L follows a quadratic function in relation to the coil current I_c according to equation (4.3) [122].

$$P_m = \frac{1}{2} L I_C^2 \tag{4.3}$$

A proportional heat gain from an increased energy was expected, which finally results in a quadratic relation on the generator current (4.4).

$$h_r \sim I_C^2 \tag{4.4}$$

The predicted quadratic relation on the generator current was validated by a consideration of the measured linear heating rates (Figure 4.21).

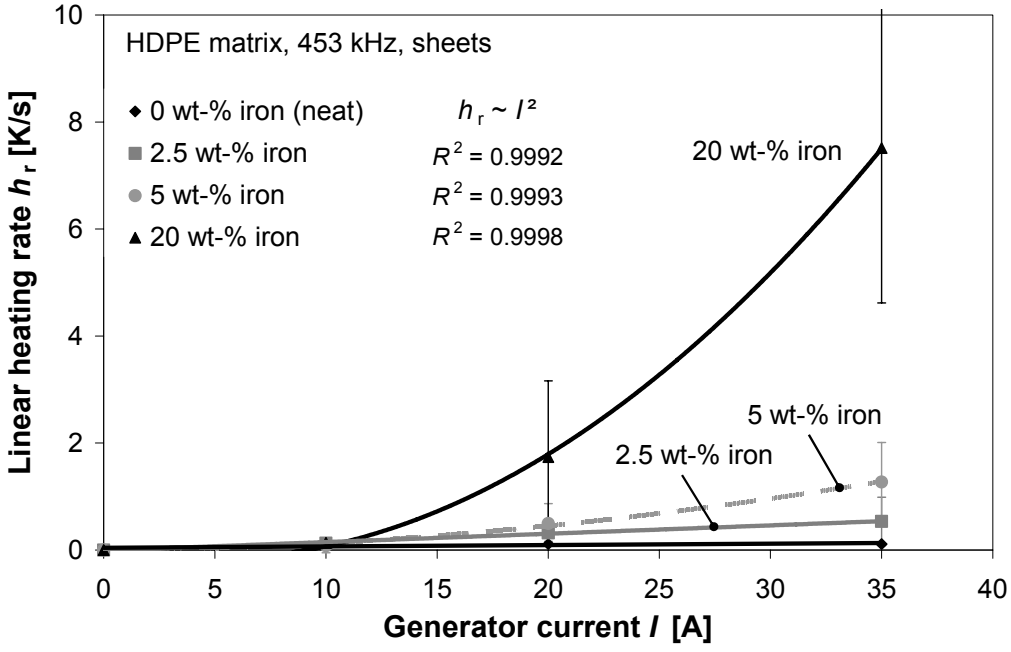

Figure 4.21: Linear heating rates of doped HDPE in respect to the generator power

4.1.3 Temperature Homogeneity of Heated Sheets

The use of the pancake coil revealed that the dome shaped magnetic field (see chapter 3.7) had a significant influence on the temperature homogeneity of the sample during static heating. The higher magnetic field strength in the area of the coil center caused increased heating in the center of the sample, whereas the edges remained cold. This effect could be best validated with a thermographic image of a sample. The sample was placed in the center of the coil but was actually larger than the coil (Figure 4.22). The specimen's center heated up very rapidly and exceeded the melting temperature of the material after a short time, whereas the material above the coil edges only reached a lower temperature. The specimen edges, which were not above the coil at all, remained at a very low temperature at the end of the experiment in comparison to the specimen center. Therefore, it was concluded that the shape of the coil and homogeneity of the electromagnetic field is a very important issue for quick homogeneous particle based induction heating.

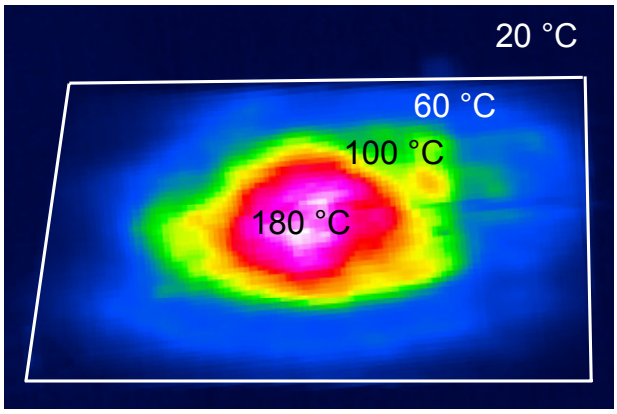

Figure 4.22: Thermographic image of a particle induction heated HDPE sample (120 x 120 mm²)

To overcome the homogeneity problem caused by inhomogeneous electromagnetic fields, the modification of the thermoplastics with thermally conductive carbon black particles was considered. This incorporation aimed at improving the composite's overall thermal conductivity without a reasonable weight gain. The higher thermal conductivity was expected to lead to increased temperature homogeneity. In the ideal case, the temperature for sample center and edge had been identical.

Table 4.2: Thermal conductivity of selected materials

Material	Thermoplastic polymers	Cast iron	Graphite	CNT
Thermal conductivity [W/mK]	0.2 - 0.6	40 - 50	120 - 160	~6000

The experiments with 5 wt-% cast iron susceptors reveal that the two recorded temperatures converge with increasing carbon black fraction (Figure 4.23).

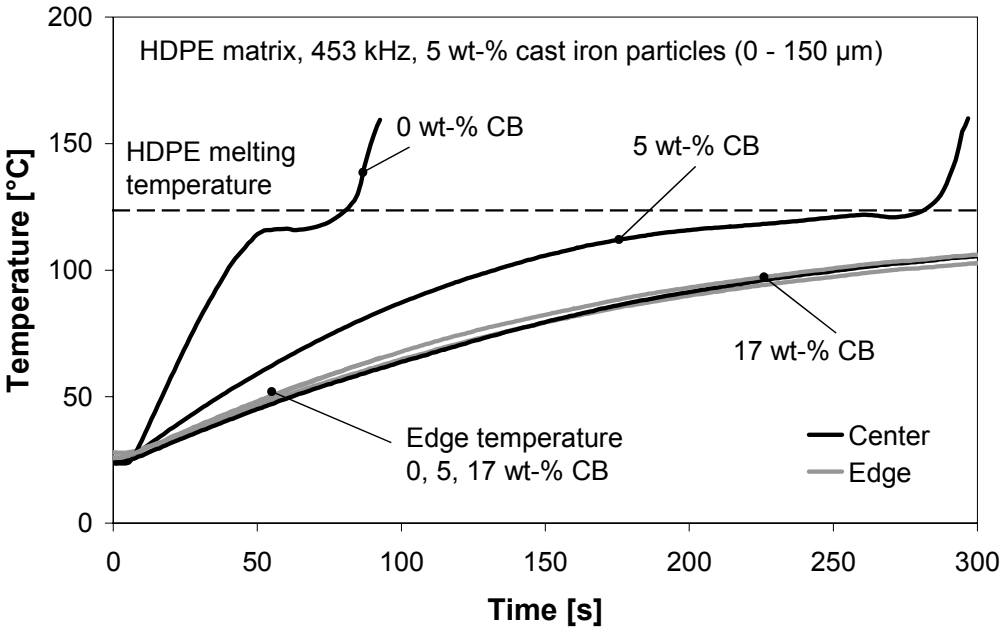

Figure 4.23: Attempt to increase temperature homogeneity between sample center and edge by the incorporation of carbon black particles

The edge temperature did not change significantly in any of the experiments, whereas the center took longer for reaching the polymer's melting temperature. By thermal image recording was observed that a larger area around the specimen's center was heated. The area gain was still so small that the thermocouple, positioned at the edge, was not measurably affected by the distributed energy from the improved thermal conductivity but only heated by the activated surrounding particles. For this reason, the achieved homogeneity increase was only viable in a very small area.

The described effect was observed more significantly with higher susceptor fraction. For 10 wt-% cast iron, the temperature difference between center and edge for samples with different carbon black filler nearly remained the same (Figure 4.24).

Only the time for reaching a distinct temperature at the center prolongated. This indicated that the improved temperature distribution was limited to a local zone around the center with the highest magnetic field strength, whereas the composite edges did not benefit from the incorporated carbon black particles. By these means, the composite heating could not be homogenized in the desired way. Instead of the material, the machine setup was, thus, modified to improve temperature homogeneity (see chapter 6.1).

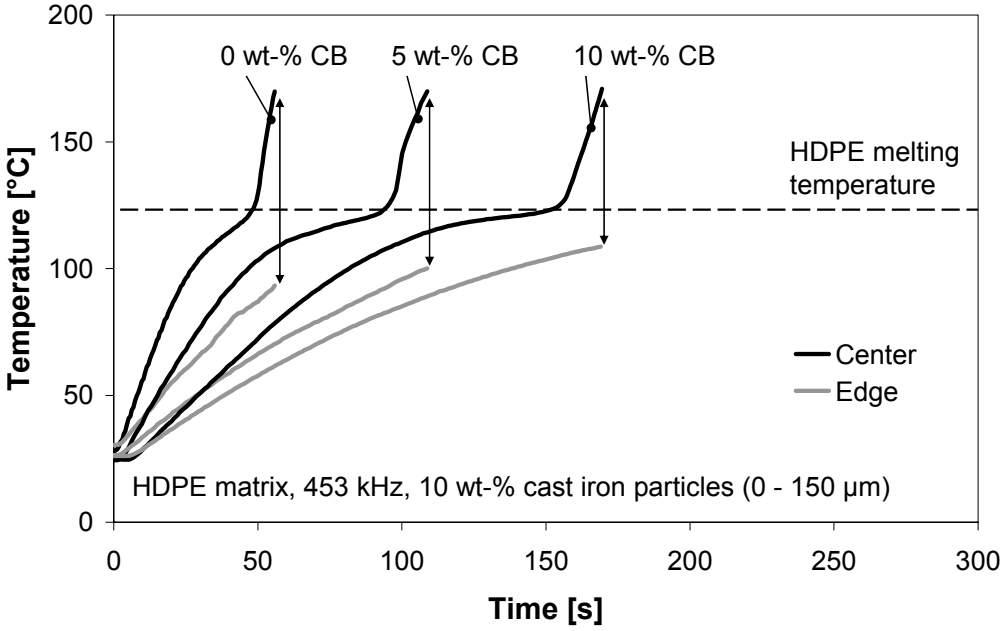

Figure 4.24: Change of heating evolution by the incorporation of additional carbon black in iron doped HDPE

By concerning the temperature homogeneity, also the drop formation of matrix melt was considered a possible problem (Figure 4.25). A computer tomographic scan revealed that the influence of gravity had reduced the coupling distance between particles and coil within the matrix melt (Figure 4.26). The image furthermore depicts a particle alignment in melt flow direction. If the coil is placed under the specimen and a melt drop formation is possible as observed in the experimental series, the particles with decreased coupling distance are subjects to an increased heating effect. Since these particles are already surrounded by matrix melt, this would be a self-harming effect, where the molten zone is even heated more. To avoid this in industrial applications, the coil's position has to be located above the sample. A melt flow would increase the distance between coil and susceptor which results in a self-

adjustment of the particle heating. If a melt flow is unwanted at all, a carrier film has to be applied.

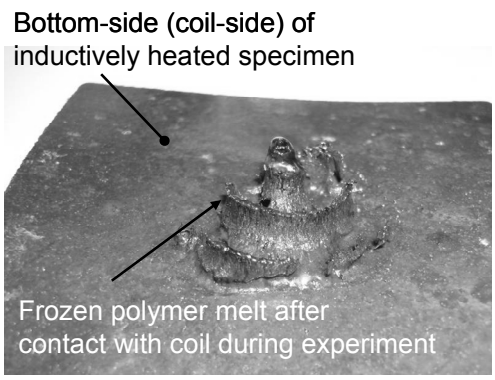

Figure 4.25: HDPE sample revealing contact with the coil due to melt flow during heating

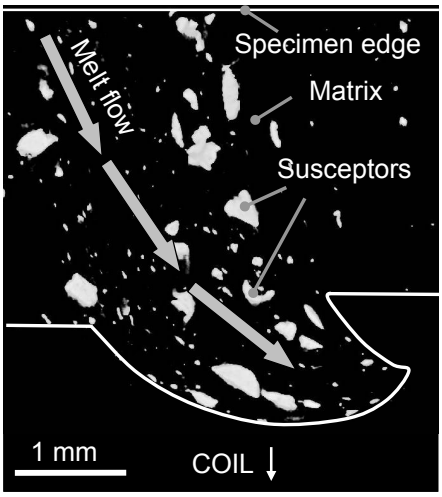

Figure 4.26: Computer tomographic image (µCT scan) of a heated particle doped sample (coil located at the bottom side of the image)

4.1.4 Thermal Polymer Degradation Caused by Heated Particles

As a disadvantage of intrinsic heating by particulate susceptors, a hot spot occurrence was anticipated. The particle surrounding zone is exposed to a higher temperature than distant areas. Consequently, the hot spot near material was assumed to suffer from thermal degradation. Since most degradation methods aim at surface analysis which is not feasible for the investigation of intrinsic heating, a comparative procedure by using DSC measurement was developed.

As references for induction heated material, neat and iron doped HDPE samples were exposed to different heating methods, which included short-wave infrared and laser heating. For the laser experiments, a LDL40-500 (Laserline GmbH, Germany) was applied with a wavelength of 980 nm providing a spot size of 4 x 12 mm². To minimize reflection, the specimens were irradiated under an angle of 0°.

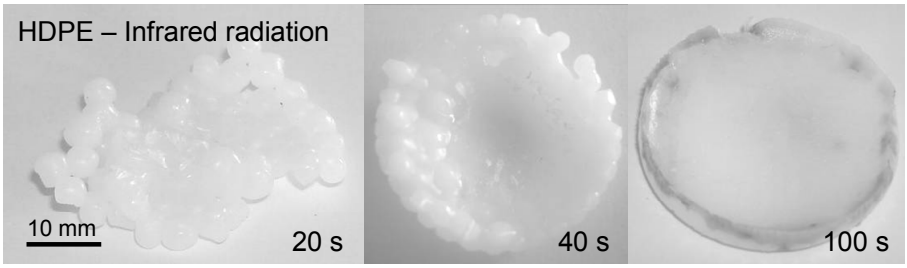

Figure 4.27: Surface morphology of HDPE pellets after 20, 40, and 100 s infrared radiation

The neat HDPE samples allowed the visual gathering of degradation effects. With increasing infrared radiation time, the samples turned from bright white into dark brown. The color shift was accompanied by an increasing emergence of smoke (Figure 4.27). The energy input was sufficient to visibly damage the samples after 30 to 40 s. For both HDPE compounds, neat and iron doped, the infrared radiation was found to have a significant influence on the melting peak temperature detected by DSC (Figure 4.28).

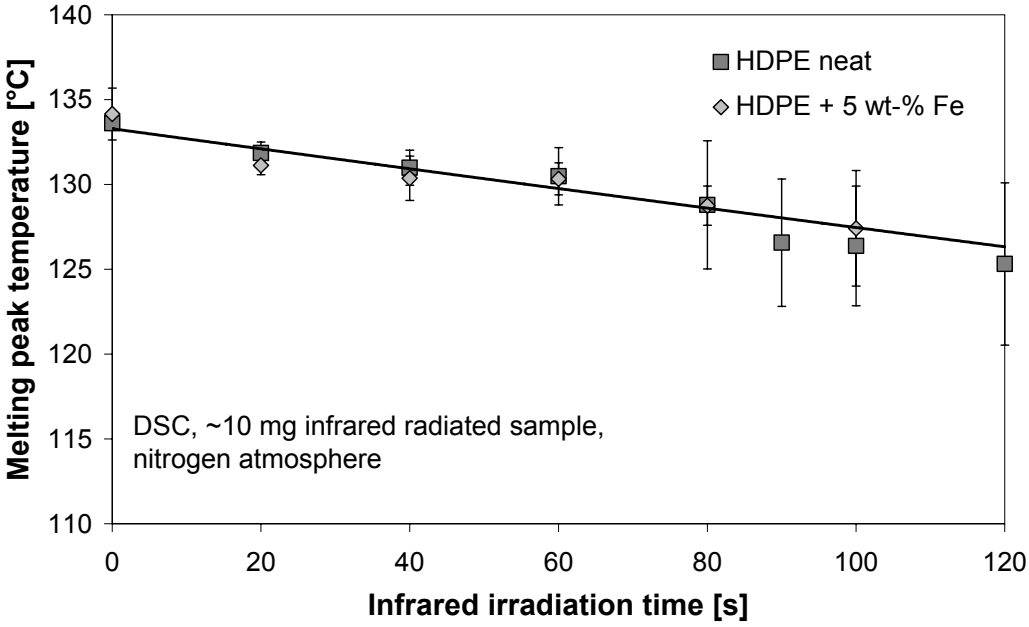

Figure 4.28: Melting peak temperature decrease caused by infrared irradiation

The melting peak temperature decreased quasi-linearly with increasing infrared radiation time in the investigated experimental boundaries. The neat as well as the filled HDPE revealed similar behavior: an influence of the iron particles was negated in this case. The observed declining melting peak temperature conformed to

experiments with long-cycle heated HDPE materials, which were previously investigated by Földes et al. [147]. Other researchers assigned the decreasing effect to chain scissoring and polymeric transformation. In these studies, the infrared radiation led to a reduced melting peak temperature as observed in the presented work [148,149].

In order to relate the degradation induction heating to competing contactless heating techniques, the melting temperature shift was compared: the quickest temperature decrease was reached with laser heating (Figure 4.29).

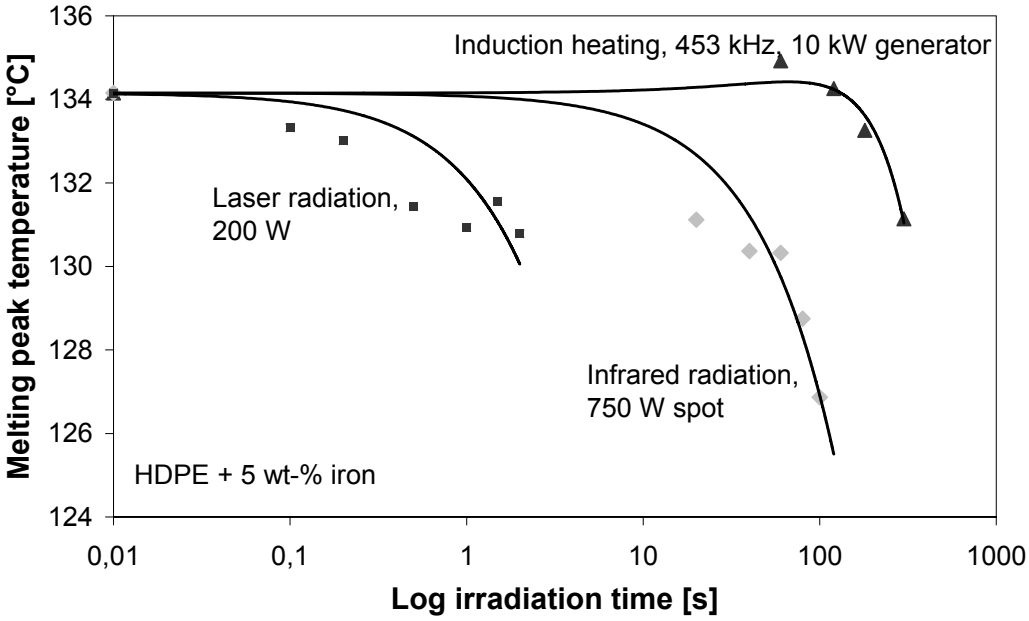

Figure 4.29: Melting peak temperature change of HDPE at different heating methods

Although only 200 W laser power was used, the declining gradient was remarkably high and resulted in a decrease of approx. 4 K after an irradiation time of only 2 s. The infrared temperature drop began one chronological decade after the temperature decrease caused by lasering. The melting temperature reduced approx. 8 K after 100 s. In comparison to laser and infrared irradiation, the intrinsic particle induction heating manifested a different behavior. The melting temperature evolution of a particle induction heated sample increased slightly up to 60 s radiation time. After exceeding this time, the melting peak temperature reduced but still remained higher than its initial state. By reaching 150 s radiation time, a decrease of the melting temperature below its initial state was noticed.

A reason for the melting temperature evolution in particle induction experiments could be explained by an analysis of the temperature evolution of a particle heated sample (Figure 4.30). A complete melting was observed after 90 s. Consequently, the increase of melting temperature up to 60 s was attributed to the lower temperature of the (still non-melted) sample. Long-time heated polyethylene samples possess an increased molecular weight at temperatures below the melting temperature, due to tempering effects [54,55]. The tempering effect was assumed to be the triggering mechanism for the observed moderate melting temperature increase. In contrast, a longer irradiation time led to a higher sample temperature and a reduced melting peak temperature.

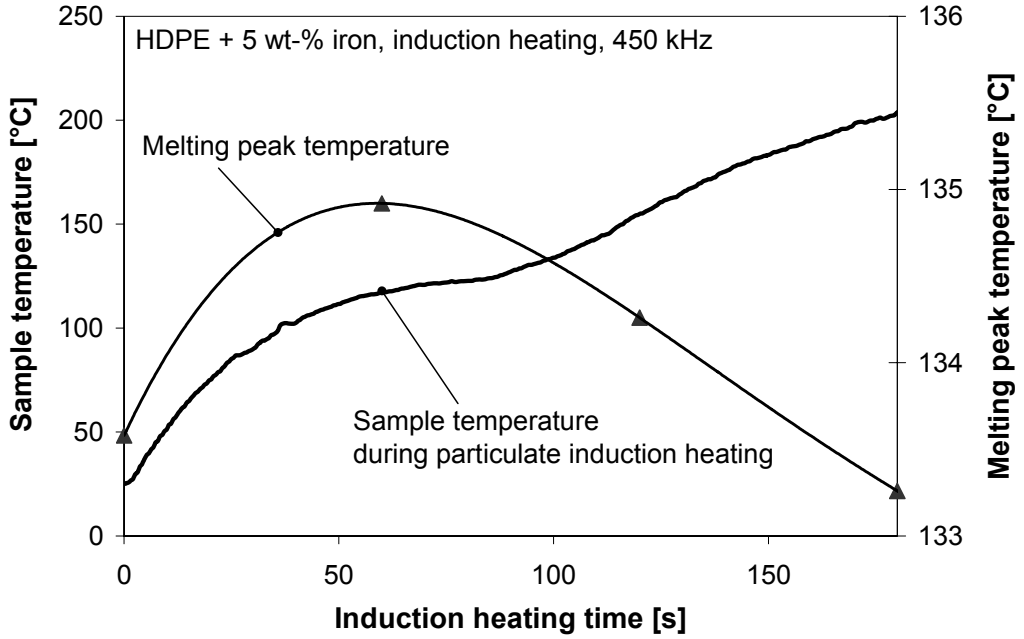

Figure 4.30: Comparison of sample temperature evolution during induction heating and resulting melting peak temperature

In contrast to the melting temperature, no significant relation was detected between degree of crystallization, visible degradation, and radiation time, respectively. The degree of crystallization remained unaffected from the degradation state at 70 to 72 % for the investigated HDPE.

In addition to the mentioned quantifiable reduction of the melting peak temperature, a qualitative difference in DSC measurements of degraded material was detected. A second melting peak was noticed at IR radiation times longer than 80 s which lay

thermally before the primary melting peak (Figure 4.31). The second peak was formed only at higher degradation states and was hence attributed to a morphological polymeric change. The second peak marked a further possibility to qualify the degradation state of HDPE material. Similar observations have been described for PEEK and polypropylene before [150,151] and were also observed with severely laser degraded material. These peaks could not be assessed with induction heated material.

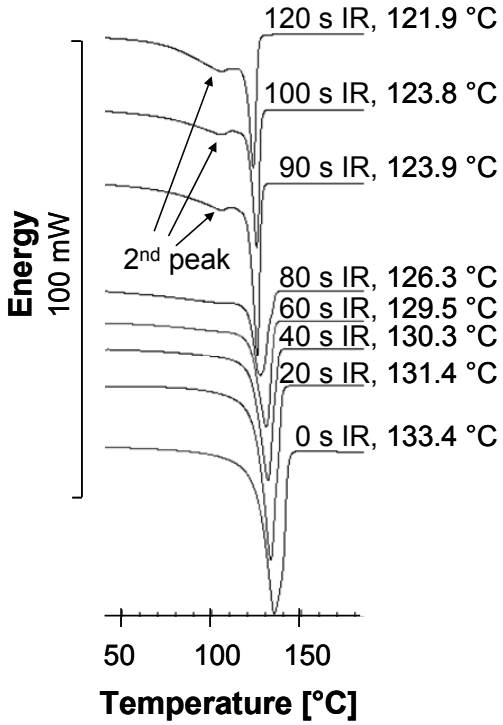

Figure 4.31: Appearance of a second melting peak observed at infrared radiated HDPE and indicating thermal degradation

By comparing a cryo-fractured surface of inductively heated iron doped HDPE with a surface of a non-heated sample, no significant differences were observed. Both samples revealed the same morphology with parts of plate-like structures as well as areas which appear more fractured. In both cases, non-heated and inductively heated, the particles were well embedded in the matrix.

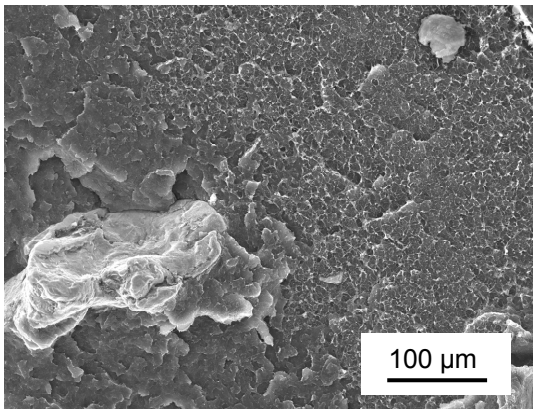

Figure 4.32: SEM image of a non-radiated HDPE sample with iron particles

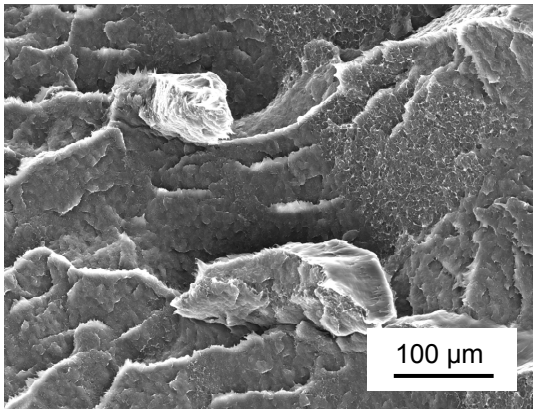

Figure 4.33: SEM image of a cryo-fractured surface demonstrating the matrix morphology around three-minute inductively heated iron particles

4.2 Impact of Susceptors on Matrix Materials

Due to the manifold quantity of tested materials and experimental results, only a representative extract for the investigated relations is presented here.

4.2.1 Tensile Strength

At low filler degrees of 5 wt-%, the tensile properties of matrixes were only marginally affected (Figure 4.34). Neither the maximum stress nor the Young's modulus changed significantly. In contrast, high particle fractions led to an embrittlement of the polymer, which was best observed at carbon black doped samples. The strain at maximum stress reduced visibly, whilst Young's moduli as well as tensile stress increased marginally. This observation was attributed to the particles representing voids within the matrix which weakened the compound. The more void forming particles, the lower was the recorded strain. A trend of this relation was found for all tested samples.

The described particle influence on tensile properties was obtained from HDPE samples and was similar for PA6 samples. The maximum stress for the PA based compounds was assessed in the range of 45 – 51 MPa with a strain of 15 – 20 %. Young's modulus varied in the range of 1.7 – 2.1 GPa.

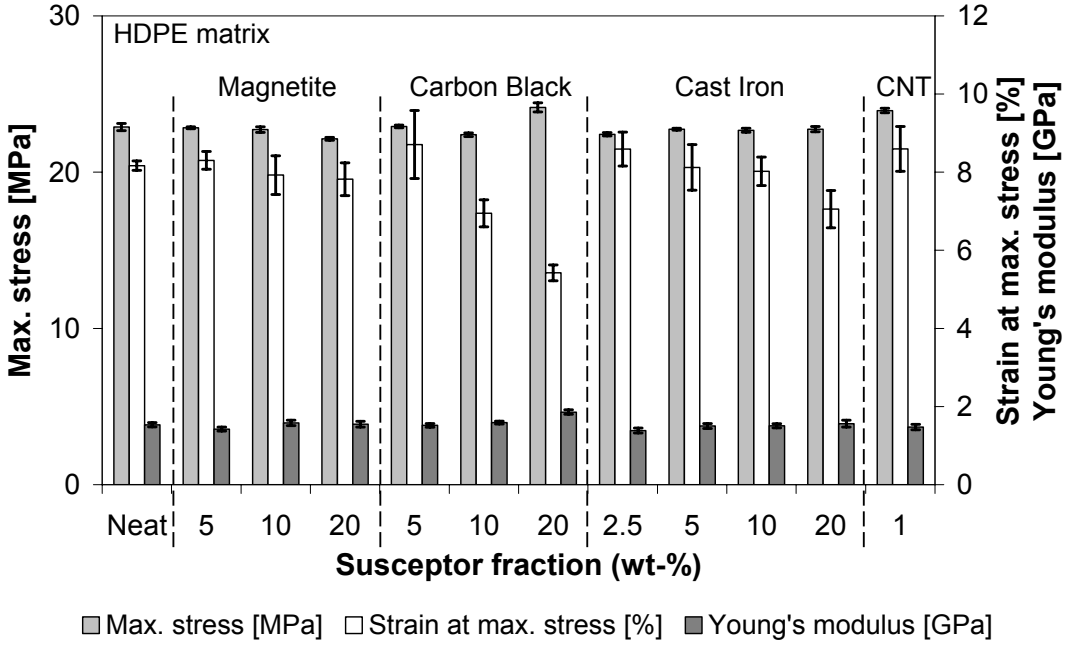

Figure 4.34: Tensile test results of particle doped HDPE matrix material

4.2.2 Notched Impact Strength

The particle fraction had an expected significant negative effect on impact resistance. The notch impact strength was reduced for all tested susceptor materials with increasing filler degree. In the presented example of HDPE composites, the impact strength declined from 7.8 kJ/m² to a minimum of 2.5 kJ/m² for 20 wt-% carbon black doped samples (Figure 4.35). In the case of cast iron particles, a decrease of around 30 % was recognized.

The lower impact resistance can be explained by regarding the particles as contaminants in the matrix, which is a homogeneous structure in neat state. Similarly, the impact strength of PA6 reduced from 4.3 kJ/m² to 2.7 - 3.2 kJ/m² resulting in a total decrease of 25 to 40 %. Also in this case, the incorporation of higher filler fractions led to the highest reduction.

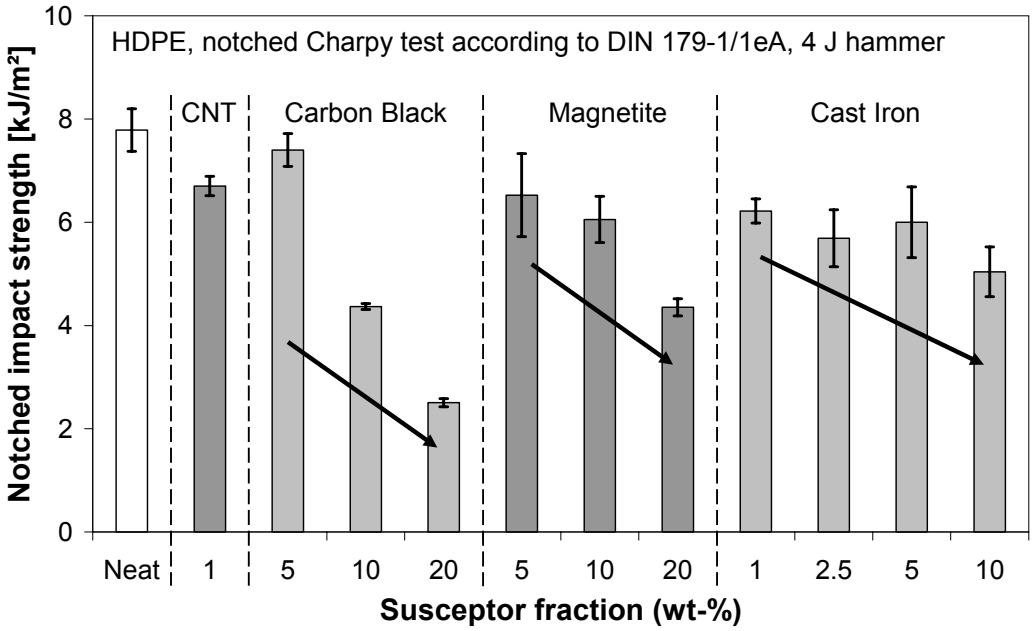

Figure 4.35: Charpy impact strength for HDPE composites (selection)

For investigating the influence of particles on the failure behavior, a SEM analysis of the surface morphology after an impact test was performed. The images revealed a common failure mode of the HDPE matrix: the matrix disintegrated by slipping-off of disk-shaped parts (Figure 4.36). The mechanism was observed around particles as well as in areas without particles. In contrast to particle-free areas which revealed a smooth micro-structure of the disks, the matrix was found coarser around particles (Figure 4.37). This morphology change was attributed to a higher stress in the soft matrix in the proximity of the tough metallic particles. In case of an impact, the particles led to stress concentrations around themselves which overloaded the surrounding matrix and resulted in a higher matrix deformation. The higher deformation led to the formation of small peaks which appear coarse in the SEM photographs.

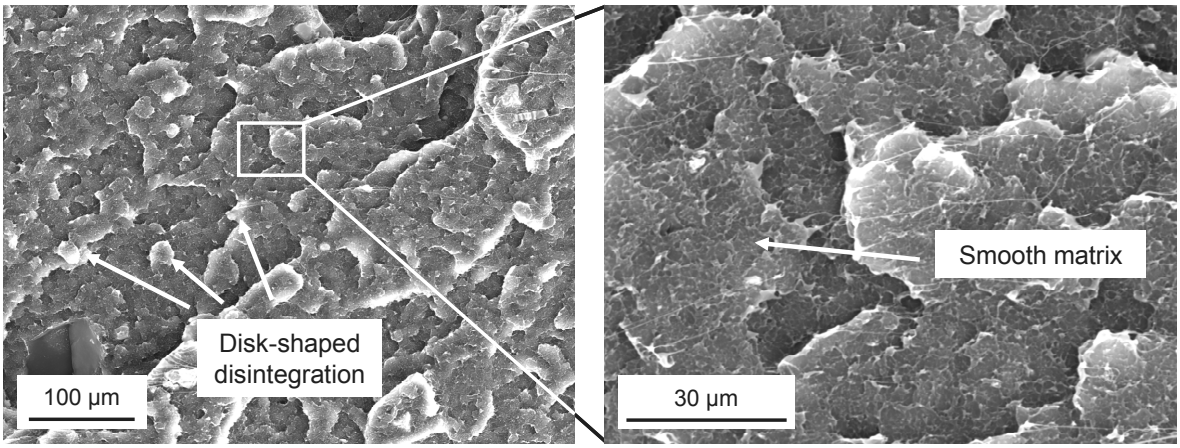

Figure 4.36: Surface morphology after an impact test of a 5 wt-% magnetite doped HDPE

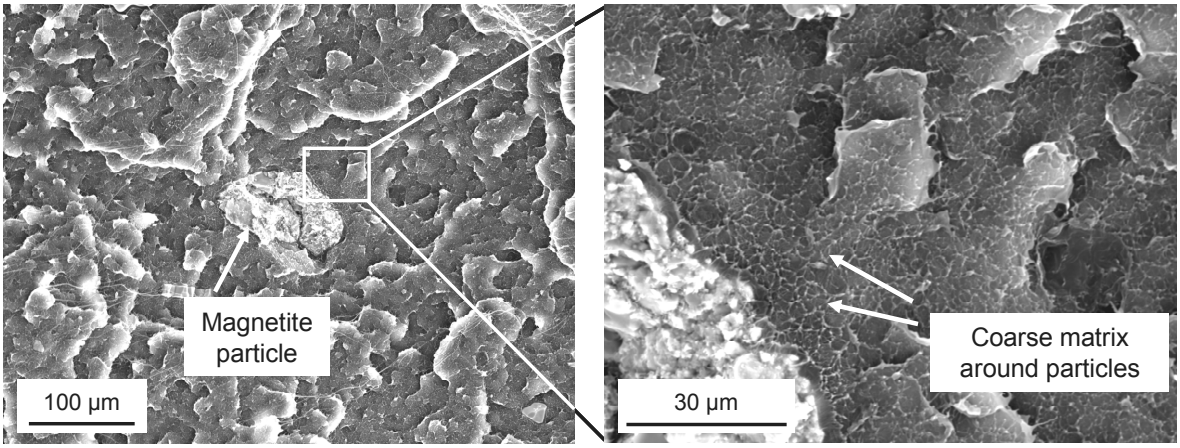

Figure 4.37: Surface morphology in the proximity of a magnetite particle of an impact tested HDPE sample with 5 wt-% magnetite doping

4.2.3 Melting Temperature and Crystallinity

The impact on melting temperature and crystallinity was analyzed by the second heating loop within a differential scanning calorimetry scan. For HDPE samples, the melting temperature was found varying around the temperature of neat material at 134.0 °C (Figure 4.38). For most of the examined particle filled HDPE composites, the melting peak temperature was slightly reduced up to 2.5 K.

The crystallinity degrees of HDPE samples were measured in the range of 75 ± 2 % which, thus, indicated that the crystallinity was not affected by the incorporated particles.

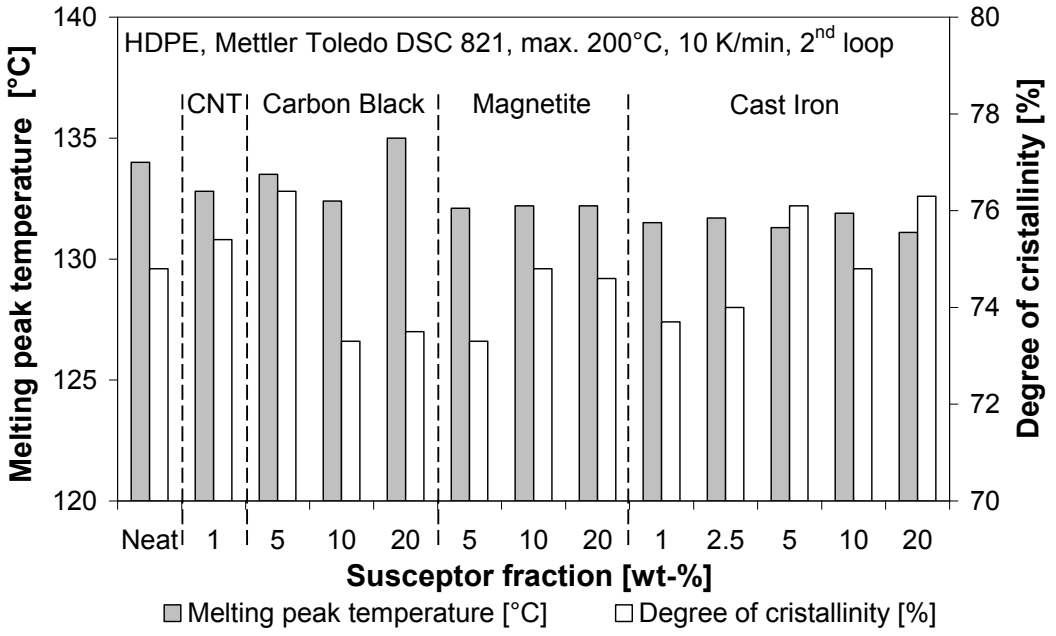

Figure 4.38: DSC results of particle doped HDPE composites (selection)

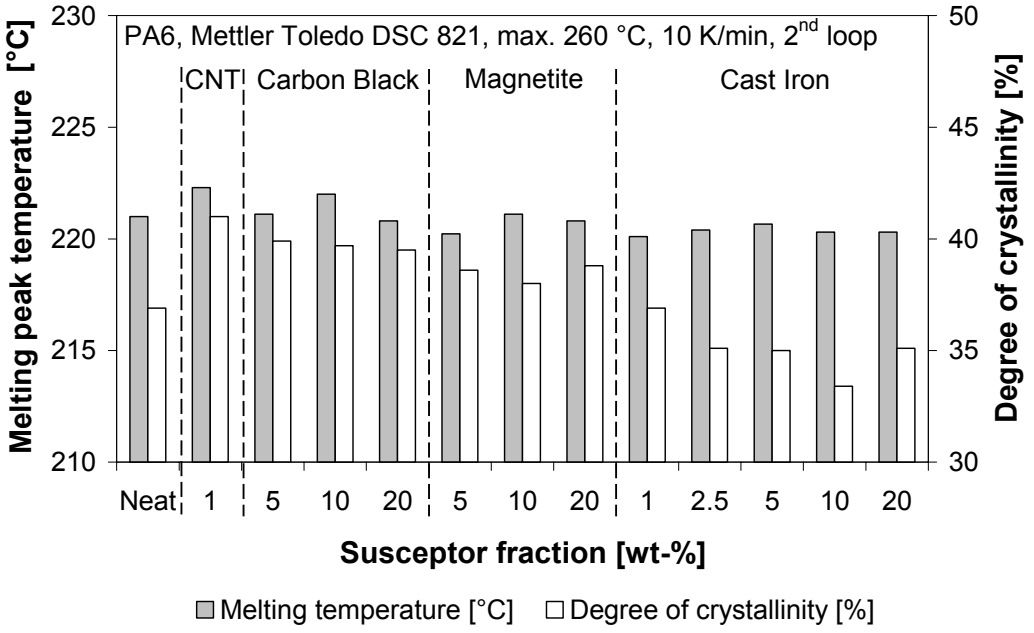

Figure 4.39: DSC results of particle doped PA6 composites (selection)

Like observed with HDPE, the melting temperature of PA6 was slightly affected, but more or less scattered around the value of neat material at 221.0 °C (Figure 4.39). In contrast to HDPE, the crystallinity degree increased with low particle fraction and decreased with higher particle fractions. The crystallinity expanded by 4 % for 1 wt-%

CNT incorporation from the neat value of 37 %. This growth could be observed with all low doped PA6 samples. Nevertheless, the particle influence was regarded as marginal in the tested limits.

4.2.4 Corrosion and Long-Term Stability of Particle Doped Matrixes

Although cast iron revealed to be the best option for particulate induction susceptors in terms of heating efficiency, its ability to react with other substances was assumed to be a knock-out criterion. HDPE samples doped either with cast iron or magnetite in filler fractions of 5 to 20 wt-%, respectively, were examined in contact with artificial sea water. A series of non-immersed samples was used as a reference (ref) for tensile and induction heating tests.

A sea water contact with cast iron doped samples resulted in a visible change of the surface particles in changing their color from black to a rusty red. The expected iron corrosion visibly occurred after a relatively short immersion time of only 24 – 36 hours. This color shift was not observed with magnetite doped samples which indicated that the non-reactive magnetite have not had interacted chemically.

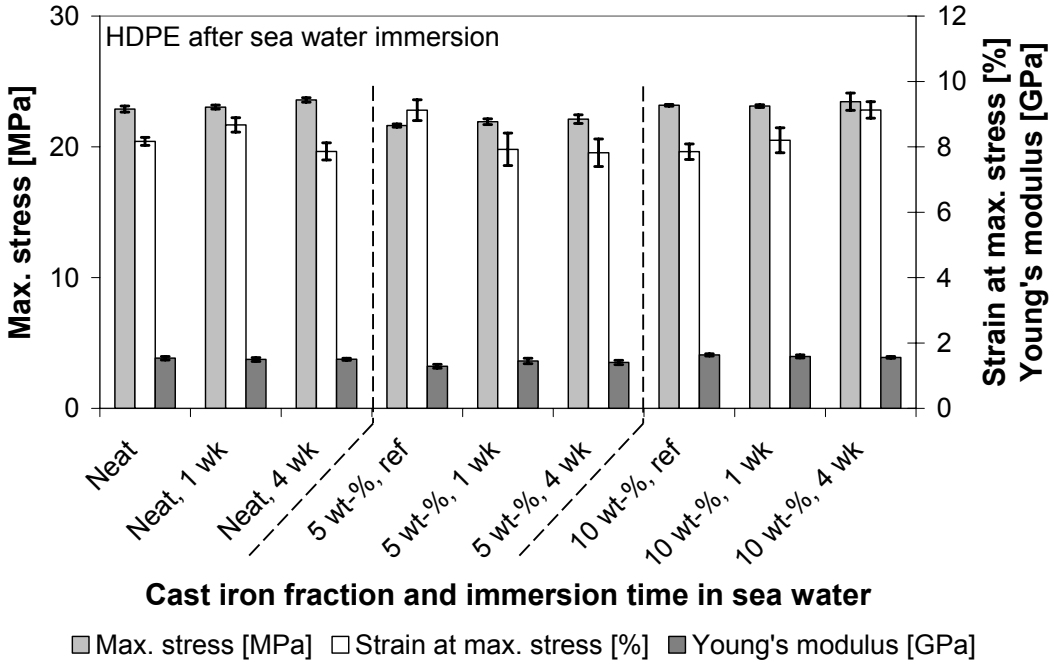

Figure 4.40: Tensile properties of iron doped HDPE after sea water immersion

From the tensile tests no significant difference in sample properties could be observed (Figure 4.40, Figure 4.41). Although a matrix embrittlement was assumed,

which Andrady best observed at a decreasing tensile strength and strain rate for polyethylene in natural sea water, the results were no clear evidence of this [152]. By concluding from the obtained tensile test results, the used susceptors, especially the corrosion of the cast iron, did not negatively affect the matrix properties.

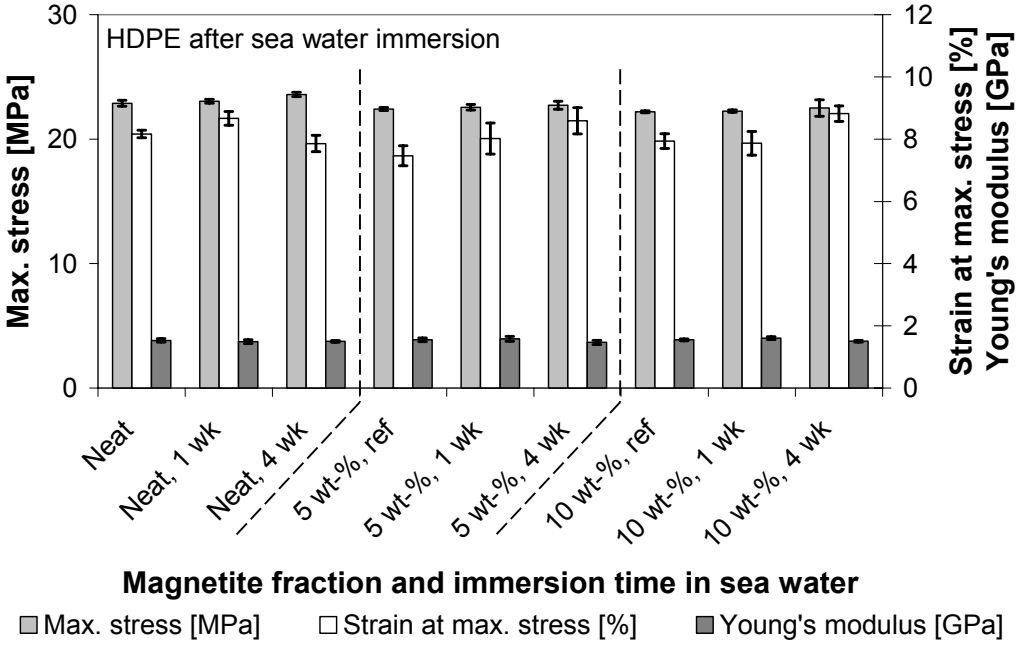

Figure 4.41: Tensile properties of magnetite doped HDPE after sea water immersion

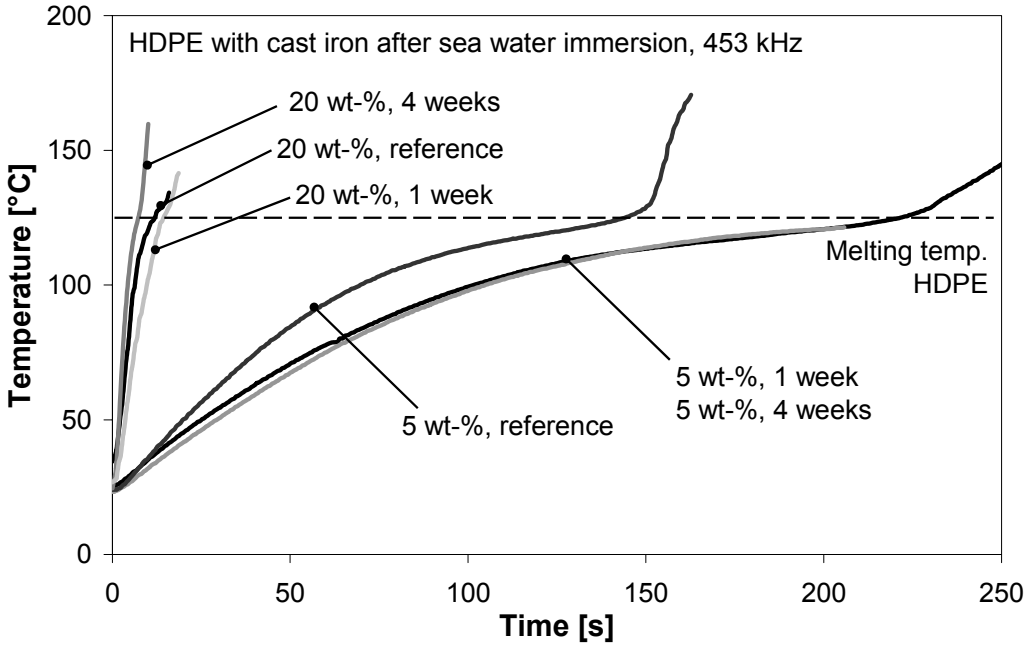

Figure 4.42: Induction heating experiments with sea water immersed HDPE samples

Heating experiments with corroded cast iron doped HDPE showed a slight reduction of efficiency with low-doped samples (Figure 4.42). The period to reach the melting temperature prolongated for approx. 50 %. This effect was even observed for samples which had been immersed in sea water for only one week (1 wk). The heating behavior did not change with increasing immersion time. For high iron doped HDPE, the effect was less dramatic: the recorded temperature evolution statistically spread around the obtained reference curves.

The results indicated that the cast iron corrosion generally reduces the heating efficiency as it has been reported for nickel particles before [130]. In case of higher filler degrees, the corrosion effect is less dramatic and can be neglected since only particles at the surface are affected (compare Figure 4.43 and Figure 4.44).

For an industrial application, the ferrous corrosion will obviously not be accepted by potential customers, and the manufacturer will decide, in this case, for the non-reactive magnetite as susceptors while accepting longer heating times.

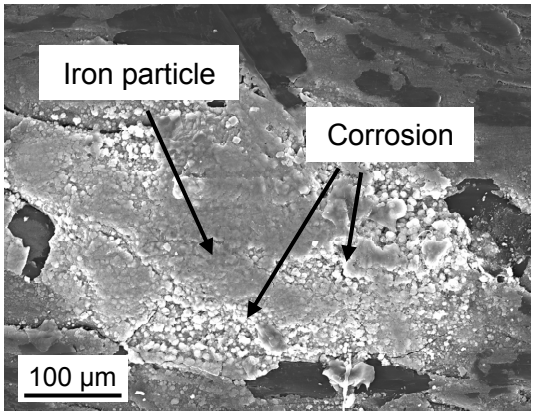

Figure 4.43: Corroded iron particle on the sample surface after sea water immersion

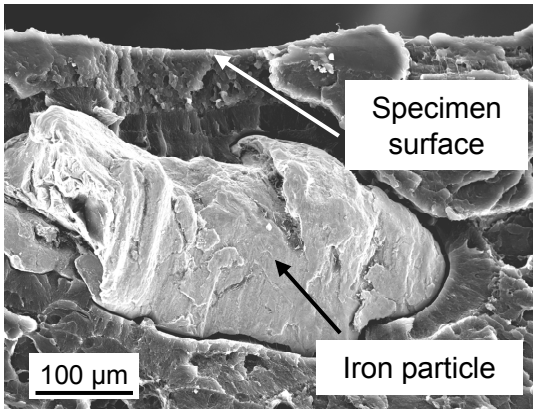

Figure 4.44: Cross-section of a specimen after sea water immersion test revealing a non-corroded iron particle in the vicinity of the surface

4.3 Particle Based Induction Heating within Polymer-Polymer Systems

The objective of this thesis was the use of induction heated susceptors for the heating of polymer-polymer composites. Therefore, the results achieved with doped matrix systems were transferred to polymer-polymer systems.

A compound consisting of a PP with 33 vol-% PET fibers provided a nominal peak melting temperature gap of 85 K (Figure 4.45) and was used for verifying the

feasibility of particle induction with SRP materials. While observing the corresponding DSC record, the melting peak temperatures and the melting zones between PP and PET were noticed to lie in a significantly different range from each other, which allowed a process window of minimum 50 K.

The process window is characterized by a shapeable matrix and a solid reinforcement. For the applied PP/PET, the window begins at the end of the matrix melting phase at approx. 180 °C and ends before the PET fibers begin to melt at approx. 230 °C. The energy curve furthermore reveals that the PP matrix melting begins at 130 °C, which is more than 30 °C lower than the melting peak temperature given in literature [27].

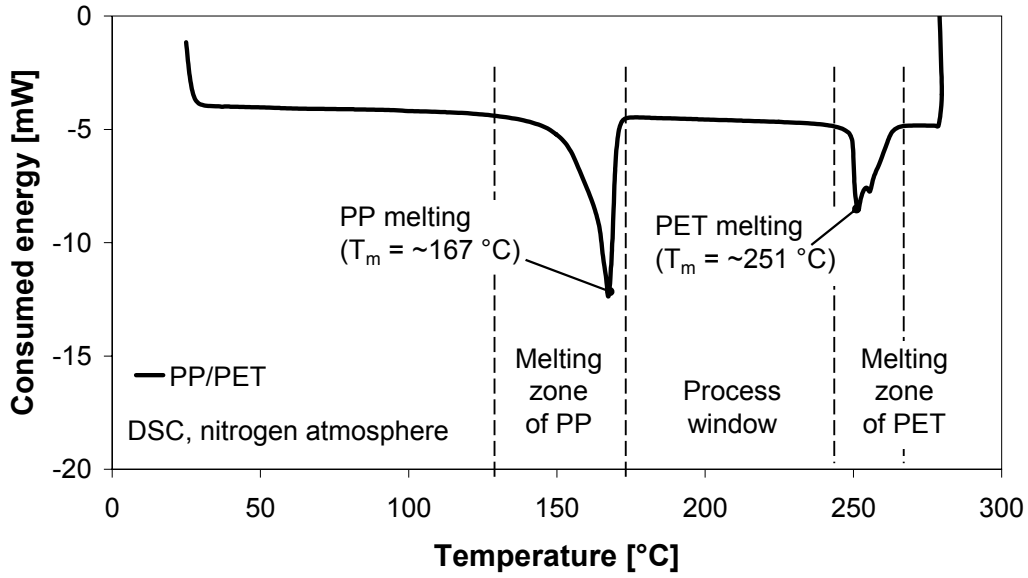

Figure 4.45: Recorded energy curve of a typical DSC measurement during the melting of a PP/PET composite

The from the energy record determined process window with the temperature range of approx. 50 K is implied in the temperature evolution of a heating experiment with iron doped PP/PET (Figure 4.46). The process window conforms to the changes of the molecular state of the matrix and the reinforcement which is indicated by the respective flattening of the temperature curve.

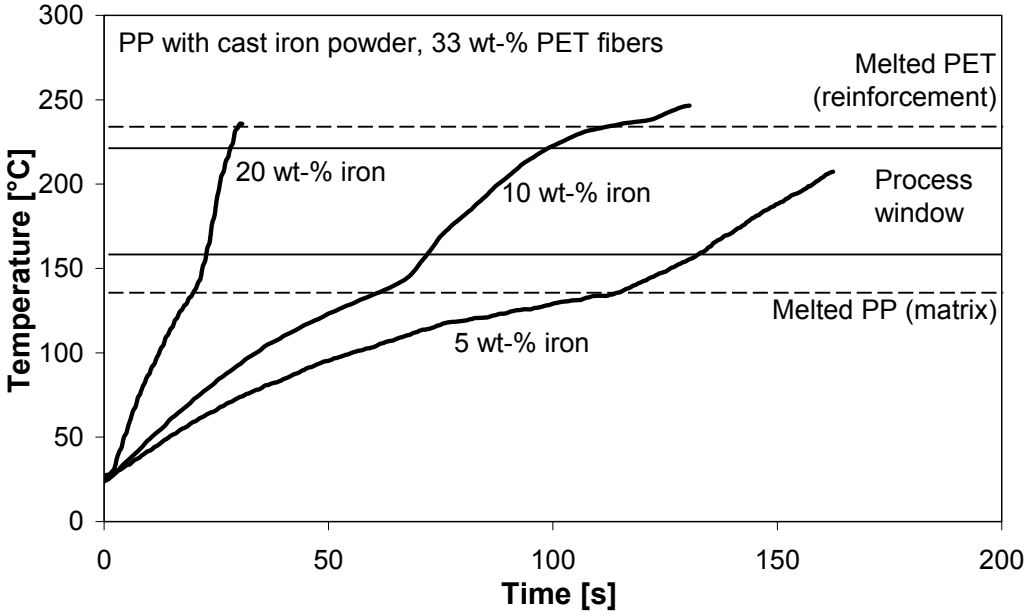

Figure 4.46: Melting of PP/PET by means of particle induction at 453 kHz

With increasing susceptor fraction, the samples reached the specific process states of matrix melting, process window, and reinforcement melting faster. This result correlated to the findings with non-reinforced matrix systems. An increased heating speed causes a shorter period of time, in which the sample is in processible state. Especially with 20 wt-% iron doping, the sample only remained 7 s in this condition. For an industrial application of this process, an accurate time control will be mandatory. Although the reduction of filler fraction extended the time within the process window, an exceeding of the reinforcement melting temperature is generally possible and must be avoided. The external approach for this problem consisted of controlling the inductive field by simultaneous reduction of the generator power. By adjusting the generator energy and consequently the magnetic field strength with the help of an additional controller and an external pyrometer, the sample temperature could be maintained at the lower border of the process window (Figure 4.47).

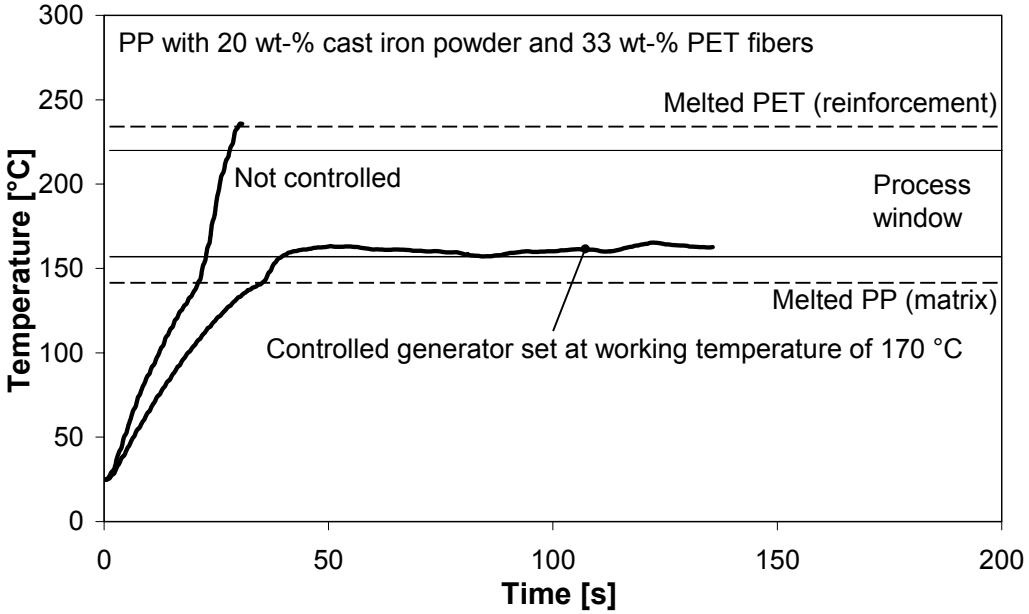

Figure 4.47: Controlled induction heating of polymer-polymer organic sheet

A possibility to limit the heating without an external control can be realized by means of susceptors, which possess a Curie point in range of the process window (compare chapter 2.4.3). Particles with the described properties existed but they were only available in small quantities at a high price. For the use with mass production SRP, they would be economically only reasonable if they were offered for a lower price and higher availability.

A polyolefin-based SRP manufactured from HDPE and 50 wt-% PP fiber reinforcement offered a significant lower process window than a PP/PET composite. The DSC measurement even revealed the energy of matrix and reinforcement melting almost overlapping (Figure 4.48). An effective process window, as described before with the PP/PET, occurs between 140 and 150 °C.

The matrix melting in case of HDPE/PP, which was indicated by a re-increasing heating rate, was found in a more progressed instant of time than the model system PP/PET. This noticeable behavior was traced back on the low melting temperature gap since the melting of PP was associated with latent heat. The latent heat has to be covered by the energy within the system and, thus, resulted in lower heating rates. As had been observed with non-reinforced doped HDPE, the melting started before the peak melting temperature. At the same time, the PP fibers lose their

stretched state, which was observed at shrinkage in the heated zone. As mentioned before, the shrinkage was attributed to the softening effect within polypropylene and caused a disintegration of the compact compound. This experiment resulted in additional air voids, which were of thermal insulating character. For an industrial application, a sample clamping is mandatory.

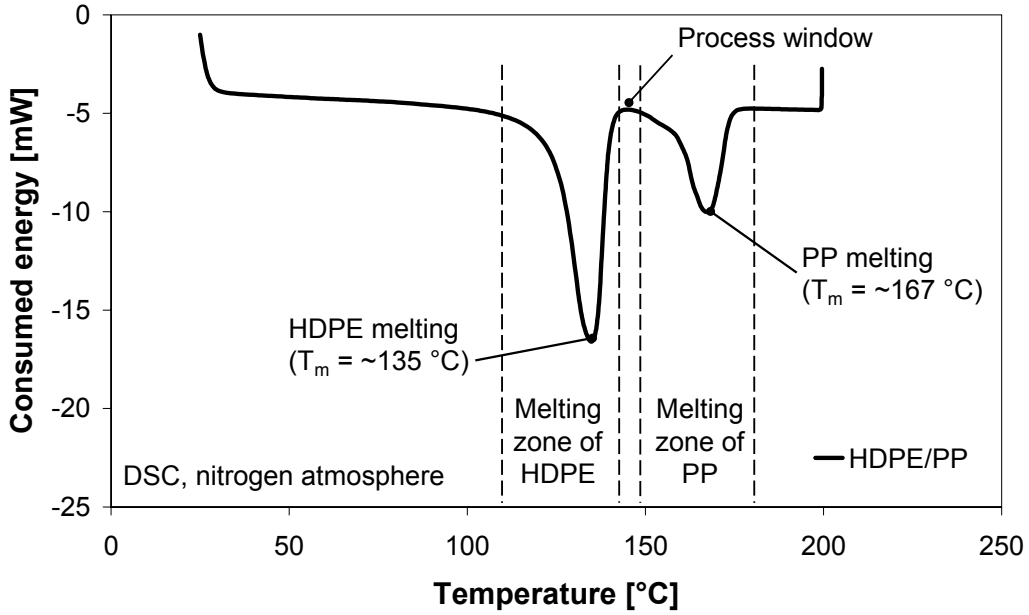

Figure 4.48: Energy curve of a differential scanning calorimetry of HDPE/PP composite containing 5 wt-% cast iron particles

The influence of susceptor doping occurred as expected: a higher doping led to faster heating and melting of the compound. The induction heating of 20 wt-% doped material resulted in an almost instant overheating of both, matrix and reinforcement, in the center of the specimen surface.

In contrast to the DSC determined overlapping melting regions of HDPE and PP, the melting could be clearly distinguished from each other, indicated by the compound with 10 wt-% cast iron doping. The temperature evolution displayed a degressive trend when the matrix starts melting and changes to a progressive increase when leaving the melting zone. Although the fiber melting did not reveal the same distinctive degression of the temperature evolution, an analogue behavior was observed when the fiber melting region was approached. The less distinctive behavior was attributed to the lower necessary latent heat needed for crystallite melting and derived from the corresponding energy record of the material. The

necessary energy for melting HDPE was more than twice the amount needed for PP within the applied sample.

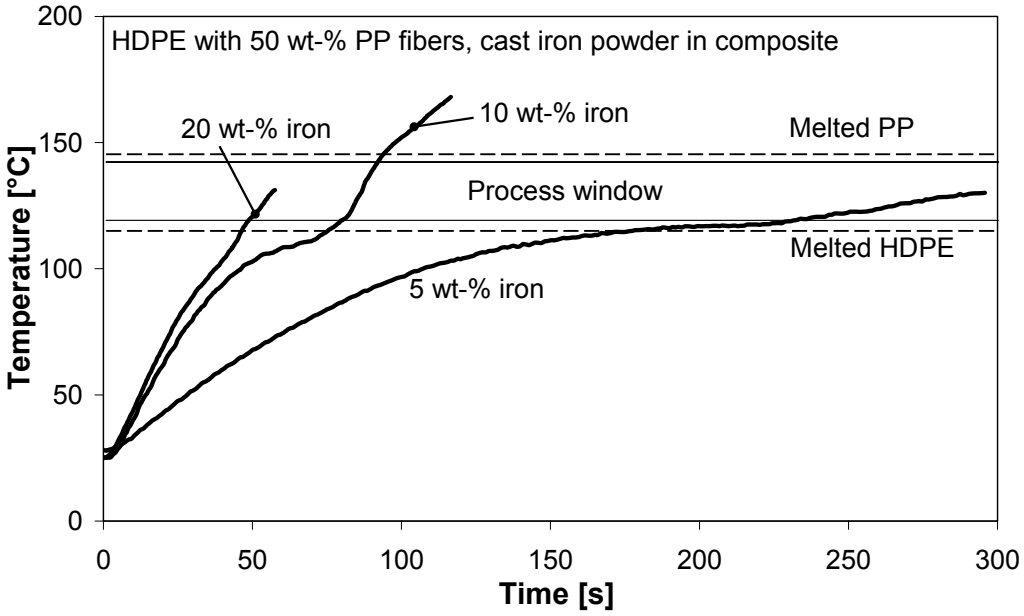

Figure 4.49: Temperature evolution of an inductively heated PP reinforced HDPE sheet

From the measurements at the surface which were opposite to the coil, a suitable process window was found between approx. 130 and 140 °C. The process window was of the same size (10 K) as the expected range determined by DSC. The previously determined temperature values could be exactly validated on the coil side of the specimen. The difference between the surfaces was attributed to the higher magnetic field strength in an area closer to the coil. This finally resulted also in a higher heating efficiency.

5 Simulation of Particle Induction Heating

A two-dimensional semi-empiric, transient, thermo-electromagnetic model based on simplified Maxwell equations was established to improve the understanding and investigation of complex problems like heat distribution, hot spot effects, and reinforcement melting. The primary objective for the setup of the model was the investigation of the selective heating performance of particle induction. Since the developed heating method works on an intrinsic level, the melting processes within the material were not observable during an experimental approach. Within the performance investigation, the focus especially lay on the analysis of the heating effect of the susceptors on the polymer reinforcement and the emerging reinforcement melting.

5.1 Mathematical Description

From the basic Maxwell equations, a simplified approach for the hysteresis heating of a magnetic volume was used for the modeling of the induction heating process in a time-varying field.

The magnetic work W_m in a volume V is generally described by equation (5.1), which depends on magnetic flux density B and magnetic field density H. The magnetic power P_m derives from (5.1) when dividing it by a time period ∂t (5.2) [153].

$$W_m = \int_V \left(\int_0^B H \cdot dB \right) dV \tag{5.1}$$

$$P_m = \int_V H \cdot \frac{\partial B}{\partial t} dV \tag{5.2}$$

Equation (5.1) corresponds to the enclosed area within the hysteresis curve of the susceptor volume, which represents the magnetic loss energy [65]. Equation (5.2) describes how often the hysteresis curve is cycled within a time step. Consequently, the hysteresis loss is closely connected to the frequency f. Since the enclosed area of the hysteresis curve can be calculated from either B or H, the integral may be

changed. With a constant susceptor volume, the heating power by hysteresis losses, P_H, can be calculated by (5.3) as also mentioned before in chapter 2.4.1.1 [67,68].

$$P_m = V \cdot f \cdot \int_0^H B_{(H)} dH = V \cdot f \cdot \frac{\mu \cdot H^2}{2} = P_H \tag{5.3}$$

The magnetic flux density of a spiral coil is described by the Biot-Savart law (5.4) [68]. According to this equation, the magnetic flux density of a coil in vacuum, B_0, depends on the number of coil windings n, the coil current I_c, the coil radius r_c, and the coupling distance r.

$$B_0 = n \frac{I_c \mu_0}{2} \frac{r_c^2}{\left(r_c^2 + r^2\right)^{\frac{3}{2}}} \tag{5.4}$$

Equation (5.4) can be combined with (5.3) by the relations (5.5), (5.6), and (5.7) [63, 65,68].

$$B = \mu H \tag{5.5}$$

$$\mu = \mu_0 \mu_r \tag{5.6}$$

$$\mu_r = \frac{B}{B_0} \tag{5.7}$$

The characteristic value μ_r represents the relative magnetic permeability. The hysteresis loss power of a single magnetic volume which is penetrated by an electromagnetic field from a spiral coil is calculated by (5.8) [67,68].

$$P_H = \frac{V \cdot f \cdot n^2 \cdot {I_c}^2 \cdot \mu_0 \cdot \mu_r \cdot r_c}{8 \cdot \left(r_c^2 + r^2\right)^3} \tag{5.8}$$

By concluding from equation (5.8), the geometric layout, including the volume and the coupling distance, is essential for the electromagnetic model. Crucial basic conditions are also represented by the magnetic properties of the susceptor material.

For the thermal part of the model, the general heat equation for conduction was used (5.9) [57,153].

$$\rho c_p \frac{\partial T}{\partial t} - \nabla \cdot (k \nabla T) = Q \tag{5.9}$$

Within this equation, the temperature evolution T is mainly dependent on thermal conductivity k and the heat capacity c_p, as well as the material's density ρ. The variable Q representing heat sources is the link between the thermal and the electromagnetic model (5.10).

$$Q = P_H \cdot t \tag{5.10}$$

The distinct thermal properties of each polymer material, k and c_p, were used as temperature dependent isotropic values and were taken from literature (see appendix) [154]. The heat transfer between components of the composite was regarded as ideal. For reducing computing efforts, convective as well as thermal radiation losses were neglected in the simulation.

5.2 Model Setup, Validation, and Simulation Results

A simulative approach for the investigation of particle induction heating in combination with polymer-polymer composites was pursued with the help of Comsol Multiphysics (version 3.5 a) software. The three-dimensional "plate-coil problem" was simplified by choosing a suitable two-dimensional simplified model (Figure 5.1).

The simplification consisted of a single coil cross section and an appropriate section of the plate. The dimension ratios of the coil and sample cross sections were equivalent to the ratios specified by the experiment. Within the sample cross section, polymer fibers and particulate susceptors were modeled. The distribution of the susceptors was analyzed in a randomized, thus well distributed, state as well as in an agglomerated condition. The surrounding air was incorporated in the model as "air box". A thermal and a magnetic continuity were chosen as boundary settings between all implied elements. Since the coil was constantly cooled in the experiment, the coil temperature was considered as constant on room temperature level in the

model. At the edges of the air box, a magnetic as well as a thermal insulation was applied.

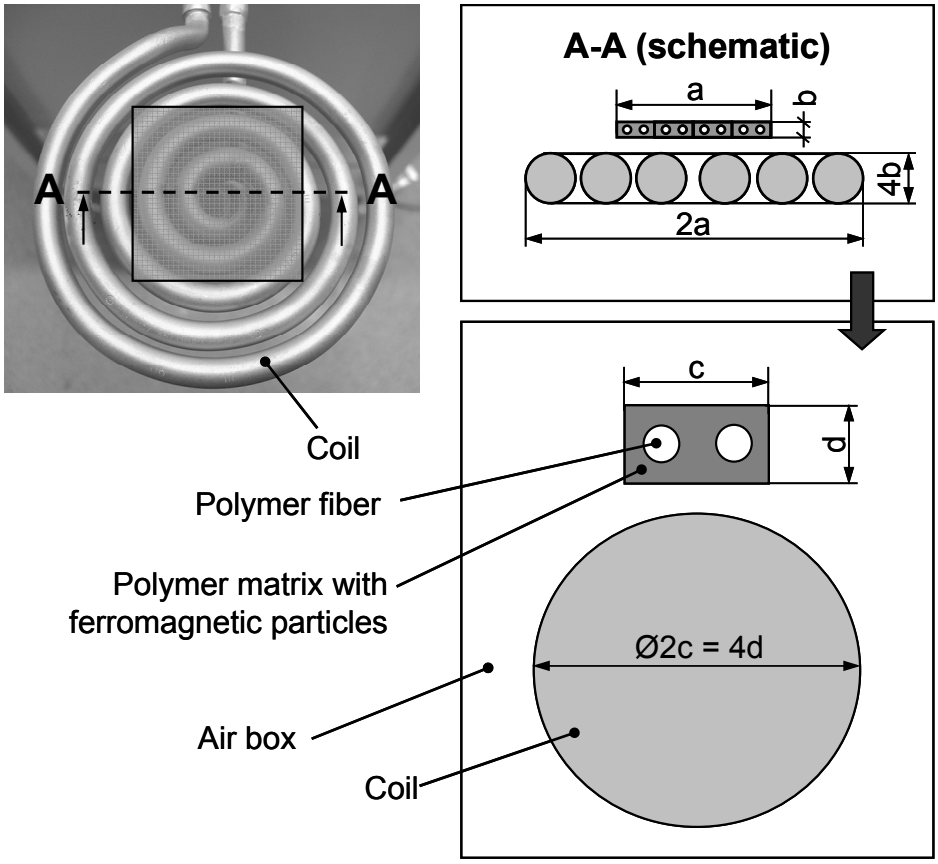

Figure 5.1: 2D model development

For meshing, second-order Lagrange elements in triangular shape were selected which are a standard for multiphysic problems and have no need of an optimization of computing time [153]. For greater accuracy, the mesh was refined in the region around susceptors and within the polymer sample (Figure 5.2).

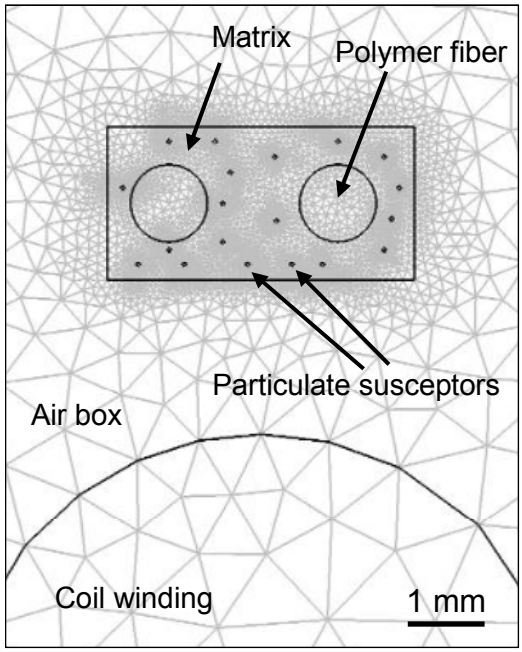

Figure 5.2: Illustration of the meshed model (detail section)

The model was once configured by an empirical fit of the unknown current in the coil for a distinct experiment with HDPE and 5 wt-% cast iron particles at a frequency of 453 kHz and a coupling distance of 2 mm (Figure 5.3).

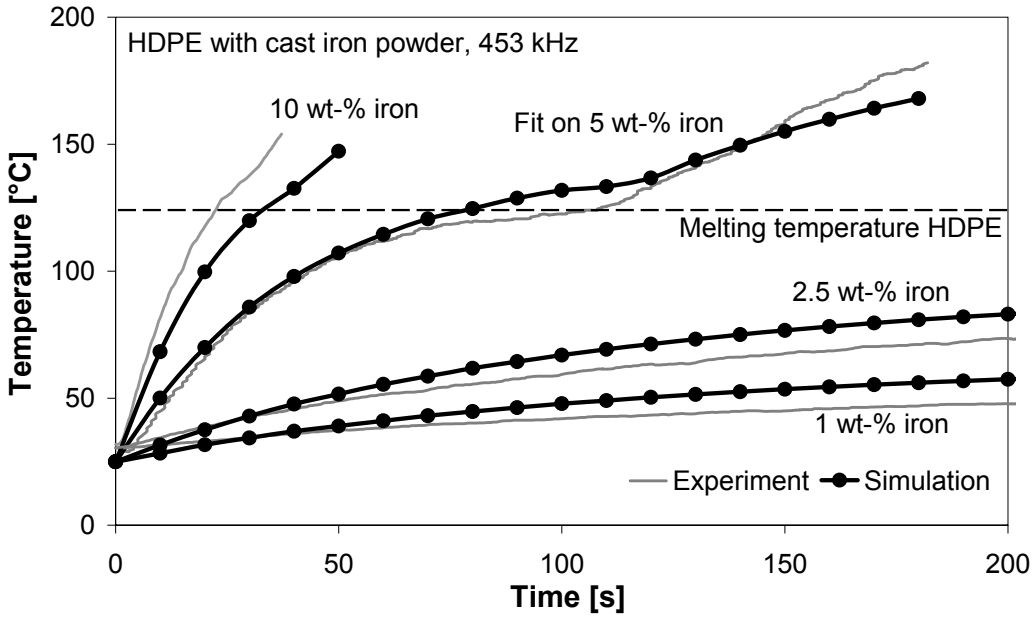

Figure 5.3: Validation between model and simulation of HDPE specimens with different filler fractions of cast iron particles

The current was used as a fit parameter due to the problematic measurement of the coil current in the experiment and the knowledge about losses within oscillating

induction setups [142]. The current fit was subsequently applied to all other simulations. By using the values from the fit, a high agreement of the model was also observed for other filler fractions. The deviation lies between 10 and 15 %, which was considered a sufficient approximation.

In the following analysis, the model was validated with several experimental setups, as for example, the influence of coupling distance (Figure 5.4). The experimental results confirmed the proper working of the model.

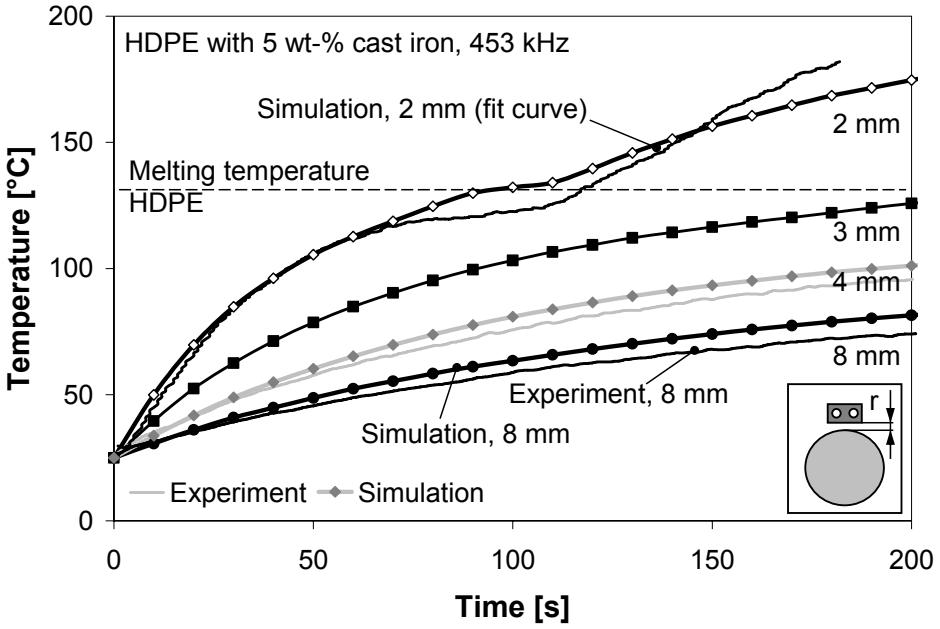

Figure 5.4: Simulation of coupling distance influence on temperature evolution of particle doped HDPE

The model realized the possibility for investigating the problem of hot spot formation in a polymer-polymer material (Figure 5.5). It was examined whether a hot spot in the coil-close region of a HDPE matrix material with 5 wt-% iron doping affected a melting of the 30 vol-% polypropylene reinforcement. The fiber diameter was set to 1 mm. For the simulative approach, the same parameters of the experimental series were used, including a frequency of 453 kHz and a coupling distance of 2 mm. The specimen's thickness was 2 mm.

The model pointed out that the matrix melting (at 135 °C) of the whole sample was reached at t_0 = 160 s. At this stage, the material should be processible, thus, it was shapeable with the reinforcement still intact. A hot spot was already noticeable in the

expected coil-close zone and even near to the temperature, at which the fibers tend to melt. During the following process seconds, the hot spot increased, and also the fibers were exposed to a temperature of 150 °C and above (yellow color), which lay in the beginning fiber melting range (see Figure 4.38). 60 seconds after the matrix melting point had been reached, the first spots were appearing, which were hotter than the nominal fiber peak melting temperature at 165 °C. The temperature at the fiber matrix interface reached 160 °C and exceeded the melting temperature after 100 s.

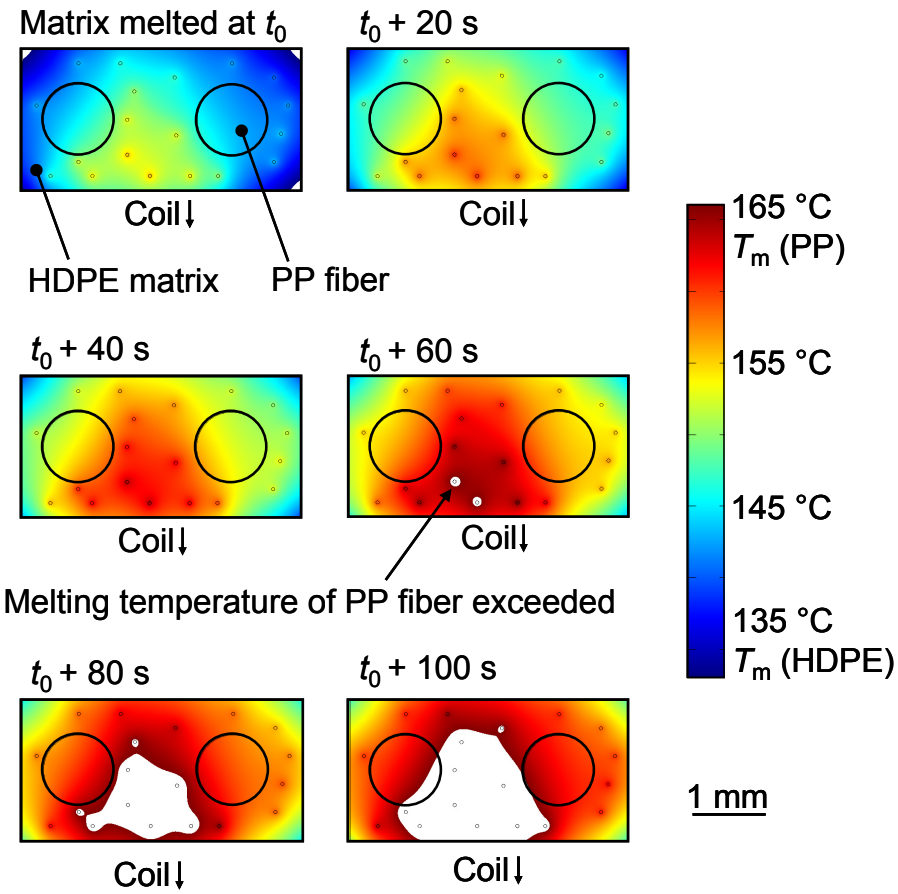

Figure 5.5: Temperature evolution of a HDPE/PP (fiber diameter 1 mm) composite containing 5 wt-% cast iron particle during particle induction heating at 453 kHz

The simulation uncovered a process window of approx. 60 to 80 seconds, which lay in the same range as the experimental results for the corresponding HDPE/PP composites. The analytical experiment indicated that selective heating was not acting like it had been expected. As predicted, the main energy input occurred in the matrix through the susceptors and led to a local heating. But the heat energy was distributed by conduction, which also affected the embedded reinforcing fibers.

Moreover, the model allows a chronological prediction of hot spot appearance and fiber overheating. The prediction can serve to define a process interruption point to preserve the intactness of the fibrous polymer reinforcement.

A significantly worse heating emerged by an inhomogeneous distribution of susceptors and agglomerates, especially in a fiber near zone. This behavior was demonstrated exemplarily at a HDPE/PP composite with 5 wt-% cast iron particles (Figure 5.6). Without proper susceptor dispersion, the reinforcement melted faster than the matrix, whereas the same amount of susceptors achieved a homogenous heating in dispersed state. The resulting heating was more effective and a processible compound was reached after 140 s.

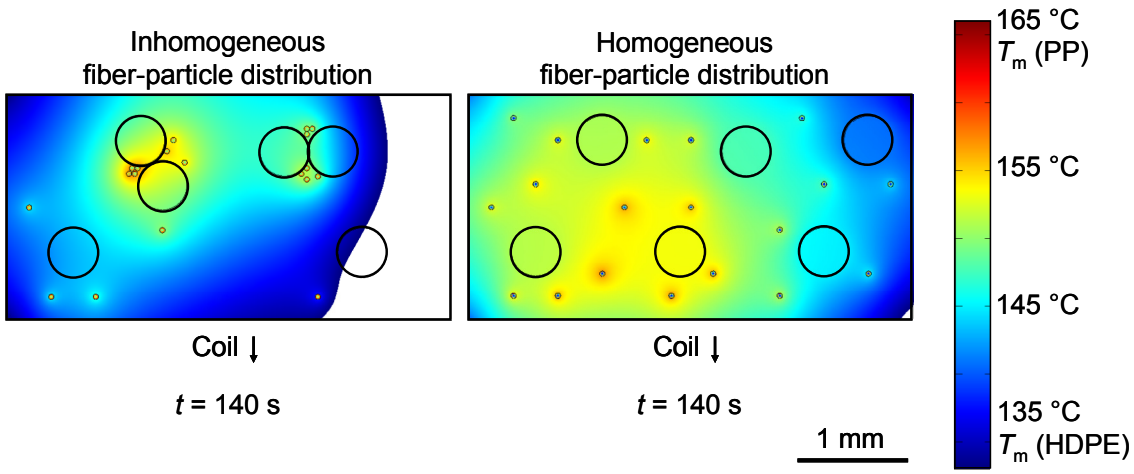

Figure 5.6: Heat distribution of PP fiber (diameter 0.5 mm) reinforced HDPE with an inhomogeneous (left) and a homogeneous (right) distribution of 5 wt-% iron particles

By concluding from the simulative results, the degree of susceptor dispersion as well as a homogeneous fiber distribution are of eminent relevance for the success of the process by limiting the presence of hot spots. The selective melting is only valid in the beginning heating: the selective character is lost with increasing time. This behavior is attributed to conduction representing the main mechanism of heat distribution. Since matrix and fiber nearly possess the same thermal conductivity, the heat energy is spread through the matrix and also affects the reinforcement.

For reaching a selective heating only of the matrix, the thermal conductivity had to be higher in order to spread the heat energy quicker in the matrix, before the fibers begin to melt. By the help of the model, the effect of increasing the matrix thermal

conductivity has been investigated analytically. A selective melting of the matrix without a fiber melting could be achieved while increasing the matrix thermal conductivity by a factor of 10^3. Nevertheless, this approach was not realistic without a significant impact on the matrix properties and a complete change of the composite setup caused by the thermal conductive additives.

Additionally to the investigated complex problems, the good accordance between model and experiment makes the simulative approach a powerful tool for feasibility studies for the future use of new material combinations and optimization processes.

6 Compression Molding and Thermoforming of SRP Compounds with Induction and Standard Heating Techniques

The processability of polymer-polymer compounds were investigated in standard compression molding as well as a in a modified thermoforming application with inductively heated sheets. This experimental series served for a qualitative analysis of limitations of these materials in the applied processes.

6.1 Compression Molding with Inductively Heated Sheets

The feasibility of the induction heating in combination with polymer fiber reinforced composites was investigated in two steps. In a preliminary test, the impact of induction heating on the performance of a HDPE/PP system was examined with a Charpy test series of inductively heated samples. In a second step, the manufacturing of a complex shaped component was proven.

For the feasibility series, inductively heated samples were compared to conduction heated references and tested on their impact strength. All samples contained 5 wt-% cast iron susceptors in the composite. The reference samples were manufactured in a laboratory hot press by using different process temperatures between 155 °C, 180 °C, and 220 °C. The temperatures served to evoke different melting states within the applied polypropylene reinforcement fiber. A temperature of 155 °C was regarded as non-critical for the fibers' performance, since their melting temperature lay higher (165 °C), but high enough to sufficiently melt the applied HDPE matrix. A value of 180 °C marked the upper border of the melting zone of the PP fiber, whereas 220 °C significantly exceeded this zone.

For the inductively heated samples, comparable reference samples, which have not been overheated, were reheated by induction until they were shapeable. The surface temperature at this state was determined with an infrared temperature sensor to 135 °C. As presented before, the problem of homogeneous heating of the whole sample appeared which was solved by a manual oscillation of the sample in the magnetic field. The overall heating time had to be extended to six minutes because a larger amount of material in contrast to the previously heated samples had to be

heated. The samples were manually deformed, afterwards reshaped into sheet form, and consolidated within the press mold at a temperature of 60 °C.

As a result from the increased fiber melting, a decrease of impact strength as well as a visible change of sample cross section with increasing process temperature above the fiber melting temperature range was expected.

Table 6.1: Results of Charpy impact tests (DIN EN ISO 179-1/3, 15 J hammer) with self-reinforced polyolefin sheets

Material	Heating method	Charpy impact resistance [kJ/m²]	Failure mode
HDPE/PP 50	Induction 135 °C	Not measurable	No break
HDPE/PP 50	Conduction 155 °C	Not measurable	No break
HDPE/PP 50	Conduction 180 °C	20.86 ± 6.23	Partial break / hinge break
HDPE/PP 50	Conduction 220 °C	5.21 ± 0.52	Complete break

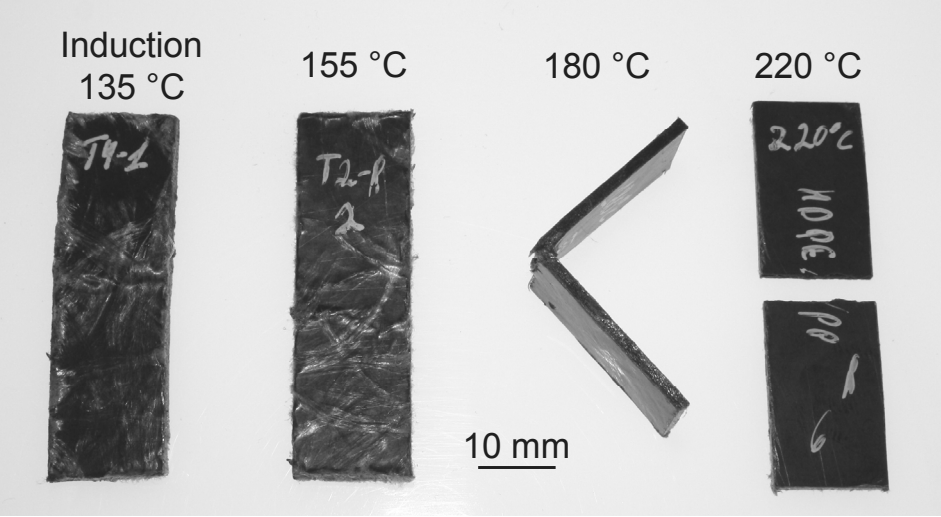

Figure 6.1: Fracture pattern of HDPE/PP samples in impact tests with different processing temperatures and methods

The reference test series showed a significant decline of impact resistance due to fiber melting at higher process temperatures (Table 6.1). At a process temperature below the reinforcement melting temperature, the reference samples did not demonstrate any break after impact. The same behavior was observed for induction heated samples, indicating that the intrinsic induction heating did not measurably

reduce the SRP's impact performance, when processed as described. By concluding from this observation, the fibers mainly remained intact during induction heating.

This assumption could be validated by the analysis of polished light micrograph sections. In both cases, induction heated and conduction up to 155 °C, the fibers were clearly visible exposing a circular shape when cut perpendicularly (Figure 6.2 and Figure 6.3). Significant fiber damage was not found around the ferrous susceptors in the induction heated sample. In contrast, the intentionally overheated surfaces revealed an increasing fiber fusion with increasing temperature (Figure 6.4 and Figure 6.5). At 180 °C, the fibers had mainly lost their circular shape but could still be distinguished from each other. The 220 °C sample did not possess any detectable fiber – the compound consisted of large zones from both of the two applied polymers forming a blend structure.

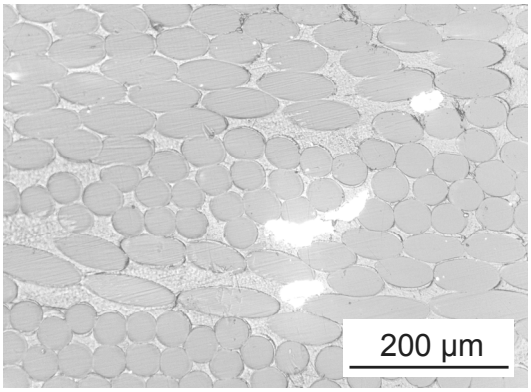

Figure 6.2: Inductively heated HDPE/PP50 (135 °C on surface)

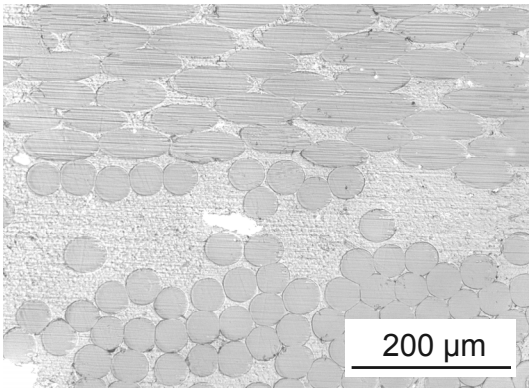

Figure 6.3: HDPE/PP50 consolidated at 155 °C

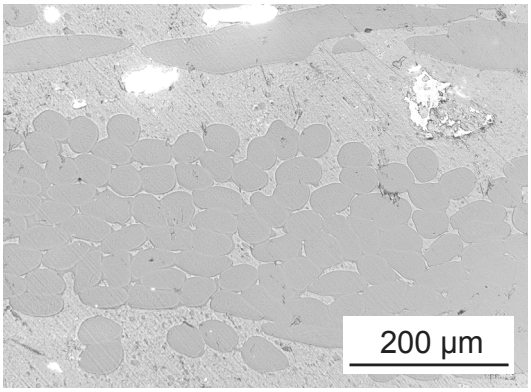

Figure 6.4: HDPE/PP50 consolidated at 180 °C

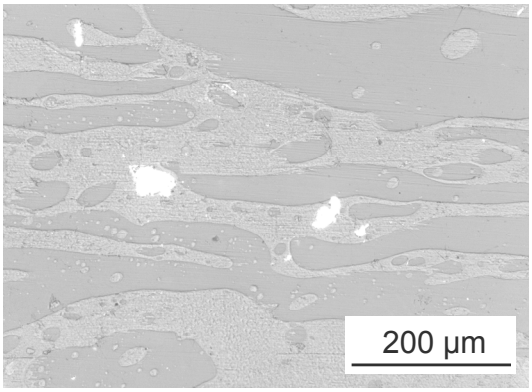

Figure 6.5: HDPE/PP50 consolidated at 220 °C

For the manufacturing of a complex shaped demonstrator (Figure 6.6) in an adapted thermoforming process, a safety shoe cap mold was applied (Figure 6.8). The mold only demanded a little amount of hot material for proving the feasibility of the induction particle heating method.

Figure 6.6: Safety shoe cap geometry and position within a safety shoe [155]

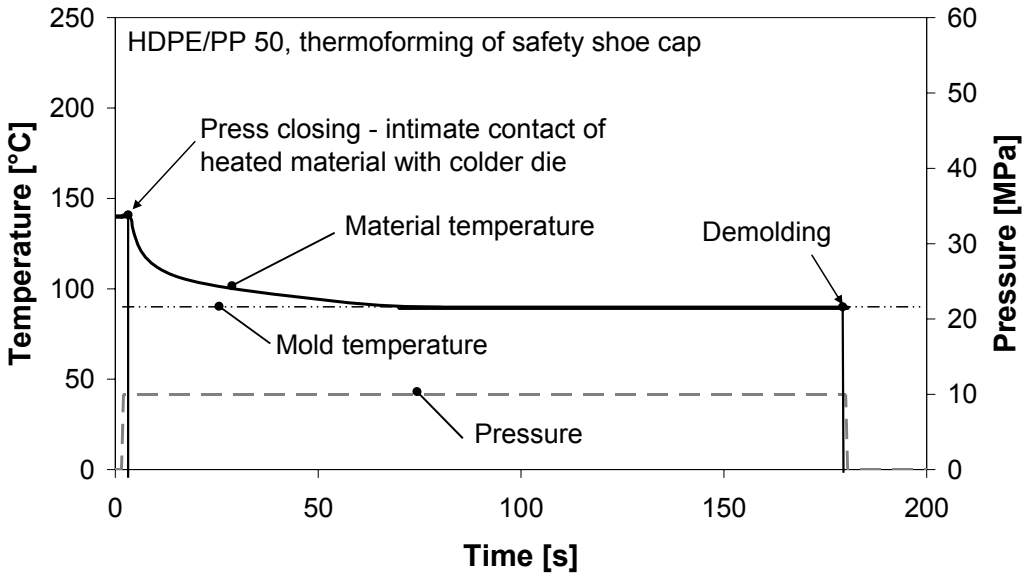

Figure 6.7: Exemplary cycle for the thermoforming of HDPE/PP

Since the applied pancake coil provided an inhomogeneous magnetic field, a static heating was excluded for this reason. To overcome this problem without a new

generator-coil setup, the previously mentioned oscillating heating was extended to a rotational movement instead. By performing this, the heating of a HDPE/PP 50 with 10 wt-% cast iron particles up to processible state had to be prolongated in comparison to the laboratory scale, but resulted in a homogenously heated sheet.

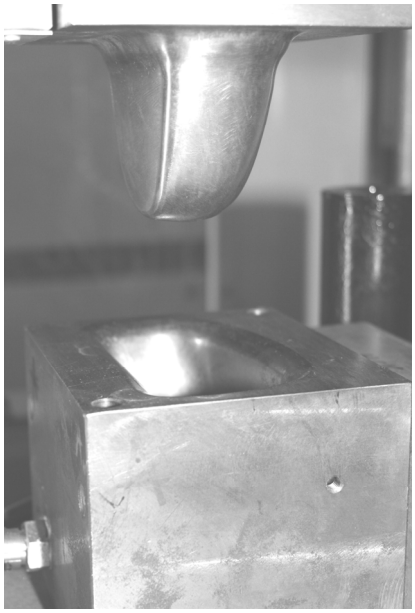

Figure 6.8: Safety shoe cap mold

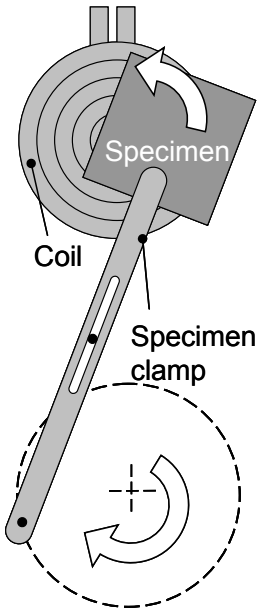

Figure 6.9: Moving principle used for the inductive heating of samples for shoe cap experiments

In contrast to a convection oven, which was used as a comparative heating method, the heating time of semi-finished sheets could be reduced by 40 %. In each heating way, the self-reinforced composite sheets revealed fiber shrinkage due to the softening of the polymer and related relaxation forces.

Additionally, the induction heating process indicated limits in terms of component size and efficiency: a lower temperature at the edges in comparison to the center of the semi-finished sheets due to thermal losses to the environment was observed. Despite this, the examination of the thermoformed demonstrators, which pointed out intact polymer fibers throughout the samples, revealed that the thermoforming of inductively heated sheets was feasible.

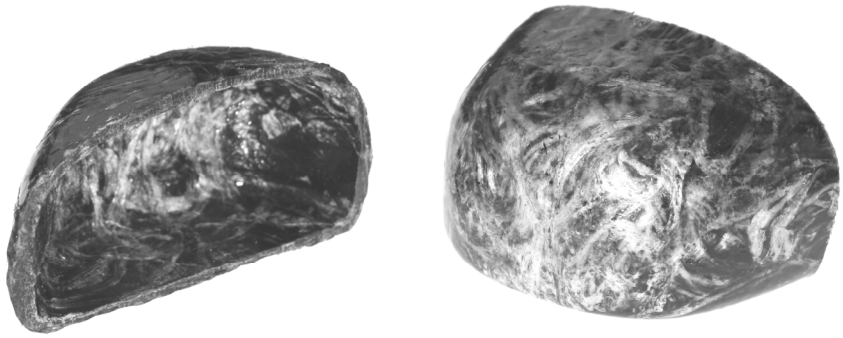

Figure 6.10: Shoe cap demonstrators manufactured from inductively heated HDPE/PP sheets

6.2 Infrared Heating

Infrared radiation was considered a competing technology for the heating of SRP. The experiments were focused on finding a proof of using infrared radiation for selective melting purposes. In this context, the application of carbonous and ferritic particles as infrared susceptors was investigated.

A dark radiator was used at various temperatures, beginning with temperatures close to the melting point of the HDPE matrix material. The aim was not the affection of the sample by convection, but by infrared radiation. A heating was not achieved in IR modes close to the melting point of HDPE. At an operating temperature of 300 °C, a significant effect on the surface of the material could be observed (Figure 6.11). The tested, 2 mm thick samples were only moderately affected within the test time of three minutes. The temperature did not exceed 100 °C in any case. Furthermore, all samples presented the same behavior, which indicated that the incorporation of particles did not have any influence on the heating by a long-wave IR radiator. This observation was independent from the used matrix material and was also valid for PA6.

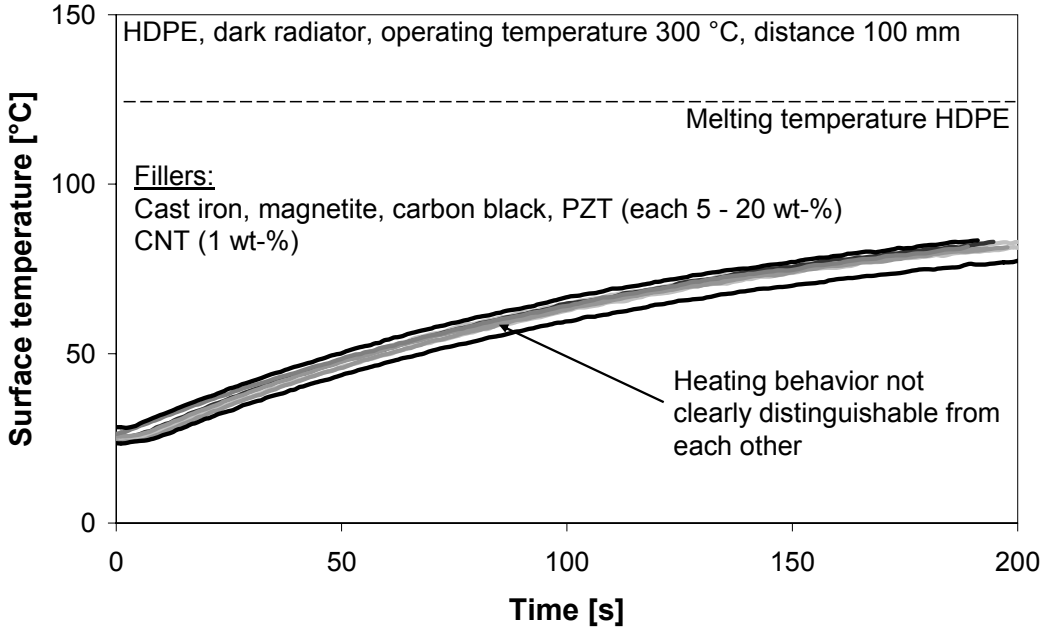

Figure 6.11: Temperature behavior of HDPE compounds during heating by a dark IR radiator

The use of the short-wave infrared spot resulted in a quicker heating of the compounds. The spotlight provided temperatures above 1000 °C, which eventually resulted in a quick degradation of the polymer surface without evoking a complete melting of the compound (Figure 6.12). This behavior was attributed to the bad thermal conductivity of the used polymers. Moreover, the mechanism of infrared radiation only took effect at the surface of the material.

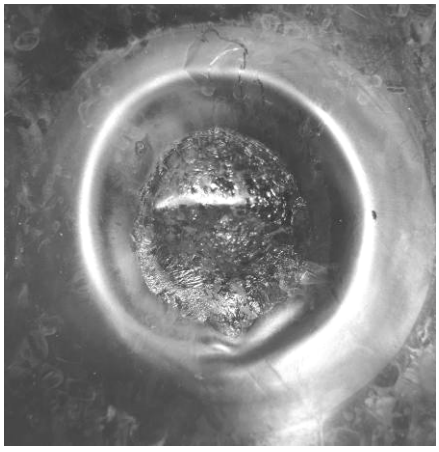

Figure 6.12: Exemplary surface of a carbon black doped HDPE sample after infrared heating with a short-wave radiator

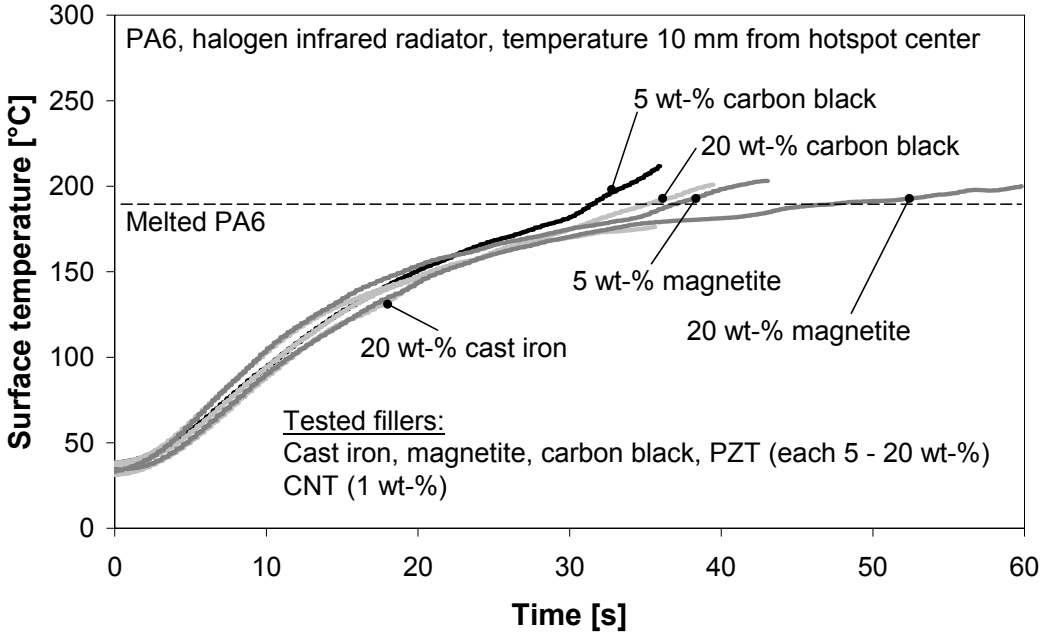

Figure 6.13: Temperature evolution of PA6 compounds during heating by a short-wave IR spotlight

When being exposed to short-wave infrared radiation, HDPE and PA6 compounds heated up within one minute but did not indicate any clear trend caused by the incorporation of susceptors. Within PA6 samples for example (Figure 6.13), the temperature curves of high and low doped materials were found so close to each other that an influence of fillers fraction could be neglected. This was also validated for HDPE. The surfaces illustrated severe damage after heating, whereas the opposite side of the exposed surface remained nearly unaffected in many cases. The surface damage was in most of the cases accompanied by an emergence of intense smoke.

The infrared heating could not be used as a selective fast heating method for temperature sensitive materials since the infrared trials demonstrated no influence on different susceptors. Furthermore, the tests indicated that a heating was not realized by intrinsic mechanisms. Therefore, the samples were heated from the surface and the heat was conducted through the whole sample without sparing polymer fiber parts. This behavior would lead to reinforcement melting in case of use with SRP materials.

Consequently, a dark radiator could be used as a conservative heating method by adjusting it to a temperature lower than the polymer fiber melting point. However, this would exceed the demanded maximum heating time of three minutes. As a consequence, the compression molding with infrared heating for SRP materials was not further investigated.

6.3 Conduction Heating

6.3.1 Adaption of LFT and GMT Process Chain for SRP

The developed SRP pellets (PP/PET and PET-A/PET-C) were tested on their compatibility with an adapted LFT process chain. They were melted in an extruder and a predefined material mass placed in a mold for flow molding. The cycle time for the heating of 1 kg material was approx. four minutes. The experiments revealed the temperature sensitive behavior of the material, which is characterized by low mechanical properties at higher temperatures and furthermore by lower viscosity which is needed for the filling of complex molds. In case of PP/PET, the material could be well processed with a complete filling of a complex mold at 180 °C mass temperature.

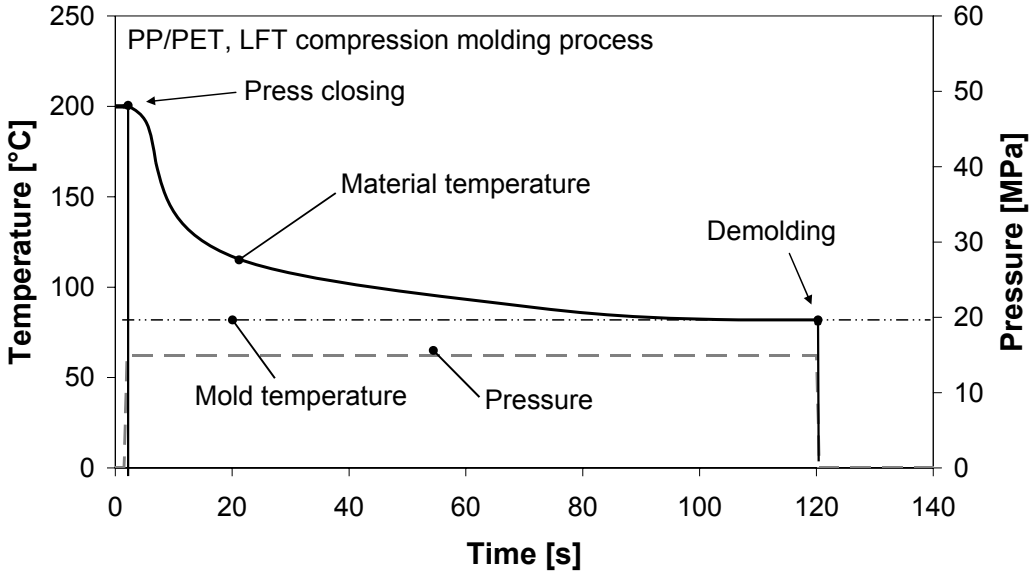

Figure 6.14: Exemplary parameters for the processing of melted PP/PET pellets in a shear edge mold

The polypropylene matrix could be clearly distinguished from the polyethylene terephthalate part by optical microscopy even after using a process temperature exceeding the melting temperature of the reinforcement (Figure 6.15).

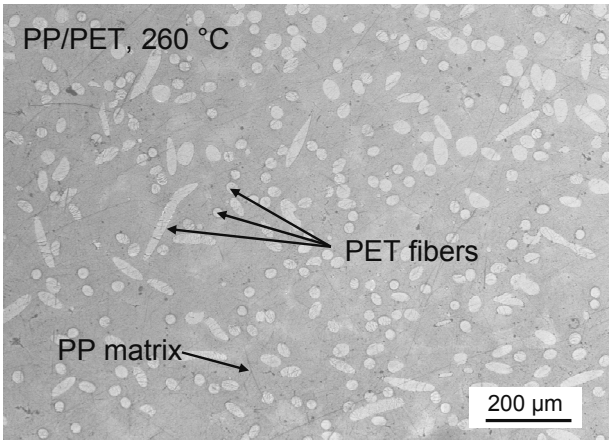

Figure 6.15: Light microscopic image of a PP/PET sample processed at 260 °C

Since the optical investigation did not reveal a significant influence of process temperature, Charpy impact tests were performed. The composite could be observed losing its mechanical performance at higher process temperatures. This result indicated the PET fibers loss of their reinforcing effect and consequently their integrity (Figure 6.16).

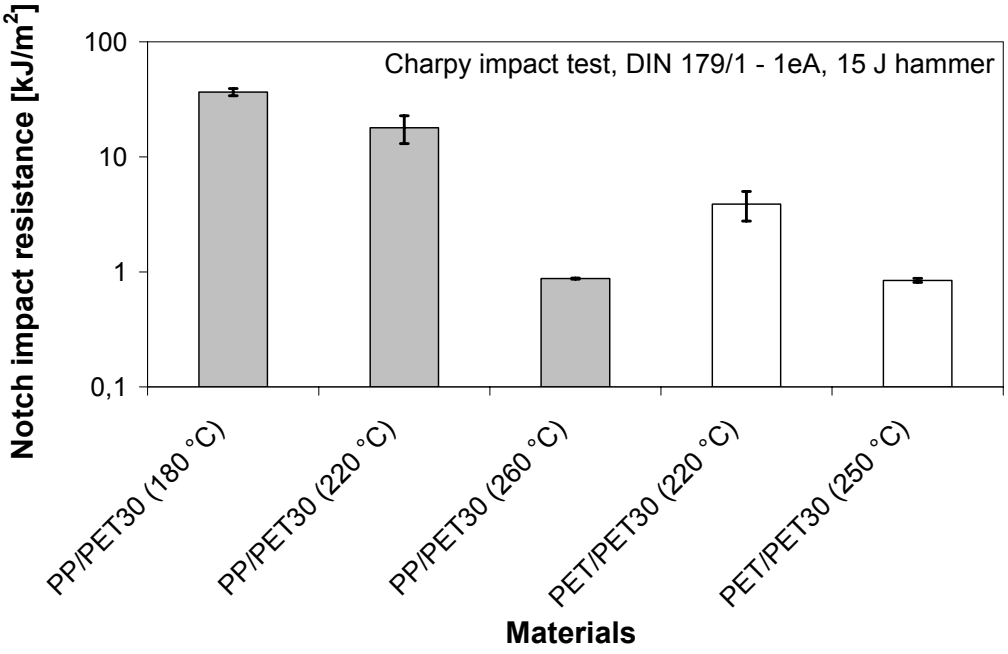

Figure 6.16: Influence of LFT process temperature on impact resistance of SRP

Similar results were found for self-reinforced PET as reference. The impact resistance decreased with higher temperature, whereas the processability was easier at higher temperatures due to the observed lower viscosity. The filling of a complex, ribbed mold could not be realized with the PET/PET due to the high viscosity and instant material freezing. In this way, the material also revealed extreme shrinkage, which made a deforming nearly impossible. By increasing the mold temperature from 60 to 80 °C, the flowability and deformability were improved. Yet, the material temperature at the end of the molding cycle remained higher than the glass transition temperature, which caused warpage during deforming. As a consequence, the tested self-reinforced polyester (srPET) material was not suitable for complex molds in a compression molding based LFT process, whereas the SRP model material PP/PET could be well processed, but the fibers were also damaged at increased temperature.

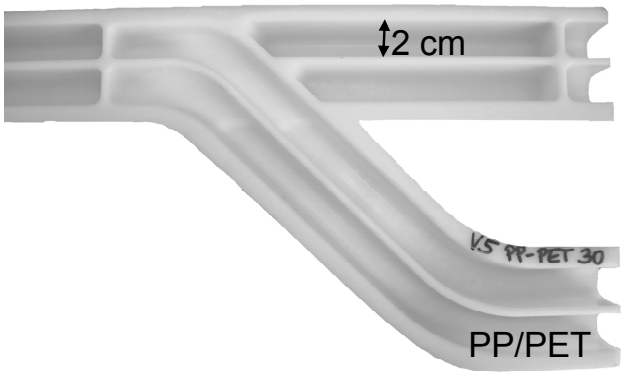

Figure 6.17: Complete filling of a complex shaped mold with PP/PET

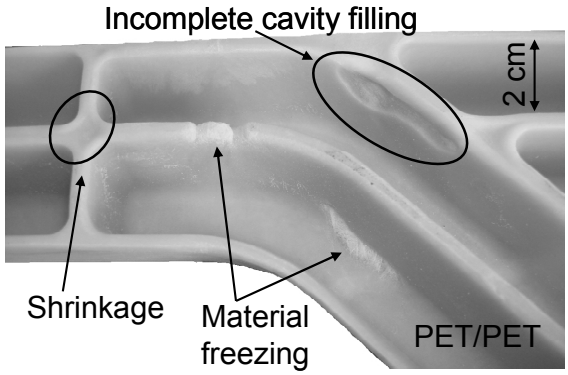

Figure 6.18: Observed challenges with PET/PET pellets in a LFT process

A GMT process chain, using a convection oven for processing of commingled PP/PET (30 wt-% fibers) and a PET/PET (30 wt-% fibers) reference as well as randomly reinforced HDPE/PP (50 wt-% fibers), was tested as a competing heating and process method of self-reinforced materials in terms of heating efficiency and material damage. The sheets were stacked in an oven without an additional dead weight for a pre-consolidation. As the oven temperatures, 150 °C for HDPE/PP, 180 °C for PP/PET, and 220 °C for PET/PET were applied. All of the used fabrics were subjects to shrinkage, at which the self-reinforced PET revealed a rate of up to 30 %. Nevertheless, the handling and compression molding in a shear edge mold was uncomplicated. The enormous observed shrinkage was regarded as a knock-out criterion for this process chain with self-reinforced materials.

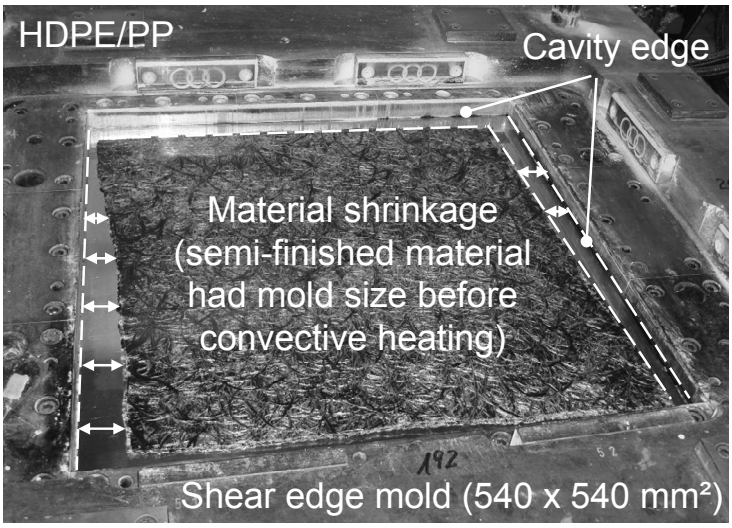

Figure 6.19: Visual shrinkage of HDPE/PP sheets after convective heating

A better way would be the adaption of a thermoforming process by using an additional frame, which tightens the fibrous reinforcement during heating and reduces shrinkage. For this method, an open mold would be mandatory.

6.3.2 Compression Molding with Heated Tool

The processability of Fibroline HDPE/PP sheets was tested with a water heated pinch-off edge mold. Four layers of HDPE/PP fabrics were placed in the mold preheated to 145 °C.

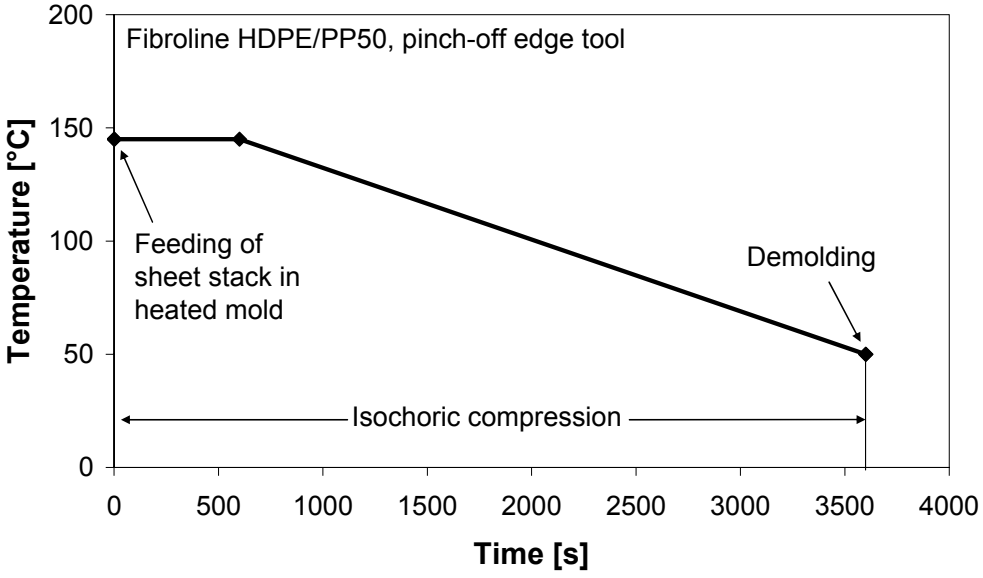

Figure 6.20: Process cycle of sheet molding with a pinch-off edge tool

For avoiding a squeeze out of the matrix, the process was isochoric. The sheets had been heated for 10 minutes in contact with the mold, before the cooling was initiated. Due to the high thermal capacity of the heavy mold, the cooling took 50 minutes to reach the demolding temperature of 50 °C.

The compression molding in this way was also feasible with all kind of tested amounts of SRP sheets. In any case, the component was well-consolidated, and the fibers were qualitatively still intact (Figure 6.21). Any shrinkage was not measurable which was attributed to the constant pressure on the material during processing. The good matrix flowability which was realized by the chosen process temperature could be observed at the components' edges, where the matrix agglomerated because of the pinch-off edge.

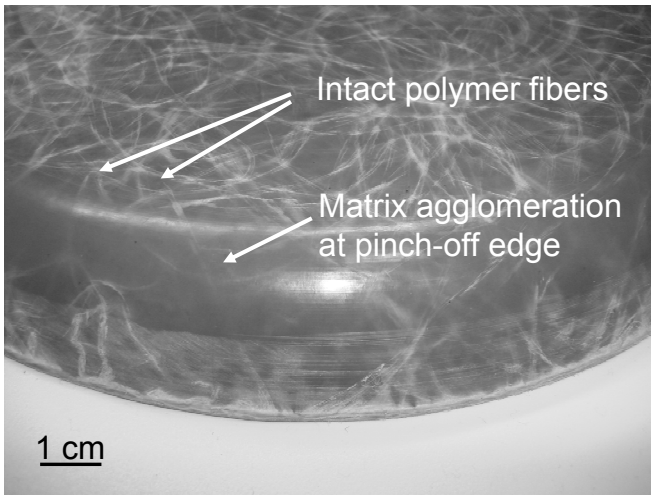

Figure 6.21: Compression molded HDPE/PP sheet with pinch-off edge tool

However, the cycle time of this kind of process has to be significantly reduced for an industrial realization.

Due to this reason, the use of the fast heating RocTool® mold was pursued. HDPE/PP SRP fabrics were placed in the cold mold and a constant press force of 500 kN was applied, which equaled to 18.3 bar. The mold was heated within two minutes to 145 °C and kept constant at this temperature for 10 minutes. Afterwards, mold and component were cooled to 60 °C within four minutes.

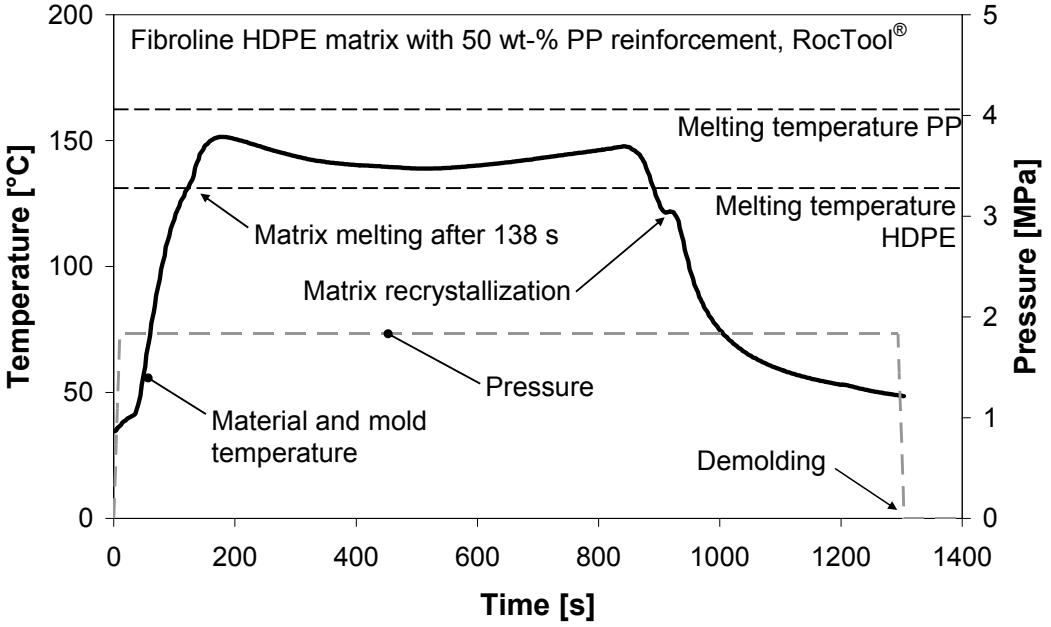

Figure 6.22: Temperature record of conduction heating with RocTool® mold

The temperature record of a within the material stack applied temperature sensor displayed that a controlled heating is only possible with certain limitation. The limitation is related to the temperature fluctuation of up to 10 K (Figure 6.22). The resulting compressed sheet did not reveal excessive shrinkage, and the fibers remained also in this case intact. The intactness could be also proven quantitatively in dart impact experiments (see chapter 6.4) and notched Charpy tests. The samples of the latter test method even did not reveal a break after impact.

6.4 Comparison of Molded SRP Sheets with Competing Materials

In order to investigate the competitiveness of the used self-reinforced particle doped material, the dart impact performance of HDPE/PP (50 wt-% reinforcement, 2.5 wt-% iron doping) SRP was compared to industrially available Curv® and TwinTex® material. The HDPE/PP and the TwinTex® semi-finished materials were consolidated in compression molding process applying a shear edge mold. The Curv® was obtained in the condition supplied to the customer as pre-consolidated sheet.

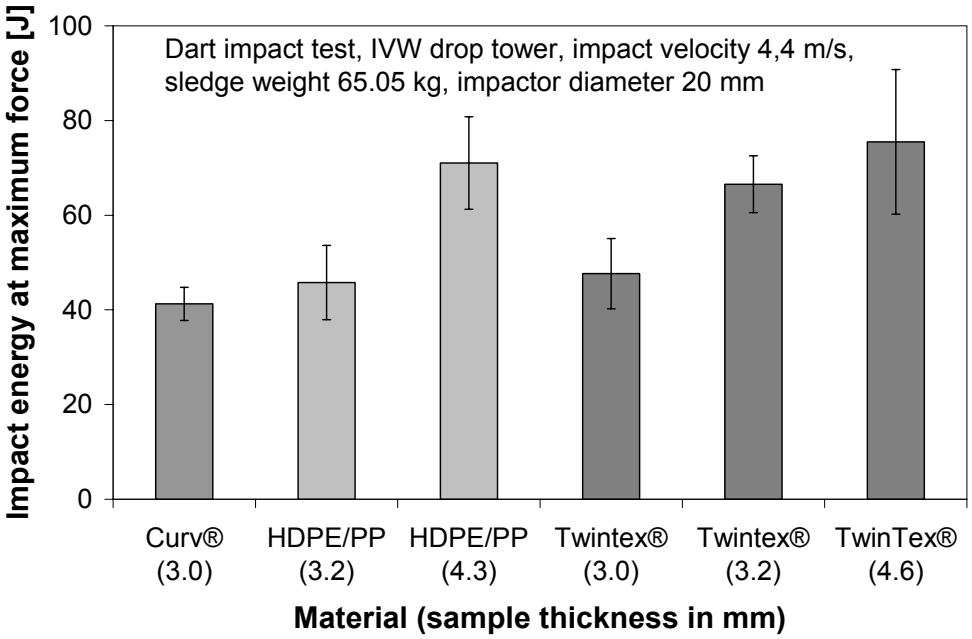

Figure 6.23: Dart impact energy of SRP and GF-reinforced composites at maximal force

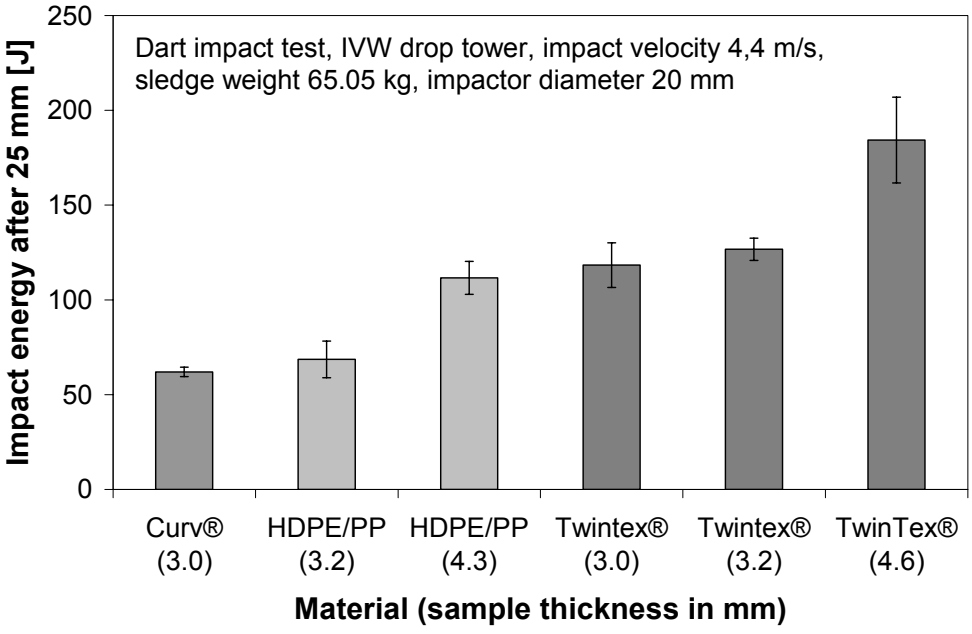

Figure 6.24: Dart impact energy of SRP and GF-reinforced composites after 25 mm from initial impactor contact

The impact energy of the compression molded 5 wt-% iron particles containing HDPE/PP was determined in the same range as the competing composites. As depicted in the standard, the nominal impact energy is in this case calculated up to the maximum force (Figure 6.23). Nevertheless, the impact energy after a

displacement of 25 mm from the impact proved to be significantly less for self-reinforced materials, in comparison to the glass fiber reinforced TwinTex® (Figure 6.25). To reach the same impact energy range after 25 mm, the SRP sheet thickness had to be increased to approx. 1 – 1.5 mm (Figure 6.24).

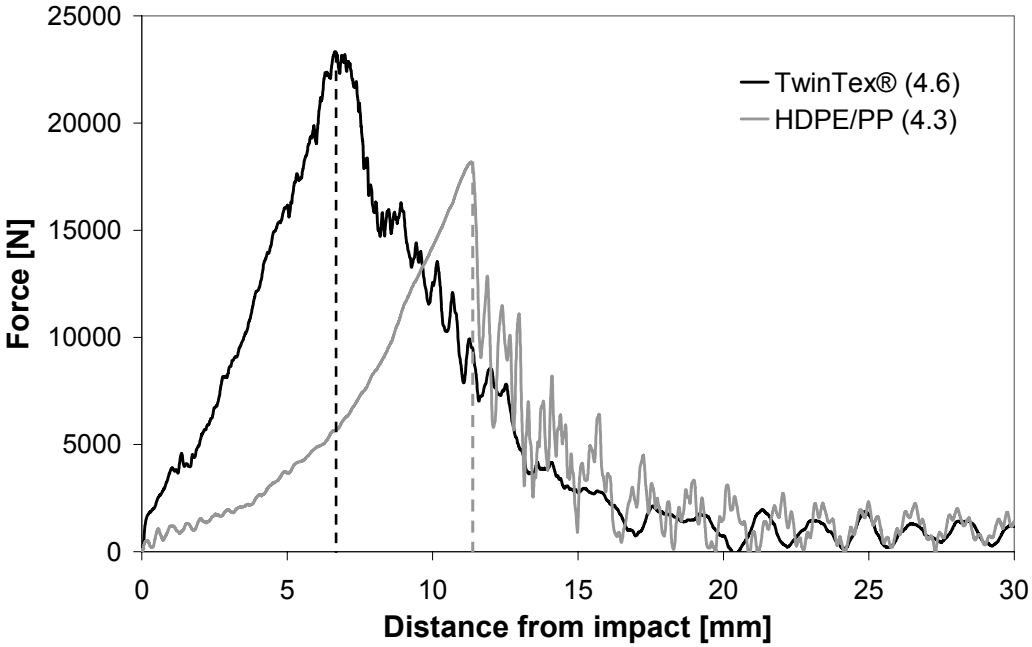

Figure 6.25: Comparison of force evolution of a self-reinforced polyolefin and TwinTex® within a dart impact test

An explanation was found in the analysis of the force-displacement curves (Figure 6.25). The impact force of the polymer-reinforced material reached its maximum later than the glass-reinforced TwinTex®, which behaved more brittle. The ductile SRP had generally a lower force peak (dotted lines in Figure 6.25), but this was compensated for the calculation of the nominal impact energy by the larger displacement. The difference in impact energy measured after 25 mm displacement resulted from the material behavior after exceeding the force peak. The force of the SRP material decreased very rapidly, whereas the GFRP followed an axially symmetrical curve. This characteristic can be explained by the higher strength and stiffness of the glass fibers, which revealed a more brittle behavior, but, in total, a higher deformation resistance in comparison to polypropylene fibers.

In a comparison of the specific energy at maximum force, which considers the density, the self-reinforced composites were able to outperform the glass fiber

reinforced TwinTex® competitors (Table 6.2). This could be best demonstrated at the HDPE/PP with a thickness of 4.3 mm tending to higher specific impact energy than the thicker TwinTex®.

Table 6.2: Comparison of specific dart impact energies

Property	**Curv®**	**HDPE / PP (2.5 wt-% Fe)**		**TwinTex®**		
Thickness [mm]	3	3.2	4.3	3	3.2	4.6
Density [g/cm³]	0.92	1.07	1.07	1.50	1.50	1.50
Specific energy at max. force [J m^3 kg^{-1}]	44.9 ±3.8	42.8 ±7.3	66.4 ±9.1	31.8 ±5.0	44.3 ±4.0	50.3 ±10.2

The impact results indicated that the particle filled HDPE/PP is able to compete with market solutions and that the susceptor doping does not negatively influence the desired mechanical performance.

7 Transfer of the Achieved Results into Industrial Applications

7.1 Concepts for an Industrial Realization of Particle Induction Heating

The successful implementation of particles in polymer-polymer composites and the associated inductive heating offers a wide range of possible application concepts. Figure 7.1 illustrates an automated heating process by transportation of particle doped sheets through a magnetic field. Since the magnetic field density needs to be of adequate strength, a transportation belt runs through the center of a solenoid coil, where the highest field strength is located. The disadvantage of this process is characterized by the necessity of a suitable generator unit, which delivers sufficient power to the coil for a heating in an adequate time frame. The generator power is dependent on the coil size and length, the number of windings, and the desired frequency. Since an unlimited generator upscale is not possible for technical and physical reasons, the generator quasi limits the feasibility of this concept. The (semi-) continuous processing and the simple heating controllability by belt speed and generator power are the concept's advantages. Besides the preheating of small-scale semi-finished SRP materials, the setup is also regarded as adequate for injection molding applications. The precondition for injection molding is the use of a high-pressure resistant electromagnetic transparent material within the coil as part of a piston injection molding machine, for instance.

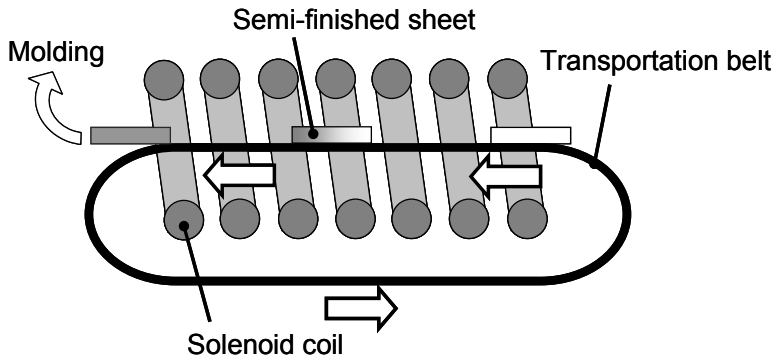

Figure 7.1: Continuous heating concept with a single-coil

The single-coil concept needs a powerful generator, which also has to provide the suitable frequency around 500 kHz. Most of the large-scale generators are not able to provide frequencies in this range, which consequently leads to a concept of using

several small- or medium-scale generators in a cascade (Figure 7.2). The concept uses a continuous approach with a transportation belt running through a magnetic field. The magnetic field is provided by several independent coil-generator systems. In contrast to the introduced single-coil approach, the coil cascade is also able to concentrate the magnetic field density in certain zones of the semi-finished material by adjustment of the individual coils. The coil-cascade concept is able to meet the needs of a continuous sheet heating at a high energy level, but still needs a high economic effort, for acquisition and consequential costs.

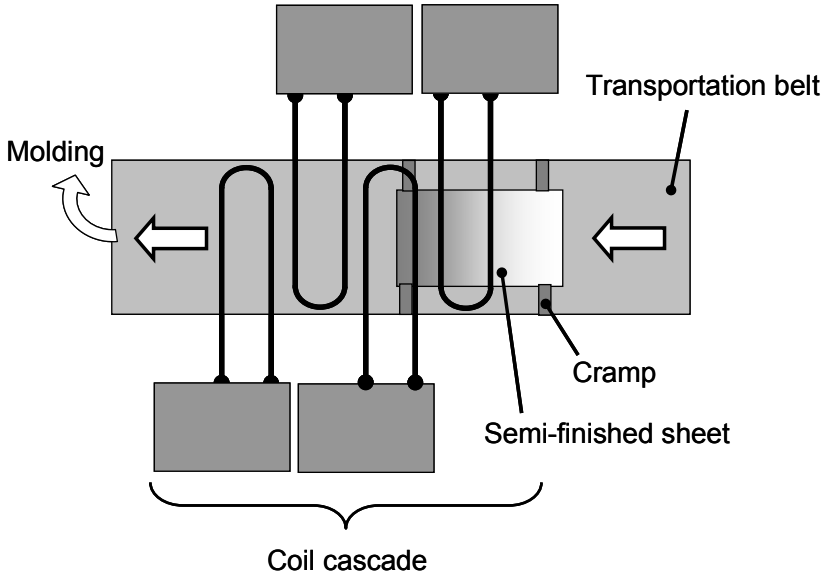

Figure 7.2: Continuous heating concept with a coil cascade

From a technical point of view, the presented concepts are not especially developed for the specific needs of polymer-polymer composites but work with any particle doped compound. As it was observed for the experiments with standard compression molding techniques, the fiber shrinkage revealed to be a problem with SRP materials in any heating case. The lowest shrinkage was either found with a constant pressure on the material during heating or during the experiments of feasibility of particle induction. A concept, which seizes the idea to avoid thermal shrinkage of the polymer reinforcement, is based on the local heating and melting of a SRP panel by inductive means for a thermoforming process (Figure 7.3). In this concept, the SRP panel is only melted in the section of a subsequent thermoforming step. The reinforcement shrinkage is limited to the hot zone, since the solid parts of the component act as a stretching frame. The fiber shrinkage in the heated area can be even valuable to

reduce warpage and undulations in the later thermoformed zone. Economically considered, the concept is of energy-saving nature because of its local applicability within a small section of the entire component. An optimized coil design can be additionally helpful to reduce energy consumption. Nevertheless, this concept is validated as not suitable for the manufacturing of complex shapes.

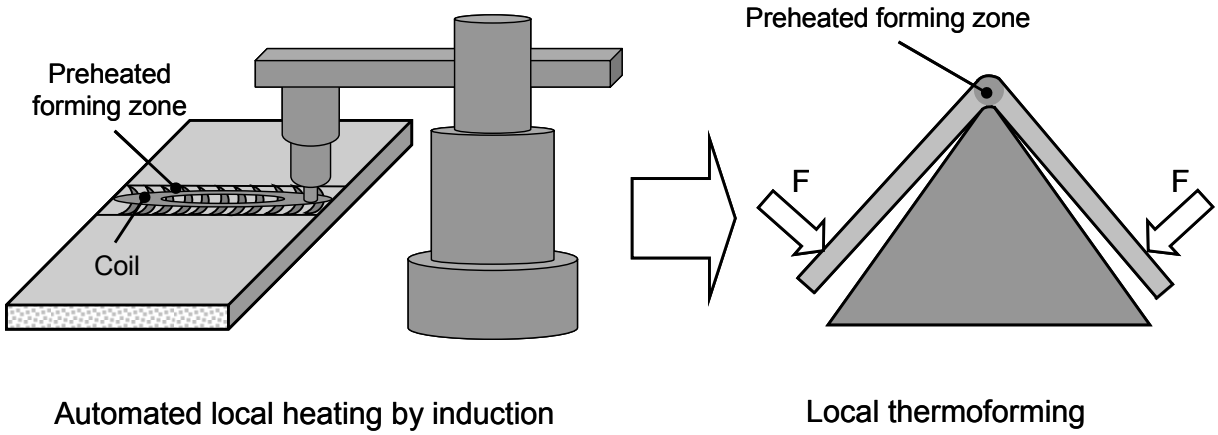

Figure 7.3: Local heating concept with subsequent local forming

7.2 Economic Considerations

The investigated low-cost susceptors are suitable for particle induction, but their use will marginally increase material as well as matrix manufacturing costs. A filler degree of 5 to 10 wt-% of ferromagnetic particles in the composites was found sufficient in the composite. This is assessed to be extremely low in comparison to matrix and reinforcement volume fractions (Table 7.1 and Table 7.2). Nevertheless, the density increase is significant. If a higher filler degree is acceptable in a compound, the heating efficiency can be improved. For this work, a further susceptor increase was rejected due to the accompanied higher density.

Table 7.1: Comparison between weight fraction and volume fraction of iron particles in HDPE/PP composite matrix

HDPE/PP50 composite with cast iron particles						
Filler fraction	wt-%	0	1	5	10	20
	vol-%	0	0.13	0.67	1.4	3.1
Composite density	[g/cm³]	0.92	0.98	1.23	1.55	2.18

Table 7.2: Comparison between weight fraction and volume fraction of magnetite particles in HDPE/PP composite matrix

HDPE/PP50 composite with magnetite particles						
Filler fraction	wt-%	0	1	5	10	20
	vol-%	0	0.18	0.92	1.93	4.24
Composite density	[g/cm³]	0.92	0.96	1.13	1.35	1.78

By the incorporation of particles, a self-reinforced composite loses its recycling character in general, but the ferromagnetic susceptors are regarded as unproblematic due to their easy separation from a polymer melt by means of gravimetric or magnetic forces during a recycling process.

The needed equipment for particle induction heating is comparable to the ones of competing processes. As in these methods, the final investment costs for the process equipment is dependent on the components' complexity such as undercuts and ribbings. An improved coil design is expected to provide an optimized magnetic field resulting in an increase of heating efficiency. The proposed use of a coil-generator cascade, which consists of several stand-alone systems, will definitely cause a higher invest effort but a reduction of heating time is expected as well.

As a further consequence, the developed particle induction heating process is considered to be best suitable for the implementation especially in local heating in small scales such as the repairing or the application of local reinforcements. This evaluation is justified by the high economic effort in terms of energy consumption of the magnetic field. The experiments have proven that the magnetic field has to be of high intensity to realize a technically reasonable heating effect.

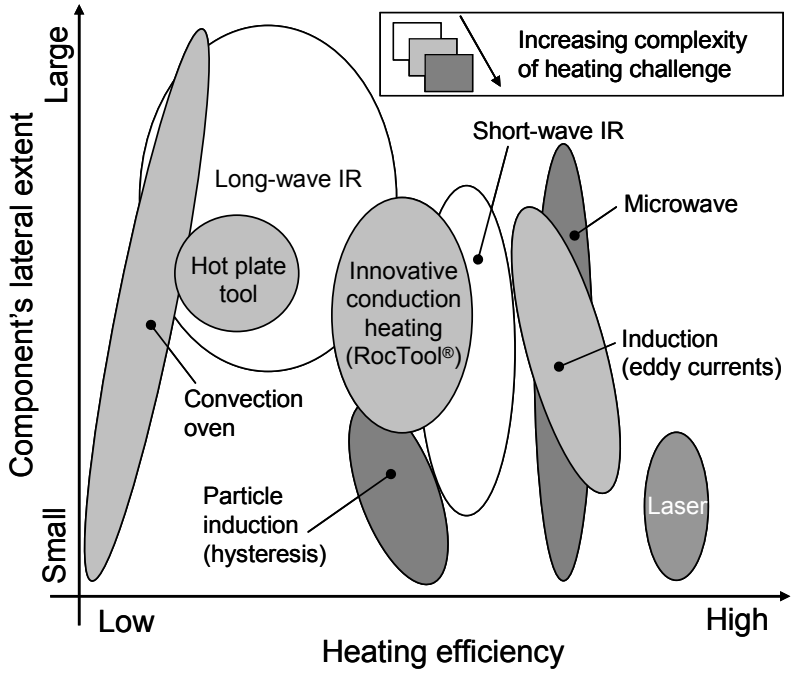

Figure 7.4: Classification of heating approaches for thermoplastic materials according to their size, efficiency, and adaptability to complex problems

On the basis of the results of this study, Figure 7.4 classifies the particle induction heating among standard heating techniques according to their respective ability to heat components or semi-finished materials of various sizes, their heating efficiency, and the heating complexity. The heating efficiency includes in this case heating time, energy consumption, as well as the overall degree of efficiency of the method. In the heating complexity, the heating of a temperature sensitive polymer-polymer material in a reasonable time without reinforcement damage were taken into account. The investigated method of particle induction is a niche method with the ability to meet local heating challenges by contactless intrinsic means.

8 Conclusion

The induction heating technique using particulate susceptors was successfully adapted for polymer-polymer composites. The heating is working on a contactless base due to its advantage to obtain the energy from an electromagnetic wave. It is intrinsic, locally applicable, and enables a precise temperature control which proved to be suitable for temperature sensitive composites.

The studies included the investigation of material related variables, like susceptor material and fraction, as well as process related variables, like magnetic field strength and coupling distance. The heating was successfully achieved with ferromagnetic particles, cast iron and magnetite, at a filler fraction of a minimum of 5 wt-%. The electromagnetic field was driven with a frequency of 453 kHz at the maximum power level of 10 kW. By using these parameters, PA6 and HDPE samples as well as the investigated self-reinforced polymer systems, HDPE/PP and PP/PET, could be melted within three minutes. The fiber integrity was observed by means of microscopic and mechanical analysis and was not found to be significantly damaged during the heating process.

On the one hand, cast iron was examined to deliver higher heating rates than competing magnetite particles. On the other hand, environmental studies have revealed a surface corrosion of iron particles. The corrosion does not decrease the heating ability and the matrix properties, but limits the applicability of the cast iron particles. In contrast, magnetite offers a higher applicability due to its impotence to corrode and to interact with other chemicals. In contrast, longer process cycles or higher susceptor fractions have to be accepted with magnetite.

The expected selective character of a heat transfer by particles could only be validated to a certain extend. After the electromagnetic activation of particles, the thermal conduction was identified as one of the driving mechanism of particle induction. The particles heat the macroscopic sample in an intrinsic way, whereas on a microscopic scale, the heat transfer does not distinguish between reinforcement and matrix. As a consequence, reinforcement melting is theoretically also possible

with particle induction but strongly depends on susceptor distribution. For spreading the induced heat mainly in the matrix, the matrix thermal conductivity had to be increased by the factor of 10^3, which was analytically investigated on the basis of the developed FEM model. Nevertheless, the necessary increase in thermal conductivity to homogenize the heating is not realizable in practice. The FEM model can moreover help potential customers to decide on the required amount of heating susceptors in future applications and to evaluate the time until the material processability is reached.

The induction heating principle could be successfully implemented in a thermoforming process in lab-scale. The scale-up is assumed to be possible by larger economic efforts, namely the use of cascades of more than one electromagnetic field source or by larger generators that are able to drive larger coils. By concluding from these necessary high machine investment costs for an industrial realization, the application of particle based induction as heating method will not be able to replace standard conduction heating methods, but serve as an additional option for heating sensitive materials at increased speed. Furthermore, the local applicability also enables a subsequent local machinability, including weldability and local repairability.

A reasonable application considers the particle based induction as a heating method within thermoforming processes. Within this concept, only zones which are subjects to a subsequent molding or thermoforming process are heated, whereas plane surfaces remain unaffected. In this way, the observed thermal shrinkage of the investigated polymer-polymer composites can be reduced by benefitting from this local heating approach.

Particle induction heating offers promising approaches for the use in polymer industry while providing high speed heating with local application and an intrinsic character.

9 References

[1] Kaiser, W.: Kunststoffchemie für Ingenieure. Hanser Verlag, München, 2008.

[2] Schürmann, H.: Konstruieren mit Faser-Kunststoff-Verbunden. 2. bearb. und erw. Aufl., Springer (VDI-Buch), Berlin, 2007.

[3] Cheung, H.; Ho, M.; Cardona, F.; Hui, D.: Natural fibre-reinforced composites for bioengineering and environmental engineering applications. Composites: Part B, Vol. 40 (2009), 655-663.

[4] Schuster, J.; Govignon, Q.; Bickerton, S.; Bhattacharyya, D.: Vacuum Assisted Resin Transfer Molding with Biobased Resins and Natural Fibre Reinforcement. International Conference on Composite Materials (ICCM-18), Jeju, Korea, Aug. 22-26, 2011, TH28-5.

[5] Shibata, M.; Nakai, K.: Preparation and Properties of Biocomposites Composed of Bio-Based Epoxy Resin, Tannic Acid, and Microfibrillated Cellulose. Journal of Polymer Science: Part B: Polymer Physics, Vol. 48 (2010), 425-433.

[6] Summerscales, J.; Dissanayake, N. P. J.; Virk, A. S.; Hall, W.: A review of bast fibres and their composites. Part 2 - Composites. Composites: Part A, Vol. 41 (2010), 1336-1344.

[7] Bledzki, A. K.; Gassan, J.: Composites reinforced with cellulose based fibres. Progress in Polymer Science, Vol. 24 (1999), 221-274.

[8] Summerscales, J.; Dissanayake, N. P. J.; Virk, A. S.; Hall, W.: A review of bast fibres and their composites. Part 1 - Fibres as reinforcements. Composites: Part A, Vol. 41 (2010), 1329-1335.

[9] Meichsner, A.: Herstellung, Charakterisierung, Modellierungsansätze und Simulation von edelstahltextilverstärkten Polypropylen (ETV-PP) und Langglasfaserthermoplasten mit PP-Matrix (ETV-PP/GF). Dissertation, TU Kaiserslautern, 2009.

[10] Voll, N.: Experimentelle Untersuchung, Simulation und Materialmodellierung von edelstahltextilverstärkten Langfaserthermoplasten. Dissertation, TU Kaiserslautern, 2011.

[11] Kmetty, Á.; Bárány, T.; Karger-Kocsis, J.: Self-reinforced polymeric materials: A review. Progress in Polymer Science, Vol. 35 (2010), 1288-1310.

[12] Mead, W. T.; Porter, R. S.: The Preparation and Tensile Properties of Polyethylene Composites. Journal of Applied Polymer Science, Vol. 22 (1978), 3249-3265.

[13] Capiati, N. J.; Porter, R. S.: The concept of one polymer composites modelled with high density polyethylene. Journal of Materials Science, Vol. 10 (1975), 1671-1677.

[14] Peijs, T.: Composites for recyclability. Materials Today, Vol. 6 (2003), No. 4, 30-35.

[15] Kolf, A.: Curv® – bridging gaps in the composite world! JEC Composites Show 2010, Technical Sales Presentation, Paris, April 13-15, 2010.

[16] Don & Low Limited: Armordon Self Reinforcing Polypropylene (srPP) – panels. Company publication, http://www.armordon.com/wp-content/uploads/2009/04/panels-insert.pdf (10/02/2011).

[17] Samsonite: Cosmolite Spinner 74cm silber. Company website, http://www.samsonite.de/cosmolite-spinner-74cm-silber/product-de.htm?or=6708260248&shs={94132c30-36ae-4b8f-ab01-bfe7babb9206} (30/11/11).

[18] Daimler AG: Mercedes-Benz E-Klasse. Company publication, published online under “Spiegel online”, http://www.spiegel.de/fotostrecke/fotostrecke-51009-5.html (30/11/11).

[19] Engelhorn Sports Shop: Nike Schienbeinschoner - Protegga Shield III. http://sports.engelhorn.de/sportarten/fussball/ausruestung/schienbeinschoner/nike-schienbeinschoner-protegga-shield-iii--70546--99037--200/ (26/04/12).

[20] Lauster, F.: Elektrowärmetechnik. B.G. Teubner Verlagsgesellschaft, Stuttgart, 1963.

[21] Kashevsky, B. E.; Prokhorov, I. V.; Kashevsky, S. B.: Audio-frequency heating of particulate magnetic systems. China Particuology, Vol. 5 (2007), 84-92.

[22] Candeo, A.; Dughiero, F.: Numerical FEM Models for the Planning of Magnetic Induction Hyperthermia Treatments With Nanoparticles. IEEE Transactions on Magnetics, Vol. 45 (2009), No.3, 1658-1661.

[23] Bae, S.; Lee, S. W.; Hirukawa, A.; Takemura, Y.; Jo, Y. H.; Lee, S. G.: AC Magnetic-Field-Induced Heating and Physical Properties for a Hyperthermia Agent in Medicine. IEEE Transactions on Nanotechnology, Vol. 8 (2009), No.1, 86-94.

[24] Hergt, R.; Dutz, S.; Röder, M.: Effects of size distribution on hysteresis losses of magnetic nanoparticles for hyperthermia. Journal of Physics: Condensed Matter, Vol. 20 (2008), 1-12.

[25] Moser, L.; Mitschang, P.; Schlarb, A. K.: Induction Welding of Thermoplastic Polymer Composites Using Robotic Techniques, Sampe Journal, Vol. 44 (2008), No. 5, 43-49.

[26] US patent US006056844A: Temperature-Controlled Induction Heating of Polymeric Materials, 02/05/2000.

[27] LyondellBasell: Moplen HP500V. Company publication, http://polymers.lyondellbasell.com (15/02/2011).

[28] Propex Fabrics: Curv® – Technical Data Sheet C100A. Company publication, http://www.curvonline.com/deutsch/pdf/datasheet_long.pdf (10/02/2011)

[29] Don & Low Ltd: Armordon Mechanical Data, Self reinforcing polypropylene (srPP). Company publication, issue 2, July 2011, http://www.armordon.com/ wp-content/uploads/2009/04/Mechanical-Data1.pdf (28/10/11).

[30] Lankhorst Pure Composites bv: PURE® - Technical Data Sheet, PURE® - sheets. Company publication, version 30-03-07, 2007.

[31] Milliken & Co.: Tegris Sheet Stock, Technical Data Sheet. Company publication, 2007.

[32] Lankhorst Pure Composites bv: The principle of PURE®. Company publication, http://www.epicos.com/epicos/extended/netherlands/lankhorst/lankhorst_pure. html (28/10/11).

[33] Nextrusion GmbH: Product Information kaypla®, High-Performance Tapes. Company publication, http://www.kaypla.de/fileadmin/user_upload/kaypla_doc/ product_informations/product_information_kaypla_tapes.pdf (28/10/11).

[34] Lankhorst Pure Composites bv: PURE® - Technical Data Sheet. PURE®-tape. Company publication, version 30-03-07, 2007.

[35] Don & Low Ltd.: Self reinforceing Poylpropylene (srPP), tape. Company publication, http://www.armordon.com/wp-content/uploads/2009/04/tape-insert.pdf (28/10/11).

[36] Barkoula, N. M.; Peijs, T.; Schimanski, T.; Loos, J.: Processing of Single Polymer Composites Using the Concept of Constrained Fibers. Polymer Composites, Vol. 26 (2005), No. 1, 114-120.

[37] Barkoula, N. M.; Alcock, B.; Reynolds, C. T.; Cabrera, N. O.; Govaert, L. E.; Peijs, T., 31.05.-03.06.2004: Temperature and Strain Rate Dependant Mechanical Behaviour of All-PP Composites - Comparison with GMT and NMT. 11th European Conference on Composite Materials (ECCM 11), Rhodes, Greece, May 31 - June 3, 2004.

[38] Bailey, P. B. S.; Hodzic, A.; Hayes, S. A.; Fairclough, J. P. A.; Marginson, S.: Development of Biodegradable Polymer-Polymer Composites. In: Proceedings of the 14th European Conference on Composite Materials (ECCM-14), Budapest, Hungary, June 7-10, 2010.

[39] Bjekovic, R.: Monocomposite Schichtwerkstoffe auf Basis von Polypropylen. Dissertation, Universität Kassel, VDI-Verl., Düsseldorf, 2003.

[40] Li, W.: PET/PP-Based Polymer Composites: Effects of Compatibilizer and Nanofillers on the Processing-Structure-Property Relationships. Dissertation, TU Kaiserslautern, 2009.

[41] Trznadel, M.; Kryszewsk, M.: Thermal Shrinkage of Oriented Polymers. Journal of Macromolecular Science, Part C: Polymer Reviews, Vol. 32 (1992), No. 3-4, 259-300.

[42] Emri, I.; von Bernstorff, B.; Voloshin, A.: Effect of Heating on Fiber Shrinkage. SEM Annual Conference & Exposition on Experimental and Applied Mechanics, St. Louis, USA, June 4-7, 2006.

[43] Urudzhev, R. S.: Chemistry and Technology of Man-Made Fibers. The Thermal Shrinkage of Textile Fibers. Fibre Chemistry, Vol. 7 (1976), No. 5, 471-473.

[44] Karger-Kocsis, J.: Interphase with lamellar interlocking and amorphous adherent - a model to explain effects of transcrystallinity. Advanced Composites Letters, Vol. 9 (2000), No. 3, 225-227.

[45] Oberbach, K. (ed.): Saechtling – Kunststoff Taschenbuch. 28th issue, Hanser Verlag, München, 2001.

[46] Ehrenstein, G. W.; Riedel, G.; Trawiel, P.: Praxis der thermischen Analyse von Kunststoffen. 2. Auflage, Hanser, München, 2003.

[47] Yang, R.; Liu, Y.; Yu, J.; Wang, K.: Thermal oxidation products and kinetics of polyethylene composites. Polymer Degradation and Stability, Vol. 91 (2006), 1651-1657.

[48] Phillips, R.; Glauser, T.; Manson, J.-A. E.: Thermal Stability of PEEK/Carbon Fiber in Air and its Influence on Consolidation. Polymer Composites, Vol. 18 (1997), No. 4, 500-508.

[49] Göpferich, A.: Mechanisms of polymer degradation and erosion. Biomaterials, Vol. 17 (1996), 103-114.

[50] La Mantia, F. P.; Valenza, A.; Acierno, D.: Thermomechanical Degradation of Blends of Isotactic Polypropylene and High Density Polyethylene. Polymer Degradation and Stability, Vol. 13 (1985), 1-9.

[51] Gulmine, J. V.; Janissek, P. R.; Heise, H. M.; Akcelrud, L.: Degradation profile of polyethylene after artificial accelerated weathering. Polymer Degradation and Stability, Vol. 79 (2003), 385-397.

[52] Hussein, I. A.; Ho, K.; Goyal, S. K.; Karbashewski, E.; Williams, M. C.: Thermomechanical degradation in the preparation of polyethylene blends. Polymer Degradation and Stability, Vol. 68 (2000), 381-392.

[53] Zahedi, M.; Ahmadi, M.; Nekoomanesh, M.: Influence of Microstructure and Morphology on Stress–Strain Behavior of Commercial High Density Polyethylene. Journal of Applied Polymer Science, Vol. 110 (2008), 624-631.

[54] Holmström, A.: The Course of Thermooxidative Degradation of LD- and HD-Polyethylene under Accelerated Testing Conditions. In: Eby, R. K. (Ed.): Durability of Macromolecular Materials. American Chemical Society Washington, 1979, 45-62.

[55] Holmström, A.; Sörvik, E. M.: Thermooxidative Degradation of Polyethylene. I and II. Structural Changes Occuring in Low-Density Polyethylene, High-Density Polyethylene, and Tetrateracontane Heated in Air. Journal of Polymer Science: Polymer Chemistry Edition, Vol. 16 (1978), 2555-2586.

[56] Chan, C. M.; Venkatraman, S.: Crosslinking of Poly(arylene Ether Ketone)s. 1. Rheological Behavior of the Melt and Mechanical Properties of Cured Resin. Journal of Applied Polymer Science, Vol. 32 (1986), 5933-5943.

[57] Baehr, H. D.; Stephan, K.: Wärme- und Stoffübertragung. 7th ed., Springer-Verlag, Berlin, Heidelberg, 2010.

[58] Welty, J. R.: Engineering heat transfer. Wiley, New York, 1974.

[59] Fletcher, L. S.: Heat transfer and thermal control systems. American Institute of Aeronautics and Astronautics, New York, 1978.

[60] Yousefpour, A.; Hojjati, M.; Immarigeon, J.-P: Fusion Bonding/Welding of Thermoplastic Composites. Journal of Thermoplastic Composite Materials, Vol. 17 (2004), 303-341.

[61] Mehdizadeh, M.: Microwave, RF applicators and probes for material heating, sensing, and plasma generation. A design guide. 1. ed., William Andrew, Amsterdam, 2010, available online: http://www.sciencedirect.com/science/book/9780815515920 (07/09/2011).

[62] Nußelt, W.: Das Grundgesetz des Wärmeüberganges. Gesundheits-Ingenieur, Vol. 38 (1915), 477-482.

[63] Kegel, K. (Ed.): Elektrowärme – Theorie und Praxis. W. Girardet, Essen, 1974.

[64] Maxwell, J. C.: A Dynamical Theory of the Electromagnetic Field. Philosophical Transactions of the Royal Society of London, Vol. 155 (1865), 459-512.

[65] Bosse, G.; Wiesemann, G.: Grundlagen der Elektrotechnik II – Das magnetische Feld und die elektromagnetische Induktion. VDI-Verlag, Düsseldorf, 1996.

[66] Border, J.; Salas, R.: Induction Heated Joining of Thermoplastic Composites without Metal Susceptors. In: 34th International SAMPE Symposium, May 8-11, 1989, 2569-2578.

[67] Meyer, E.: Die Eisenverluste in elektrischen Maschinen. Dissertation, ETH Zürich, 1932 .

[68] Knauf, B. J.; Webb, D. P.; Liu, C.; Conway, P. P.: Low frequency induction heating for the sealing of plastic microfluidic systems. Microfluidics and Nanofluidics, Vol. 9 (2010), 243-252.

[69] Rudnev, V.; Loveless, D.; Cook, R.; Black, M.: Handbook of Induction Heating. Marcel Dekker AG, Basel, 2003.

[70] Zhang, X.; Li, Y.; Xiao, J.: Theroretical and experimental analysis of magnetic inductive heating in ferrite materials. Journal of Applied Physics, Vol. 93 (2003), No. 10, 7124-7126.

[71] Yarlagadda, S.; Fink, B. K.; Gillespie, J. W. [JR].: Resisitive Susceptor Design for Uniform Heating during Induction Bonding of Composites. Journal of Thermoplastic Composite Materials, Vol. 11 (1998), 321-337.

[72] Moser, L.; Mitschang, P.: In the Shifting Magnetic Field. Kunststoffe International, Vol. 100 (2010), No. 7, 26-28.

[73] Wacker, M.; Moser, L.; Schlarb, A. K.; Tradt, H.-R.: Flexible 3D joining process for complex fibre composite components. Joining Plastics, Vol. 2 (2008), No. 4, 266-271.

[74] Mitschang, P.; Velthuis, R.; Emrich, S.; Kopnarski, M.: Induction Heated Joining of Aluminum and Carbon Fiber Reinforced Nylon 66. Journal of Thermoplastic Composite Materials, Vol. 22 (2009), 767-801.

[75] Velthuis, R.: Induction welding of fiber reinforced thermoplastic polymer composites to metals. Dissertation, TU Kaiserslautern, 2007.

[76] Heraeus Noblelight GmbH: Infrared Basics and Technology. Company presentation,http://heraeus-noblelight.de/de/divisions/infrared/furtherinformation/irlinks/ir_links.aspx (07/09/11).

[77] Heraeus Noblelight GmbH: Infrarot-Wärme für die Kunststoffverarbeitung. Company publication, http://heraeus-noblelight.de/media/webmedia_local/media/pdf/ip/applications_7/kunststoff/plastics_brochure_d.pdf (07/09/11).

[78] Belhamra, A.; Diabi, R.; Moussaoui, A.: Technology and Applications of Infrared Heating in the Industrial Area. Journal of Engineering and Applied Sciences, Vol. 2 (2007), No. 7, 1183-1187.

[79] Anhalt, M.: Magnetische Eigenschaften weichmagnetischer Composite. Dissertation, TU Clausthal, 2008.

[80] Keller, R.; Schmidbauer, E.: Magnetic properties and rotational hysteresis losses of oxidized ≈250 nm Fe_3O_4 particles. Journal of Magnetism and Magnetic Materials, Vol. 162 (1996), 85-90.

[81] Svoboda, J.: Magnetic methods for the treatment of minerals, Elsevier, Amsterdam, 1987.

[82] Stacey, F.D.; Banerjee, S. K.: The Physical Principles of Rock Magnetism. Elsevier, Amsterdam, 1974.

[83] Suwanwatana, W.; Yarlagadda, S.; Gillespie, J. W. Jr.: Influence of particle size on hysteresis heating of nickel particulate polymer films. Composites Science and Technology, Vol. 66 (2006), 2825-2836.

[84] Suwanwatana W.; Yarlagadda S.; Gillespie J. W. Jr.: Hysteresis heating based induction bonding of thermoplastic composites. Composites Science and Technology, Vol. 66 (2006), 1713-1723.

[85] Mohr, R.; Kratz, K.; Weigel, T.; Lucka-Gabor, M.; Moneke, M.; Lendlein, A.: Initiation of shape-memory effect by inductive heating of magnetic nanoparticles in thermoplastic polymers. Proceedings of the National Academy of Sciences, Vol. 103 (2006), No. 10, 3540-3545.

[86] German patent DE 10037884A1: Verfahren zur beschleunigten Klebstoffaushärtung, 3/8/2000.

[87] German patent DE 10037883A1:Ferromagnetische Resonanzanregung und ihre Verwendung zur Erwärmung teilchengefüllter Substrate, 3/8/2000 .

[88] Hilger, I.; Andrä, W.; Bähring, R.; Daum, A.; Hergt, R.; Kaiser, W. A.: Evaluation of Temperature Increase with Different amounts of Magnetite in Liver Tissue Samples. Investigative Radiology, Vol. 32 (1997), No. 11, 705-712.

[89] Zhao, D.-L.; Wang X.-X.; Zeng, X.-W.; Xia, Q.-S.; Tang, J.-T.: Preparation and inductive heating property of Fe_3O_4-chitosan composite nanoparticles in an AC magnetic field for localized hyperthermia. Journal of Alloys and Compounds, Vol. 477 (2009), 739-743.

[90] Zhao, D. -L; Zhang, H. -L; Zeng, X. -W; Qi-Sheng, X.; Tang, J. -T: Inductive heat property of Fe_3O_4 / polymer composite nanoparticles in an ac magnetic field for localized hyperthermia. Biomedical Materials, Vol. 1 (2006), 198-201.

[91] Jordan, A.; Scholz, R.; Wust, P.; Fahling, H.; Felix, R.: Magnetic fluid hyperthermia (MFH): Cancer treatment with ac magnetic field induced excitation of biocompatible superparamagnetic nanoparticles. Journal of Magnetism and Magnetic Materials, Vol. 201 (1999), 413-419.

[92] Hergt, R.; Andrä, W.; d'Ambly, C. G.; Hilger, I.; Kaiser, W. A.; Richter, U.; Schmidt, H.–G.: Physical Limits of Hyperthermia Using Magnetite Fine Particles. IEEE Transactions on Magnetics, Vol. 34 (1998), No. 5, 3745-3754.

[93] Fortin, J.-P.; Wilhelm, C. ; Servais, J. ; Ménager, C. ; Bacri, J.-C. ; Gazeau, F.: Size-Sorted Anionic Iron Oxide Nanomagnets as Collodial Mediators for Magnetic Hyperthermia. Journal of the American Chemical Society, Vol. 129 (2007), 2628-2635.

[94] Dutz, S.; Hergt, R.; Mürbe, J.; Müller, R.; Zeisberger, M.; Andrä, W.; Töpfer, J.; Bellemann, M. E.: Hysteresis losses of magnetic nanoparticle powders in the single domain size range. Journal of Magnetism and Magnetic Materials , Vol. 308 (2007), 305-312.

[95] Rohsenow, W. M.; Hartnett, J. P.: Handbook of heat transfer applications. 2nd ed., McGraw-Hill, New York, 1985.

[96] Standard DIN 1910-3, 1979.

[97] Quickstep Technologies Pty. Ltd.: Aerospace Composite Manufacturing | The Benefits - Quickstep Technologies. Company website, http://www.quickstep.com.au/what-is-quickstep/the-benefits (11/02/2011).

[98] RocTool S.A.: Roctool - Composite processing - Innovative Moulding Technologies. http://www.roctool.com/compositeProcessing.php (11/02/2011).

[99] Steeg, M.: Prozesstechnologie für Cyclic Butylene Terephthalate im Faser-Kunststoff-Verbund. Dissertation, TU Kaiserslautern, 2009.

[100] Davis, B.; Gramann, P. J.; Osswald, T. A.: Compression Molding. 1st edition, Hanser, München, 2003.

[101] Mitschang, P.; Neitzel, M.: Handbuch Verbundwerkstoffe. Werkstoffe, Verarbeitung, Anwendung, Hanser, München, 2004.

[102] Neitzel, M.; Breuer, U.: Die Verarbeitungstechnik der Faser-Kunststoff-Verbunde, Hanser, München, 1997.

[103] Hawley, R. C.; Jones, R. F: In-line Compounding of Long-fiber Thermoplastics for Injection Molding. Journal of Thermoplastic Composite Materials, Vol. 18 (2005), 459-464.

[104] Krause, W.; Henning, F.; Tröster, S.; Geiger, O.; Eyerer, P.: LFT-D – A Process Technology for Large Scale Production of Fiber Reinforced Thermoplastic Compounds. Journal of Thermoplastic Composite Materials, Vol. 16 (2003), 289-302.

[105] Geiger, O.; Henning, F.; Eyerer, P.; Brüssel, R.; Ernst, H.: LFT-D: materials tailored for new applications. Reinforced plastics, Vol. 50 (2006), No. 1, 30-35.

[106] Priebe, M.; Schledjewski, R.: Processing and properties of glass/polypropylene in long fibre compounding extrusion. Plastics, Rubber and Composites, Vol. 40 (2011), No. 6-7, 374-379.

[107] Petterson, J.; Nilsson, P.: Recycling of SMC and BMC in Standard Process Equipment. Journal of Thermoplastic Composite Materials, Vol. 7 (1994), 56-63.

[108] Palmer, J.; Savage, L.; Ghita, O. R.; Evans, K. E.: Sheet molding compound (SMC) from carbon fibre recyclate. Composites: Part A, Vol. 41 (2010), 1232-1237.

[109] Stachel, P.; Stadtfeld, H.: Pressarbeit als Messverfahren zur Verarbeitungsfähigkeit von SMC. Internationale AVK-Tagung für verstärkte Kunststoffe und technische Duroplaste, Stuttgart, 2009.

[110] Ineos Polyolefins: Rigidex HD6070EA, Product Description. Company publication, 2008.

[111] DSM Engineering Plastics: Akulon K222D (dry). Company publication, 2009.

[112] Fibroline SARL: General description of the process. http://www.fibroline.com/general-description.htm (22/04/2011).

[113] Performance Fibers: Polyester Fiber and Resin. Company publication, 2004.

[114] Noll, A.; Burkhart, T.: Electrical, Mechanical and Thermal Properties of Multiwall Carbon Nanotube Modified Linear Poly(P-Phenylene Sulfide) Manufactured via Twin Screw Extrusion. 14th European Conference on Composite Materials (ECCM-14), Budapest, Hungary, June 7-10, 2010.

[115] Noliac Ceramics s.r.o.: Properties of piezoceramic materials. Company publication, 2008.

[116] Columbian Chemicals Company: Raven® L Ultra, Carbon Black for Geomembrane and Film Applications. Company publication, 2004.

[117] Mineralmühle Leun, Rau GmbH & Co. KG: Specification Ilmenit AU, SG. Company publication, no. 2005-04-14, 2005.

[118] Mineralmühle Leun, Rau GmbH & Co. KG: Specification Ilmenit 90 W. Company publication, no. 2005-02-28, 2005.

[119] Nanocyl S.A.: NANOCYL™ NC7000 series – Product Datasheet – Thin Multi-Wall Carbon Nanotubes. Company publication, http://www.nanocyl.com/en/content/download/417/2536/file/DM-Qual-05-TDS%20NC7000-V05.pdf (19/10/11).

[120] Gotthart Maier Metallpulver GmbH: Technisches Datenblatt, Eisenoxid-Pulver. Company publication, 2009.

[121] Gotthart Maier Metallpulver GmbH: Technical Data Sheet, Cast Iron Grit. Company publication, 2009.

[122] Lee, H.-B; Song, H. J.: Efficient Magnetic Field Calculation Method for Pancake Coil Using Biot-Savart Law. 12th Biennial IEEE Conference on Electromagnetic Field Computation, Miami, USA, April 30 - May 3, 2006, PC2-7.

[123] Hayt, W.H.; Buck, J.A.: Engineering Electromagnetics. 5th ed., McGraw-Hill Higher Education, Boston, USA, 1989.

[124] Hüttinger Elektronik GmbH + Co. KG: TruHeat HF 5010. Technical Description. Company publication, no. 24148352 EN, 2010.

[125] Standard DIN EN ISO 527-2, 1996.

[126] Standard DIN EN ISO 179, 1997.

[127] Standard DIN EN ISO 6603-2, 2002.

[128] Standard DIN 53765, 1994.

[129] Standard DIN EN ISO 11357, 1999.

[130] Suwanwatana, W.; Yarlagadda, S.; Gillespie, J. W. Jr.: An investigation of oxidation effects on hysteresis heating of nickel particles. Journal of Materials Science, Vol. 38 (2003), 565-573.

[131] Standard DIN 50905-4, 1987.

[132] Standard DIN EN ISO 3915, 1999.

[133] Heraeus Noblelight GmbH: Infrarot-Strahler für industrielle Prozesse. Company publication, 2006.

[134] Research Inc.: Model 4085 Instruction Manual, Spot IR Infrared Heaters. Company publication, Nov. 2008, http://www.researchinc.com/Resources/PDF/SpotIR%20Model4085%20User%20Manual.pdf (14/06/11).

[135] Research Inc.: Infrared Heaters for Controlled Concentrated Heating, Model 4085. Company publication, http://www.researchinc.com/Resources/PDF/SpotIR%20Model4085%20Data%20Sheet.pdf, (14/06/11).

[136] Kaiser, R.; Gottschalk, G.: Elementare Tests zur Beurteilung von Meßdaten. Soforthilfe für statistische Tests mit wenigen Meßdaten, B.I.-Wissenschaftsverlag, Mannheim, 1972.

[137] Golt, M. C.; Yarlagadda, S.; Gillespie, J. W. Jr.: Magnetic and Dielectric Properties of Composites Consisting of Oriented, Iron Flake Filler within a Thermoplastic Host: Part I. Material Fabrication and Electromagnetic Characterization. Journal of Thermoplastic Composite Materials, Vol. 22 (2009), 551-567.

[138] Ma, M.; Wu, Y.; Zhou, J.; Sun, Y.; Zhang, Y.; Gu, N.: Size dependence of specific power absorption of Fe_3O_4 particles in AC magnetic field. Journal of Magnetism and Magnetic Materials, Vol. 268 (2004), 33-39.

[139] Frauenhofer, M.: Schnellhärtung struktureller Verbundklebungen mittels elektromagnetischer Wechselfelder. Diss., TU Carolo-Wilhelmina zu Braunschweig, Shaker Verlag, Aachen, 2010.

[140] Heck, C.: Magnetic materials and their applications. Butterworths, London, 1974.

[141] Nagata, T.: Rock Magnetism. Maruzen Company Ltd., Tokyo, 1961.

[142] Orfeuil, M.: Electric process heating. Technologies, equipment, applications, Battelle Press, Columbus, Ohio, 1987.

[143] Mohr, R.; Kratz, K.; Weigel, T.; Lucka-Gabor, M.; Moneke, M.; Lendlein, A.: Initiation of shape-memory effect by inductive heating of magnetic nanoparticles in thermoplastic polymers. Proceedings of the National Academy of Sciences, Vol. 103 (2006), No. 10, 3540-3545.

[144] Namkung, M.; Wincheski, B.; Bryant, R. G.; Buchman, A.: Effects of heat treatment on the magnetic properties of polymer-bound iron particle cores. Journal of Applied Physics, Vol. 83 (1998), No. 11, 6474-6476.

[145] Hergt, R.; Hiergeist, R.; Zeisberger, M.; Glöckl, G.; Weitschies, W.; Ramirez, L. P.; Hilger, I.; Kaiser, W. A.: Enhancement of AC-losses of magnetic nanoparticles for heating applications. Journal of Magnetism and Magnetic Materials, Vol. 280 (2004), 358-368.

[146] Leuchtmann, P.: Einführung in die elektromagnetische Feldtheorie, Pearson Studium, München, 2005.

[147] Földes, E.; Iring, M.; Tüdós, F.: Degradation of HDPE and LLDPE in closed mixing chamber: a comparison. II. Changes of some physical and machanical properties. Polymer Bulletin, Vol. 20 (1988), 89-96.

[148] Day, M.; Suprunchuk, T.; Cooney, J. D.; Wiles, D. M.: Thermal Degradation of Poly(aryl-Ether-Ether-Ketone) (PEEK): A Differential Scanning Calorimetry Study. Journal of Applied Polymer Science, Vol. 36 (1988), No. 1097-1106.

[149] Nam, J.-D.; Seferis, J. C.: Generalized Composite Degradation Kinetics for Polymeric Systems Under Isothermal and Nonisothermal Conditions. Journal of Polymer Science: Part B: Polymer Physics, Vol. 30 (1992), 455-463.

[150] Kenny, J. M.; Torre, L.; Nicolais, L.: Short- and long-term degradation of polymer-based composites. Thermochimica Acta, Vol. 227 (1993), 97-106.

[151] Yan, R. J.; Jiang, B.: Melting Behavior of Drawn Polypropylene. Journal of Polymer Science: Part B: Polymer Physics, Vol. 31 (1993), 1089-1094.

[152] Andrady, A. L.: Weathering of Polyethylene (LDPE) and Enhanced Photodegradable Polyethylene in the Marine Environment. Journal of Applied Polymer Science, Vol. 39 (1990), 363-370.

[153] Comsol AB: COMSOL Multiphysics Modeling Guide. Company publication, 2008.

[154] Verein Deutscher Maschinenbau-Anstalten; Verband Deutscher Maschinen- und Anlagenbau: Kenndaten für die Verarbeitung thermoplastischer Kunststoffe. Teil 1, Hanser, München, 1979.

[155] Uvex safety group: Sicherheitsschuhe. Extrem sportlich – extrem sicher. Online catalogue, http://www.uvex-safety.com/fileadmin/editors/de_DE/Online-catalogue/KAT_2012_Sicherheitsschuhe_D/index.html#/38 (16/02/12).

10 Appendix

Material Combinations and Design of Experiments

Table 10.1: Survey of considered material combinations and realized experiments

Material	HDPE	PA6	PP/PET	HDPE/PP
Cast iron	Filler fraction, frequency variation, particle size, coupling distance, generator power, pellets	Filler fraction, frequency variation, pellets	Filler fraction, tapes	Filler fraction
Magnetite	Filler fraction, frequency variation, coupling distance, pellets	Filler fraction, frequency variation, pellets	Filler fraction, tapes	Filler fraction
Carbon black	Filler fraction, frequency variation, pellets	Filler fraction, frequency variation, pellets	-	-
PZT	Filler fraction, frequency variation, pellets	Filler fraction, frequency variation, pellets	-	-
CNT	Filler fraction, frequency variation, pellets	Filler fraction, frequency variation, pellets	-	-
Nickel	Filler fraction, frequency variation, particle size	-	-	-
Ilmenite	Filler fraction, frequency variation	-	-	-

Applied Parameters in the Simulation Model Source Code

Constant Values

Frequency	453000 Hz
Coil current (1 winding, fit)	160 A
Starting temperature T_0	298.15 K

Density

Copper	8.93 g/cm³
Iron	7.87 g/cm³
PET	1.41 g/cm³
HDPE	0.95 g/cm³
PP	0.91 g/cm³
Air density (standard conditions)	1.293 g/cm³

Thermal conductivity

Copper	384 W/mK
Iron	80.2 W/mK
Air	0.0253 W/mK

Heat capacity

Copper	340 J/kgK
Iron	440 J/kgK
Air	1010 J/kgK

Relative permeability μ_r

Iron	10000
Air, HDPE, PP, PET	1

Temperature Dependent Values

Temperature dependent electric resistivity of iron

$$\frac{1}{0.125\frac{\Omega mm^2}{m}\left(1+0.0056\frac{1}{K}(T-T_0)\right)}$$

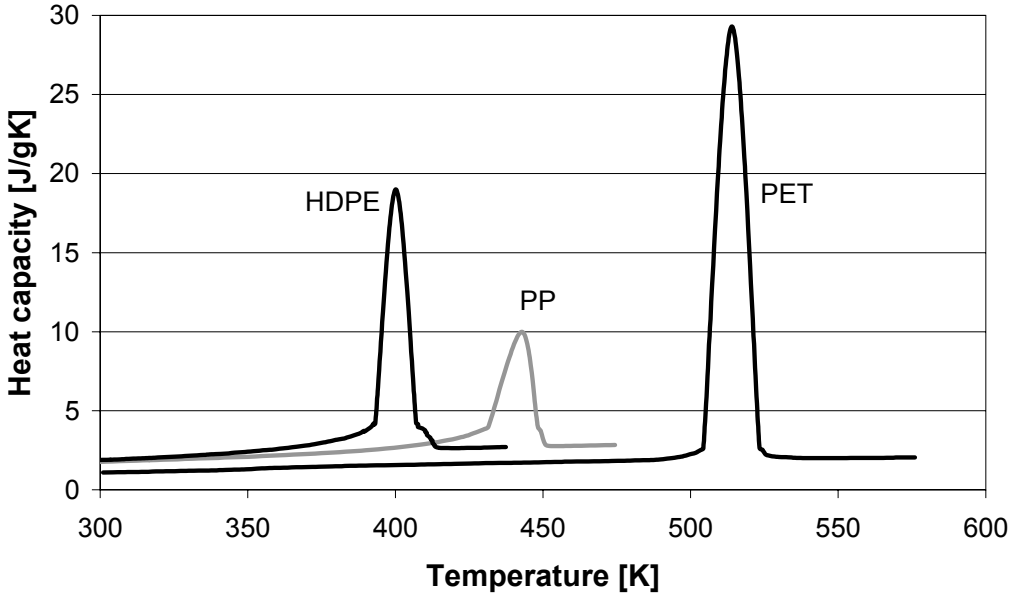

Figure 10.1: Temperature dependent heat capacity with respect to the respective latent heat of used thermoplastics

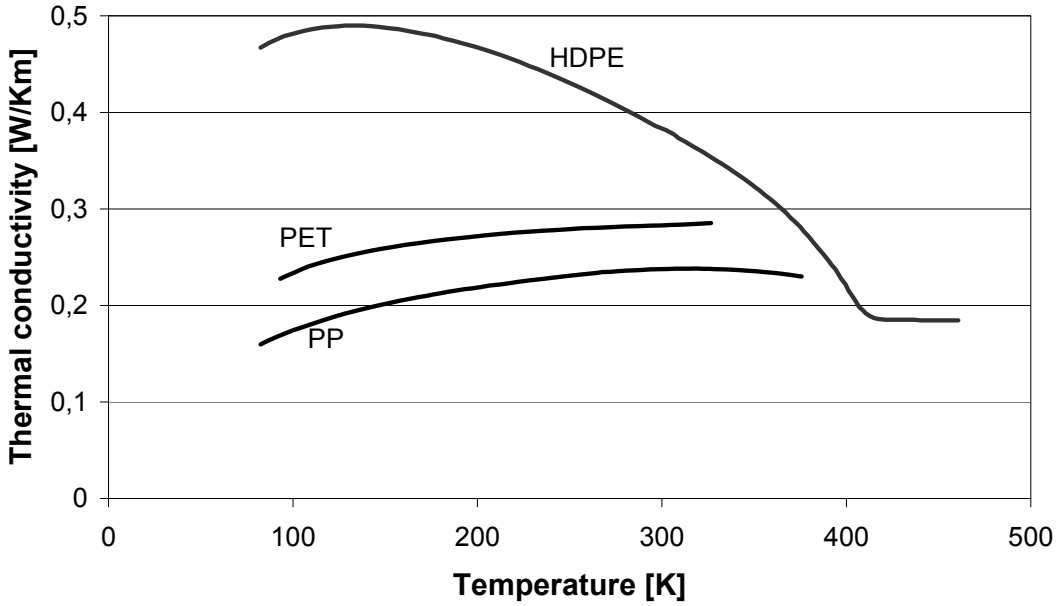

Figure 10.2: Thermal conductivity of the modeled polymers in relation to temperature

List of Publications

1. Schlottermüller, M.; Bayerl T.; Schledjewski, R.: Steigerung der Effizienz des duroplastischen Wickelprozesses. Verbundwerkstoffe und Werkstoffverbunde, Vol. 15 (2005), 535-540.

2. Bayerl, T.; Floeck, M.; Schlarb, A. K.; Haupert, F.; Friedrich, K.: Schweißeignung von peekbasierten Gleitlagerschichten und deren tribologisches Verhalten. Zeitschrift Kunststofftechnik/Journal of Plastics Technology, Vol. 4 (2007), 1-14.

3. Bayerl, T.; Schlarb, A. K.: Schweißeignung von PEEK-Tribokompositen mit metallischen Substraten. IVW-Kolloquium 2008, Kaiserslautern, September 16-17, 2008.

4. Bayerl, T.; Schlarb, A. K.: Welding capability of tribological optimized polyetheretherketone composites with metallic substrates. 2nd International Conference on Advanced Tribology (iCAT), Singapore, December 3-5, 2008.

5. Gebhard, A.; Bayerl, T.; Schlarb, A. K.; Friedrich, K.: Galvanic corrosion of polyacrylnitrile (PAN) and pitch based short carbon fibres in polyetheretherketone (PEEK) composites. Corrosion Science, Vol. 51 (2009), 2524-2528.

6. Bayerl, T.; Schlarb, A. K.: Welding of tribologically optimized polyetheretherketone films with metallic substrates. Tribology International, Vol. 43 (2010), 1175-1179.

7. Gebhard, A.; Bayerl, T.; Schlarb, A. K.; Friedrich, K.: Increased wear of aqueous lubricated short carbon fiber reinforced polyetheretherketone (PEEK/SCF) composites due to galvanic fiber corrosion. Wear, Vol. 268 (2010), 871-876.

8. Bayerl, T.; Schledjewski, R.; Mitschang, P.: Inductive Heating of Polymer Matrixes by Particulate Heating Promoters. 14th European Conference on Composite Materials (ECCM-14), Budapest, Hungary, June 7-10, 2010.

9. Bayerl, T.; Schledjewski, R.; Mitschang, P.: Induktive Erwärmung von Kunststoffverbunden über partikelförmige Additive. IVW-Kolloquium 2010, Kaiserslautern, November 16-17, 2010.

10. Brzeski, M.; Bayerl. T.; Mitschang, P.: Comparison of Methods to Detect Thermal Degradation of Short-Time Heated Carbon Reinforced Thermoplastic Composites. 5th Asia-Europe Symposium on Processing and Properties of Reinforced Polymers, Dresden, May 29 - June 1, 2011.

11. Bayerl, T.; Mitschang, P.: Heating of Polymer-Polymer Composites by Inductive Means. 18th International Conference on Composite Materials (ICCM-18), Jeju Island, Korea, August 21-26, 2011, TH11-1.

12. Bayerl, T.; Benedito Borrás, A.; Andrés Gallego, J. I.; Galindo Galiana, B.; Mitschang, P.: Melting of polymer-polymer composites by particulate heating promoters and electromagnetic radiation. Synthetic Polymer-Polymer Composites, 2011, in press.

13. Bayerl, T.; Schledjewski, R.; Mitschang, P.: Induction Heating of Thermoplastic Materials by Particulate Heating Promoters. Polymers & Polymer Composites, Vol. 20 (2012), No. 4, 333-341.

14. Bayerl, T.: Novel heating and processing for thermoplastic. Innovative Composites Summit, Paris, March 27-29, 2012.

15. Benedito, A.; Galindo, B.; Hare, C.; Bayerl, T.; Mitschang, P.: Selective Heating Applications for the Processing of Polymer-Polymer Materials. 15th European Conference on Composite Materials (ECCM-15), Venice, Italy, June 24-28, 2012, accepted for publication.

16. Bayerl, T.; Valchev, H.; Natter, E.; Mitschang, P.: Processing of Long-Polymer-Fiber Reinforced Thermoplastic Pellets by Compression Molding. 11th International Conference on Flow Processing in Composite Materials (FPCM-11), Auckland, New Zealand, July 9-12, 2012, accepted for publication.

List of Supervised Student Research and Graduation Projects

Grieser, T.: Konstruktion und Inbetriebnahme einer Umformvorrichtung für beschichtete wärmeimpulsgeschweißte Metall/Faser-Kunststoff-Verbunde, IVW-Bericht 08-035, 2008.

Džalto, J.: Konzeption einer induktiven Heizvorrichtung für eigenverstärkte Fließpressmassen, IVW-Bericht 11-003, 2011.

Zou, J.: Experimentelle Untersuchung der Heizwirkung von Kohlenstofffasern in duroplastbasierten Glasfaserkompositen, IVW-Bericht 11-005, 2011.

Kühn, F.: Parameterstudie zur induktiven Partikelerwärmung von Thermoplasten, IVW-Bericht 11-006, 2011.

Valchev, H.: Presstechnische Verarbeitung von eigenverstärkten thermoplastischen Verbundwerkstoffen, IVW-Bericht 12-019, 2012.

List of Supervised Student Internships

Sánchez Sansano, J. A.: Adhesion of Thermoplastic Composites in Cold and Warm State, 2008.

Martínez-Tafalla López, M.: Thermal Degradation Analysis of HDPE and PEEK after Short Cycle Heating, 2010.

Andrés Gallego, J. I.: Simulation of the Thermal Conditions during the Inductive Heating of Particle-Filled Polymers, 2010.